Abhishek Banerjee

Engineered Iron Oxide Nanoparticles: Potential for Stimuli-Responsive Drug Delivery Systems

February 2021

Master's thesis

2021

Abhishek Banerjee

NTNU
Norwegian University of Science and Technology
Faculty of Natural Sciences
Department of Materials Science and Engineering

NTNU
Norwegian University of Science and Technology

NTNU
Norwegian University of Science and Technology

NTNU

Norwegian University of
Science and Technology

Engineered Iron Oxide Nanoparticles: Potential for Stimuli-Responsive Drug Delivery Systems

Abhishek Banerjee

Materials Science and Engineering (MSMT)
Submission date: February 2021
Supervisor: Prof. Mari-Ann Einarsrud
Co-supervisor: Dr. Sulalit Bandyopadhyay
Anuvansh Sharma, PhD

Norwegian University of Science and Technology
Department of Materials Science and Engineering

Declaration of Compliance

I, Abhishek Banerjee, hereby declare that this is an independent work according to the exam regulations of Norwegian University of Science and Technology (NTNU).

Place and Time: Trondheim – Gløshaugen, February 2021.

Acknowledgement

I would like to show my sincerest gratitude to my supervisor, Prof. Mari-Ann Einarsrud, at Department of Materials Science and Engineering, NTNU, for the continuous support throughout the course of this thesis. Her patience, immense knowledge, insightful comments, and motivation have helped me see through tough times. I could not have imagined having a better advisor and mentor for my master's thesis.

Secondly, I am heartily grateful to Dr. Sulalit Bandyopadhyay, Postdoctoral Researcher at Department of Chemical Engineering, NTNU, for showing faith in my abilities and encouraging me till the very end. His unparalleled knowledge and mentoring skills have proven to be of huge help in theoretical as well as practical work. This project work would have not seen light had it not been for his insight.

Thirdly, I would like to thank Anuvansh Sharma, PhD scholar at Department of Materials Science and Engineering, NTNU for all his insightful advice and practical help provided while working in NTNU nanolab and Ugelstad Laboratory. Another special mention was all the microscopy assistance throughout the course of the work using High Resolution Transmission Electron Microscopy (HRTEM) provided from his side. I would also like to extend my gratitude to Nathan Church, Researcher at Department of Geoscience and Petroleum for providing immense support with training and teaching about magnetic materials and its associated characterization techniques.

I would also like to show my appreciation to all the people working at the Ugelstad Laboratory and in my study-room for their generous support and for making working at the Chemical Engineering Department fun.
Last but not least, my family, for their ever-growing love and undying support.

Thank you everyone.

Abstract

Nanomaterials have gained a lot of attention in the past few decades as potential candidates for biomedical applications. Currently, research with different nanomaterials is being carried out for enhancing existing *in-vivo* imaging techniques, wound dressing, tissue engineering, heat induced treatment and targeted drug delivery, where polymeric and inorganic nanoparticles have shown wide potential. These materials have not only been engineered individually for specific applications, but also combined for producing hybrid systems in order to address multiple areas at once.(1) Two materials that have specifically caught attention are hydrogels and iron oxide nanoparticles (IONPs).

The high-water affinity of hydrogels makes them flexible and soft emulating properties of living tissues. They also exhibit good biocompatibility and biodegradability, thus proving to be interesting materials for usage in field of biomedicine.(2) These materials can also be engineered to incorporate multiple stimuli-responsive properties that are sensitive to light, heat, pH, radiation, and electrical signals. Thus, multi-responsive hydrogels have previously been utilized and have shown potential as targeted drug delivery devices, with low toxicity and undesired side effects as compared to conventional techniques. Parallelly, IONPs have also gained wide importance in therapeutics and theranostics over the past two decades due to the possibility of controllable synthesis, thereby producing extremely small (< 20 nm) particles, having different morphology, high monodispersity, and unique superparamagnetic properties.(3, 4) By utilizing their superparamagnetic characteristic, heat can be generated from IONPs on exposure to alternating magnetic fields (AMF), at radio frequency region.(5) This has opened up a field of treatment, called hyperthermia, whereby the heat produced from IONPs can be used for cell apoptosis (killing).(6) However, unwanted, and uncontrolled production of heat can also affect healthy cells and tissues leading to side effects. Utilizing hydrogels to surface engineer IONPs, for producing hybrid structures could be the next potential solution for mitigating the above stated problem. Henceforth, heat produced from IONPs could be localized or controlled with hydrogel coating and could be utilized to trigger release of bioactive agents from these hybrid structures, thus, making treatments more target specific with less side effects. The stimuli-responsive contribution from hydrogels could also be engineered, making these hybrid systems even more efficient.

In this work, controlled and reproducible synthesis of monodisperse IONPs (16 ± 2 nm) (in organic media) was done using thermal decomposition method. The synthesized IONPs were phase transferred from organic to aqueous media using sodium citrate, in order to make the IONPs dispersible in water, which forms the steppingstone for biomedical application. Sodium citrate electrostatically stabilized the IONPs in water, which was seen from negative zeta potential values, measured using Dynamic Light Scattering (DLS). The stability of these particles was also tested at elevated temperatures (45 ºC and 60 ºC), prolonged storage periods (2 months) and different pH conditions ranging from acidic to alkaline (pH 3 to 8) before being used further. Heat generation of these particles were also studied at optimized AMF condition (587 kHz, 12 mT). These particles showed significantly low specific absorption rates (SAR) (1.76 W/g) as compared to conventional magnetite NPs, which was also in accordance with the concept of achieving controlled heating.

Parallelly, a hydrogel, (poly- (N-isopropyl acrylamide-acrylic acid)) was tailored with thermal and pH responsive properties. These systems showed collapse efficiencies ~ 97 % at 45 ºC and also reduction in hydrodynamic size (~ 63 nm) was seen at acidic pH=3.5 condition. Two systems; phase transferred IONPs and NGs, were characterized individually and used in conjunction to synthesize hybrid NGs with potential of being utilized as drug delivery devices.

Hybrid NGs were synthesized using three different techniques - (i. In-situ, ii. Post, iii. Addition), with the idea of producing hybrid systems with different physico-chemical properties, which could open up new opportunities as novel drug-delivery systems. With difference in synthesis techniques, the hybrid systems showed different thermo-responsive properties which was analyzed by studying the collapses of these systems at elevated temperatures (45 ºC). The systems were superparamagnetic and also pH responsive, which showed retention of magnetic properties from IONPs and pH responsive properties from NGs polymeric structures when combined together. Henceforth, successful synthesis of hybrid systems with thermal, pH and magneto-responsive properties were shown in this study.

The hybrid systems were then loaded with a model protein, Cytochrome C (cyt C), and the effect of thermal and pH responsive properties of hybrid systems on release of cyt C was studied under condition – 40 ºC and pH (3.5). The release of cyt C was tracked using UV-Vis spectroscopy (UV-vis) for ~ 20 hours and the release profiles obtained were fitted with common mathematical models

and analyzed. Hybrid NGs synthesized via *in situ* technique showed slowest release rates for the first two hours (0.08 $hour^{-1}$) as compared to other hybrid systems, showing potential as slower or sustained release systems.

Lastly, to understand how magneto-responsive properties of these hybrid systems effected release of cyt C, release studies were done under AMF condition for 10 hours. A major challenge faced during this study, was unwanted production of background heat from water due to formation of eddy currents. Henceforth, optimizations were tried, to mitigate the background heat signal. Real-time monitoring of the temperature within the systems were performed for the entire duration of the study. No noticeable changes in release profile of cyt C was seen on exposure to AMF condition. This was because the release signal of cyt C due to controlled heat produced from hybrid systems were masked by background heating effects.

Table of Contents

List of Figures

List of Tables

Background

Motivation

Nanomaterials are materials that have at least one dimension in the size range of one billionth of a meter (10^{-9} m). For the past two decades, considerable research has been conducted on developing and engineering magnetic nanomaterials. Magnetic nanomaterials form very effective energy harvesting systems which have the potential to transform the existing therapeutic and diagnostic methods. One such example of magnetic nanomaterial is iron oxide nanoparticles (IONPs).

Current radiation-based techniques for treatment of cancer have serious long-term health effects like hair fall, impotency, and fast ageing. IONPs, due to their magnetic properties, show heating effects on exposure to external alternating magnetic fields (AMF). This heat energy harvested from magnetic IONPs can be potentially used for direct killing of foreign antigens, harmful cells, and tissues. The process of heat induced treatment is known as hyperthermia and has been of emerging interest as a supplementary tool with current radiation techniques. But a major challenge in the field of hyperthermia is the unwanted heat production from magnetic nanoparticles which can also damage healthy cells and tissues. Hence, the main vision was to coat, or surface engineer the magnetic nanoparticles to control heat production and utilize the heat to trigger release of specific bioactive agents in the human system. This can help to overcome current challenges faced in hyperthermia technique and make treatments more specific with minimal side effects. A schematic of the motivation of the work is shown in Figure 1. Thus, magnetic nanoparticles have good potential in making existing diagnostic methods more flexible.

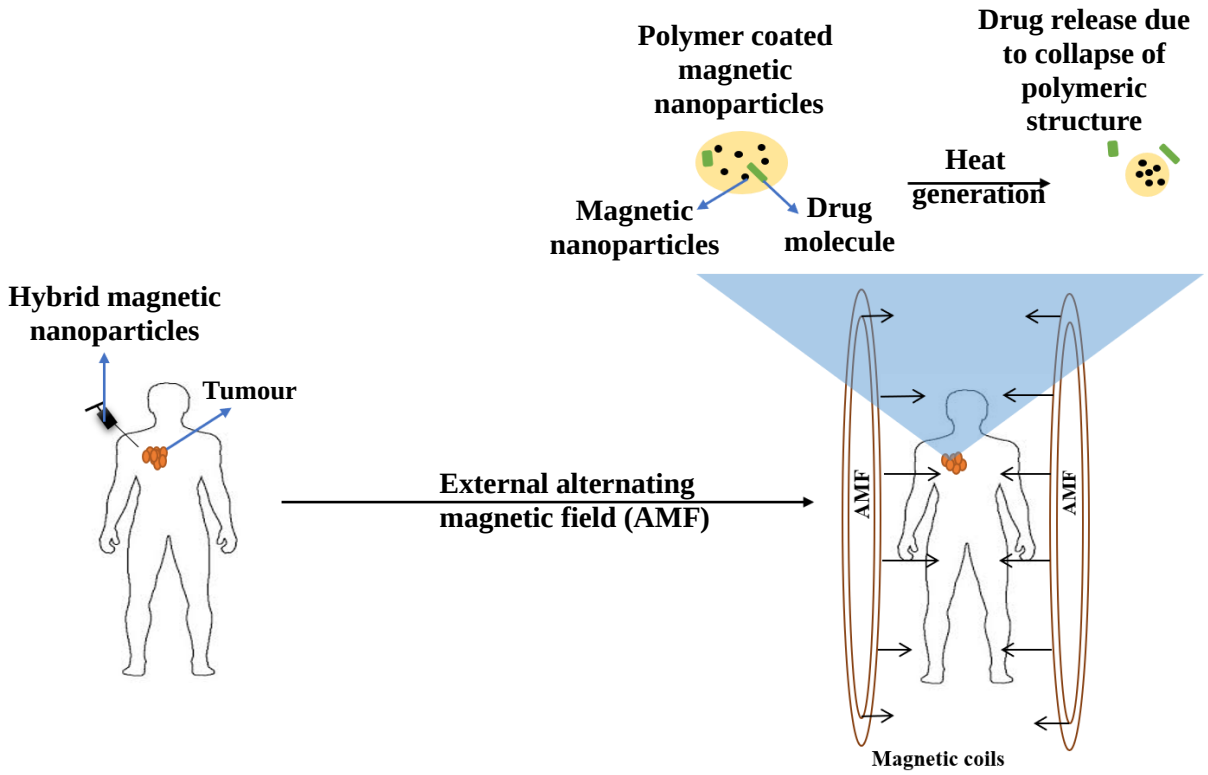

Figure 1 – Schematic showing motivation of the work.

Main Aim

The main aim of the project involves synthesis of hybrid nanoparticles with thermal, pH and magneto-responsive properties. The initial part of the work will focus on controlled and reproducible synthesis of IONPs using thermal decomposition technique in organic media. Thus, an intermediate step will be used to phase-transfer the as-synthesized IONPs from organic to aqueous media for applications in the field of biomedicine. Next, utilization of the phase transferred IONPs with a bio-compatible, thermo-responsive polymer will be used to synthesize hybrid nanoparticles. Furthermore, hybrid nanoparticles will be loaded with a drug and its releases as function of temperature and external alternating magnetic fields will be tested. A flowchart illustrating the aim is shown in Figure 2.

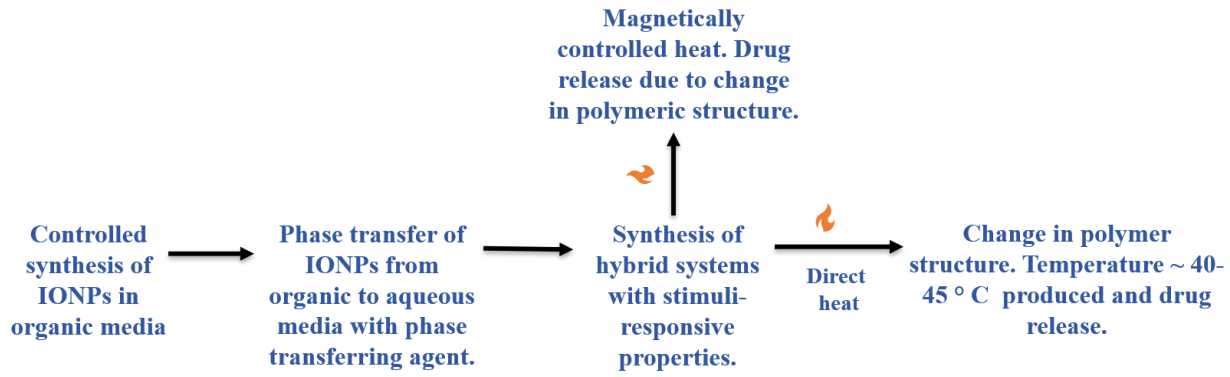

Figure 2 – Flowchart illustrating the aim of the work

Chapter 1: Introduction

Nanotechnology is the study of particles with at least one dimension less than 100 nm. Engineering at molecular level helps to provide control over macroscopic properties of material (7). Therefore, by optimizing synthesis and assembly processes of nanoparticles (NPs), the chemical and physical properties of the final product can be tuned for specific applications in fields of medicine (8, 9) , catalysis (10) and electronics (11).

The use of magnetic nanoparticles in the field of medicine has gained immense importance. Small size, controllable dispersity, surface functionalization for increasing biocompatibility and heat production properties on exposure to alternating magnetic fields are important in various medical applications, namely, cancer therapeutics, antimicrobial actions, vaccine delivery, imaging, and site-specific targeting (12).

The upcoming sections will focus on common synthesis techniques, crystallographic phases, magnetic properties, general mechanisms of heat production and surface functionalization of iron oxide nanoparticles (IONPs). The later sections will shed light on stimuli-responsive polymers and hybrid nanoparticle systems. Lastly, common pharmaceutical requirements and mathematical models for understanding drug delivery mechanisms are described.

1.1. Iron Oxide Nanoparticles (IONPs)

Iron oxide nanoparticles (IONPs) have diameters typically between 1 and 100 nm. The most common crystallographic structures of IONPs are magnetite (Fe_3O_4) and its oxidized form maghemite (γ-Fe_2O_3) (13). IONPs have attracted extensive interest due to its superparamagnetic nature. Some common applications of iron oxide nanoparticles include magnetic storage devices and high-sensitivity magnetic resonance imaging (MRI) for medical diagnosis and therapeutics.

In the following section, common synthesis routes of IONPs utilizing mechanisms of Classical Nucleation Theory (CNT) are discussed.

1.2. Synthesis of IONPs

In the past decade, synthesis of magnetic IONPs has been developed not only for understanding fundamental scientific interest but also for many bio-technological applications, such as targeted drug delivery, magnetic resonance imaging (MRI), magnetic hyperthermia and thermo ablation, bio-separation, and biosensing. IONPs have received considerable attention in the field of biomedicine as it offers unique advantages over other materials. For example, IONPs can be engineered to produce physically and chemically stable nanostructures, tunable biocompatibility, and environmentally safe (13).

This section is divided in two subsections. Firstly, general mechanisms involved in formation of nanoparticles will be touched, which will later be followed up with discussions on more specific synthesis techniques for producing IONPs.

1.2.1. General Mechanism of Nanoparticle Formation

The general formation of nanoparticles proposed by Lamer et al. involves concentration-based precipitation in a solvent. The process can be divided into two parts – 1) nuclei formation of initially precipitated solute particles followed by 2) subsequent growth of the formed nuclei (14). The Lamer`s model (shown in Figure 1.1) describes regions of nucleation and growth during nanoparticle formation as function of time. For the formation of the initial embryo, the solute concentration should be above a certain critical value (C_S). The system at this point reaches the condition of supersaturation. At solute concentrations higher than the critical nucleation concentration (C^{nu}_{min}), the embryo reaches a particular size when it starts to form the first nuclei. The further formation of nuclei reduces the supersaturation of the system. Below C^{nu}_{min}, nucleation stops, and the formed nuclei continue to grow by molecular addition.

The nucleation process can be classified into two types – 1) homogeneous nucleation and 2) heterogeneous nucleation (15). Homogeneous nucleation occurs without the presence of an external surface in the solvent and hence must overcome a larger surface energy barrier. Heterogeneous nucleation occurs in the presence of an existing surface in the system and the surface energy barrier is therefore lower (15).

For application of nanoparticles specifically in the field of biomedicine, the most important factors are controlling particle size and monodispersity to reduce agglomeration and toxicity effects (16). High monodispersity of nanoparticles can be achieved by high degree of supersaturation in the system which leads to the phenomenon of burst nucleation (formation of all nuclei at the same time) (17). Following burst nucleation, growth of the formed nuclei proceeds. This growth process can be controlled with the aid of stabilizing agents which determines the final particle size. Utilizing the above discussed nucleation and growth mechanisms, different synthesis techniques for producing IONPs is discussed in next subsection.

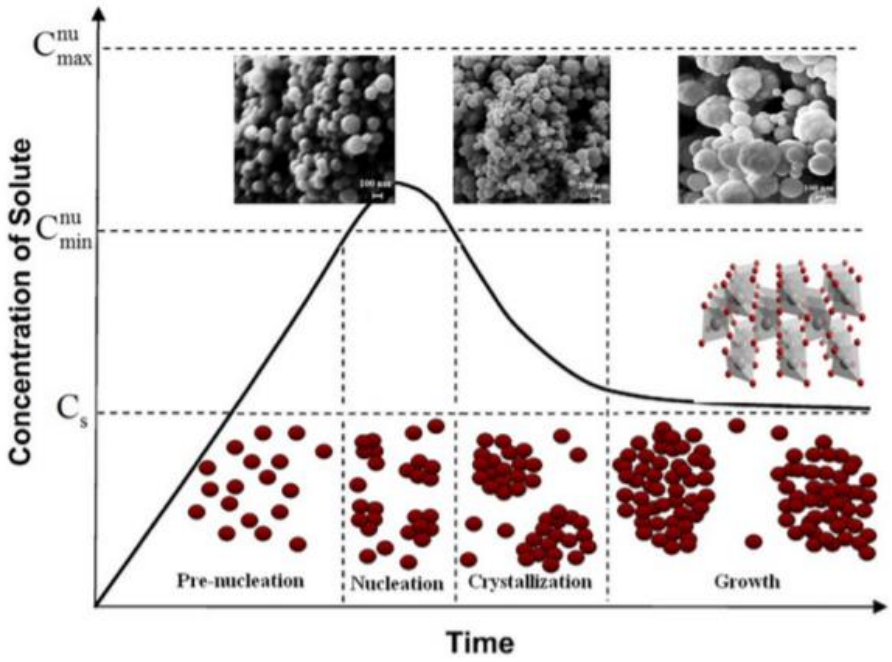

Figure 1.1 – Lamer`s model describing nucleation and growth of nanoparticles as a function of reaction time and solute concentration. Saturation concentration (C_s); minimum concentration (C^{nu}_{min}) for the formation of nuclei (18).

1.2.2. Synthesis of Iron Oxide Nanoparticles (IONPs): State of Art

IONPs have been synthesized via several routes. Two common approaches will be discussed :1) co-precipitation (19) and 2) thermal decomposition (20) .

1.2.2.1. Co-Precipitation

The basic concept of co-precipitation technique involves simultaneous precipitation of two or more solutes from its solvent. Synthesis of IONPs via co-precipitation technique was first shown by Massart et al. where an aqueous solution containing ferrous (Fe^{2+}) and ferric (Fe^{3+}) ions in stoichiometric ratio 1:2 was used, and precipitation occurred by addition of a basic solution (19). The final product obtained was black colored precipitate of IONPs.

The main advantages of this process are relatively low synthesis times as compared to other processes, inexpensive chemicals and experimental setups, and high production yields. But major challenge involves difficulty in precise control of particle size and dispersity. Due to very high supersaturation, agglomeration effect is hard to control via co-precipitation technique which might pose problems for usage in biomedicine (16, 21) . Therefore, focus will be given on thermal decomposition methods for controlled synthesis of IONPs which is discussed next.

1.2.2.2. Thermal Decomposition

Thermal decomposition is the preferred method for controlling particle size, morphology, and dispersity of IONPs (22) . The main concept revolves around thermally decomposing iron compounds with oxygen containing ligands (e.g., carbonyl, oleates, acetylacetonates or acetates) in organic solvents at elevated temperatures to cause initial nucleation of IONPs and the final growth process of IONPs is controlled via different organic stabilizing agents (23-25). The reaction conditions are chosen based on the boiling point of the solvent and stabilizing agents (26). The decomposition rate of the iron precursor determines the nucleation rate and in turn the size and dispersity of the final particles. Thus, particle size and dispersity can be controlled using precursor concentration, reaction heating rate, reaction temperature, solvent boiling point and inert reaction atmospheres (27). Previous study by Cotin et al. showed the influence of reaction heating rates on final particle size, distribution, and anisotropy (28).

The main advantages of synthesis of IONPs via thermal decomposition route is high control over particle size, shape and monodispersity while some challenges involve low yields and use of hydrophobic organic stabilizing agents like oleic acid and oleylamine which forms a

hydrophobic coating on IONPs surface (26). Therefore, particles synthesized via thermal decomposition cannot be directly dispersed in water and they require additional phase-transferring steps before being used for biomedical purposes. Thermal decomposition using two common precursors iron oleate ($C_{18}H_{33}FeO_2$) and iron pentacarbonyl ($Fe(CO)_5$) are discussed below.

Precursor Iron Oleate

Iron (III) oleate is commonly synthesized via a disproportionation reaction using iron chloride ($FeCl_3 \cdot 6H_2O$) and sodium oleate which was used as precursor for further IONPs synthesis (26). Iron (III) oleate is then thermally decomposed in an organic solvent. The solvent of the reaction is chosen based on its boiling point which should be higher than the thermal decomposition temperature of the iron oleate precursor (26). One of the common stabilizing agents used in this process is oleic acid to control the agglomeration of the IONPs.

The most important parameters to control shape, size and distribution of particles are the heating rate of the reaction. Slower heating rates would slow down the nucleation rate of IONPs thus decreasing the kinetic separation between nucleation and growth regimes of the reaction. This would eventually lead to an overlap of the nucleation and growth regions of the reaction resulting in increased average particle size and polydispersity index. Previous study by Bronstein et al. showed variation of reaction rates depending on structure of iron oleate precursor complex, which in turn affects final particle size and distribution (3). Generally, highly crystalline IONPs are produced using iron oleate as precursor (26).

Precursor Iron Pentacarbonyl

In synthesis of IONPs with iron pentacarbonyl as precursor, a common solvent previously used is octyl ether with oleic acid as stabilizing agent (26). The reaction involves mixing oleic acid with octyl ether under inert atmospheres followed by quick addition of iron pentacarbonyl (26). The inert atmosphere was maintained to prevent oxidation of the IONPs during the reaction. Particle size and distributions was controlled by varying the heating rate of the reaction (26). IONPs synthesized via iron pentacarbonyl showed relatively poor crystallinity as compared to IONPs synthesized with iron oleate (26, 29). In the following section, typical crystallographic structures

of IONPs obtained via above discussed methods are described.

1.3. Different Structures of IONPs

Eight different crystallographic phases of iron oxide are reported (30). The two most common phases seen in obtained IONPs via thermal decomposition routes are magnetite (Fe_3O_4) and maghemite (γ-Fe_2O_3) (26). This section is divided in two parts where crystallographic structures of Fe_3O_4 and γ-Fe_2O_3 will be presented, respectively. Each of these structures has unique chemical and magnetic properties which provides suitability for specific biomedical applications.

1.3.1. Magnetite

Magnetite (Fe_3O_4) has a face centered inverse cubic spinel structure (13). Fe_3O_4 differs from most other iron oxides as it contains both divalent and trivalent ions of iron (shown in Figure 1.2 - a)). Fe_3O_4 has an inverse spinel structure that consists of a cubic closed packed array of oxide ions, where all of the Fe^{2+} ions occupy half of the octahedral sites and the Fe^{3+} are evenly distributed across the remaining octahedral and tetrahedral sites. Fe_3O_4 has the lowest resistivity among iron oxides due to its small bandgap (0.1 eV) (31).

1.3.2. Maghemite

The structure of maghemite (γ-Fe_2O_3) is cubic (shown in Figure 1.2 - b)). Each unit of maghemite contains 32 O^{2-} ions, 21⅓ Fe^{3+} ions and 2⅓ vacancies (13). Oxygen anions form cubic close-packed arrays in which Fe^{3+} ions occupy the tetrahedral sites. The octahedral sites consist of the remaining Fe^{3+} ions and vacancies. Therefore, the maghemite can be considered as fully oxidized magnetite, and it is an n-type semiconductor with a bandgap of 2.0 eV (13). γ-Fe_2O_3 also has similar crystal structure as Fe_3O_4 (shown in Figure 1.2 - a)) (13). Post-annealing treatments are important for controlling the final crystallographic phase of iron oxides. Annealing treatments of magnetite phase could form maghemite phase by oxidation (26).

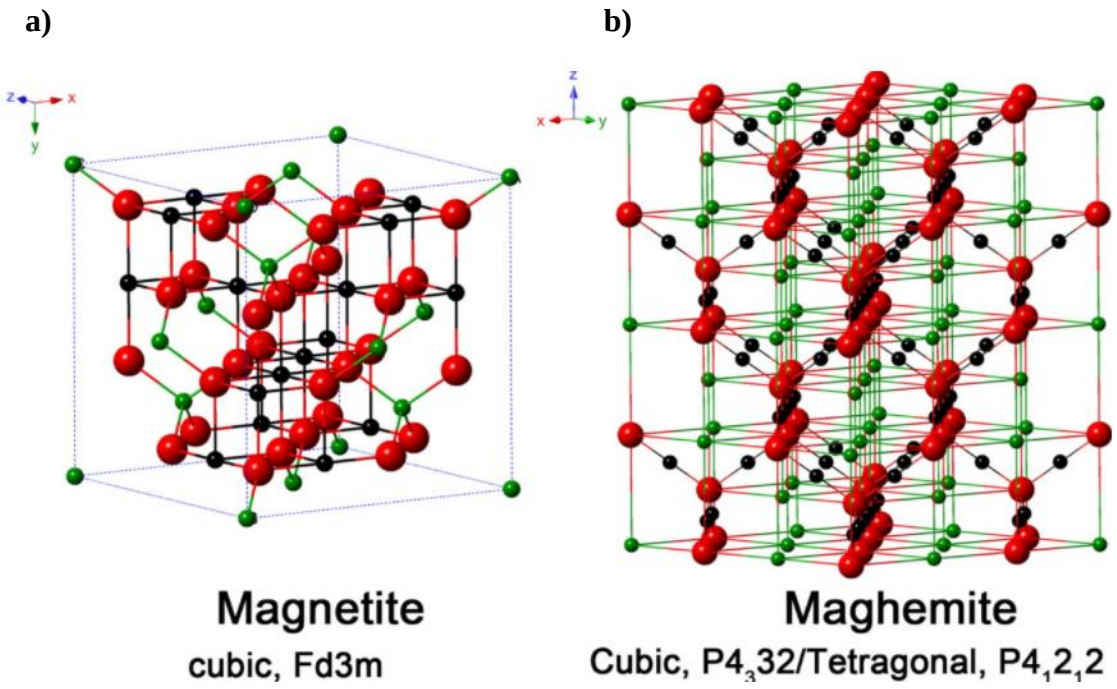

Figure 1.2 a) - Crystal structure and crystallographic data of magnetite and b) maghemite (the black sphere is Fe^{2+}, the green sphere is Fe^{3+} and the red sphere is O^{2-}) phases of iron oxide (13).

In next section, different types of magnetism and parameters governing heat generation from IONPs on exposure to external magnetic fields are discussed.

1.4. Magnetic properties of IONPs

IONPs due to its unique magnetic properties can find wide potential in field of biomedicine which involves magnetically triggered drug delivery systems, bioimaging and separation. This section contains two subsections, where firstly different types of magnetisms occurring in nature will be discussed briefly and will then be followed up with unique size dependent superparamagnetic shown by magnetic nanoparticles.

1.4.1. Different types of magnetism

Magnetism in materials arise due to magnetic moments of individual atoms. The associated magnetic moment of atoms is attributed to spin and orbital motion (probabilistic electron distributions) of the electrons. Specifically, transition metal elements with unfilled 3d orbitals (unpaired electrons) have characteristic magnetic moments. When the orbitals are filled, the net magnetic moment becomes zero and the material becomes diamagnetic. Diamagnetic materials do

not show any induced magnetism in the presence of an external magnetic field. Paramagnetic materials have unpaired electrons. At room temperature, in the absence of an external magnetic field, the net magnetic moment of the material remains zero due to random alignment of the unpaired electrons. In the presence of an external magnetic field, the unpaired electrons align in the direction of the field resulting in a net induced magnetic field (magnetic saturation) in the material.

Ferromagnetic materials are permanent magnets which retain their magnetism on removal of the external magnetic field. Ferromagnetic materials have a higher number of unpaired electrons compared to paramagnetic materials. The degree of overlap of the orbitals, dependent on the crystal structure of the material and can be understood based on two energy interactions – 1) Exchange energy interaction (parallel coupling of magnetic moments) and 2) Bonding energy interaction (antiparallel coupling of magnetic moments) (32). At large inter-orbital distances, the exchange energy interaction becomes dominant forming parallel coupling of orbitals. This gives rise to a net magnetic moment making the material ferromagnetic. Conversely, at small inter-orbital distances, the bonding energy dominates favoring anti-parallel alignment and hence total cancellation of magnetic moments happen. This type of material is known as an antiferromagnet. If the anti-parallel magnetic moments are not equal in magnitude, a net moment in the material exists showing ferrimagnetism. The different types of magnetism are illustrated in Table 1.1.

Table 1.1 - Different types of magnetism and related properties (33).

Type of Magnetism	**Susceptibility**	**Atomic Behaviour**	**Example**	**Susceptibility**
Diamagnetism	Small and negative	Atoms have no magnetic moment	Au, Cu	$-2.74 * 10^{-6}$, $-0.77 * 10^{-6}$
Paramagnetism	Small and positive	Atoms have randomly oriented magnetic moments	Sn, Pt, Mn	$0.19 * 10^{-6}$, $21.06*10^{-6}$, $66.10*10^{-6}$
Ferromagnetism	Large and positive, function of applied field, microstructure dependent	Atoms have parallel aligned magnetic moments	Fe	~ 100.00
Antiferromagnetism	Small and positive	Atoms have mixed parallel and anti-parallel magnetic moments	Cr	$3.6*10^{-6}$
Ferrimagnetism	Large and positive, function of applied field, microstructure dependent	Atoms have antiparallel aligned magnetic moments	Ba-ferrite	~ 3

1.4.2. Superparamagnetism of IONPs

Ferromagnetic materials with sizes generally less than 50 nm show a special type of magnetism called superparamagnetism (5). At such small sizes, the surfaces are more dominant as compared to their bulk counterparts. The magnetic moments for such small particles can be visualized as single domain structures which remain randomly aligned without the presence of an external magnetic field. In the presence of an external magnetic field, the randomly arranged magnetic moments align in the direction of the field producing a net magnetic moment (shown in Figure 1.3 – a)).

The special property which sets superparamagnetic materials apart from their bulk ferromagnetic counterparts is that they do not retain their magnetism at room temperature. Alike paramagnetic materials, the superparamagnetic materials also have close to zero hysteresis losses, but the magnetic susceptibility of these materials are multiple times higher and comparable to ferromagnets. This means the magnetic energy losses in the material are minimized to zero during cycles of magnetization and its reversal in presence of an external field. Figure 1.3 – a) and b) shows comparison of the hysteresis of superparamagnetic and ferromagnetic materials.

The following section will cover details of mechanisms involved in heat production from superparamagnetic IONPs on exposure to alternating magnetic fields (AMFs) and general methodologies used for quantifying the produced heat.

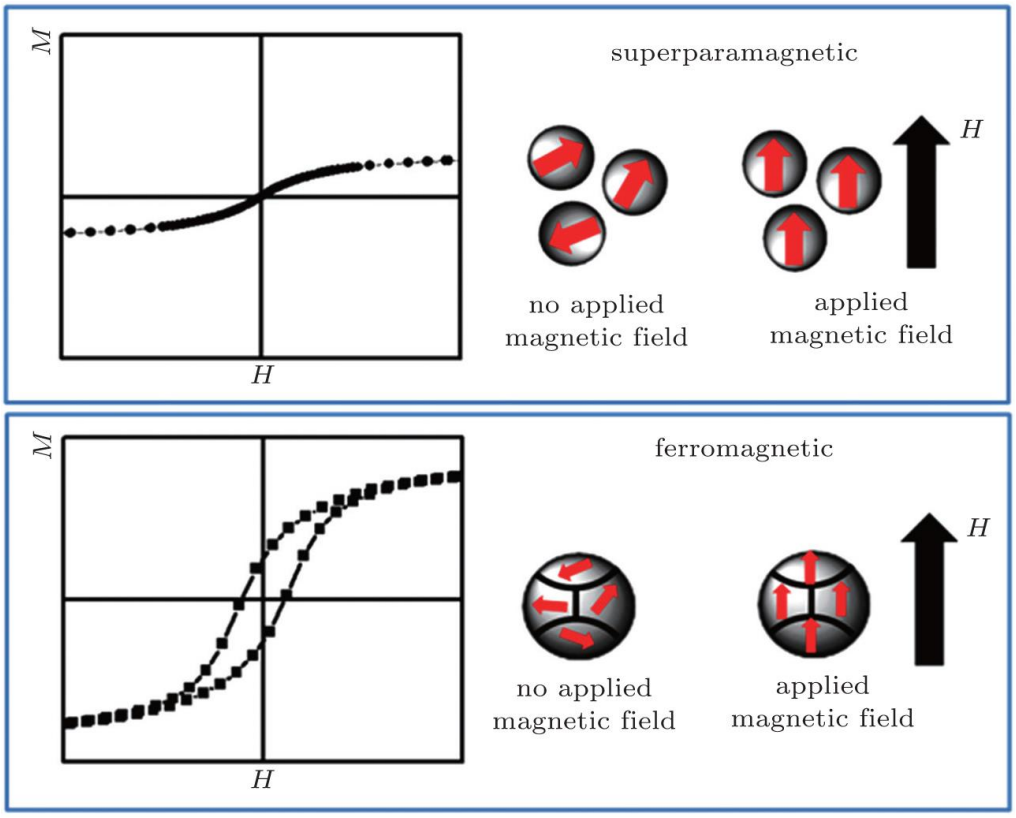

Figure 1.3 – Schematics showing the difference between paramagnetic and ferromagnetic materials. a) Superparamagnetic materials containing single-domains, randomly oriented in the absence of a magnetic field. Magnetization versus applied magnetic field curve of superparamagnetic materials showing zero hysteresis. b) Ferromagnetic materials containing multiple domains. Magnetization versus applied magnetic field curve of ferromagnetic materials showing hysteresis (34).

1.5. General Mechanisms for Heat Generation from IONPs

Superparamagnetic IONPs have high magnetic susceptibility. An external alternating magnetic field (AMF) typically in the radio frequency range (50-300 kHz) with strength close to the saturation magnetization of IONPs is required to produce a phase lag with the flipping frequency of the magnetic moments of IONPs (5). This causes loss of magnetic energy from IONPs in the form of heat energy which can find applications in targeted tumor therapy or engineered drug delivery systems (DDS). In a previous work by Riedinger et al., IONPs coated with a thermo-labile azo molecule produced controlled heating under the presence of an external AMF. The heat was utilized to release a chemotherapeutic agent, doxorubicin (4). This conversion of magnetic energy of IONPs to heat is mainly contributed by two mechanisms – 1) Neels relaxation, 2) Browns

relaxation which are discussed respectively, in the following subsections.

1.5.1. Neels Relaxation

In Neels mechanism, the individual magnetic moments of IONPs rotate in the presence of an external magnetic field while the particles remain fixed along their own crystallographic axes (shown in Figure 1.4 - a)) (5). For a superparamagnetic material, the mean flipping time of the magnetic moments to its preferred energy orientation is called the Neels relaxation time. For particle sizes less than 50 nm, the magnetic coercivity and anisotropic effects reduces as compared to their bulk counterparts. Thus, rotation of individual magnetic moments is more energetically favorable as compared to the rotation of the entire particles in the presence of an external magnetic field. This reduces Neels relaxation time of IONP making it the most dominant mechanism for heat production from particles less than 50 nm. Neels relaxation time increases exponentially with particle diameter as magnetic anisotropy and coercivity effects appear (shown in Figure 1.5). The dependence of Neels relaxation time (τ_N) on particle diameter and magnetic anisotropy (K) can be calculated by Equation 1 (5).

$$\tau_N = \tau_0/2\sqrt{(\pi kT/KV)} * e^{(K*V)/kB*T} \quad (1)$$

where V – particle volume, K – is the magnetic anisotropy, which is also dependent on shape anisotropy of IONPs, τ_0 – pre-exponential component and k_B – Boltzmann constant.

1.5.2. Browns Relaxation

In Brownian relaxation mechanism, the individual magnetic moments of particles remain fixed while the entire particle rotates about its crystallographic axis (shown in Figure 1.4 – b)) (5). In comparison with Neels relaxation, it is the preferred relaxation mechanism at larger particle diameters when magnetic anisotropic effects are more. Brownian relaxation (τ_B) time has linear variation with hydrodynamic volume (shown in Equation 2 and Figure 1.5) (5).

$$\tau_B = (3\eta V_H)/(k_B T) \quad (2)$$

where V_H – hydrodynamic volume, η – viscosity of the solution.

In practical scenarios, where size and magnetic anisotropic values of IONPs are distributions instead of single values, both mechanisms may occur simultaneously and depending on the above stated factors either one of them contributes more to the effective relaxation time (5). Calculation of the effective relaxation time ($\bar{C}$) is shown in Equation 3 (5). Apart from Neels and Browns relaxation mechanisms, production of heat due to eddy currents are also seen. This heat is due to small current loops produced in the solvent of dispersed IONPs on exposure to radio-frequency AMFs (shown in Figure 1.4 – c)). This heat contribution does not come from IONPs but is dependent on the properties of solvent like viscosity and polarity in which IONPs are dispersed (5). Henceforth, heat generation from eddy currents can be regarded as background or external heat which needs to be compensated while analyzing heating properties of IONPs.

$$1/\bar{C}=1/C_B+1/C_N \quad (3)$$

In the following section, existing methodologies for quantification of heat produced from superparamagnetic IONPs on exposure to AMFs will be discussed.

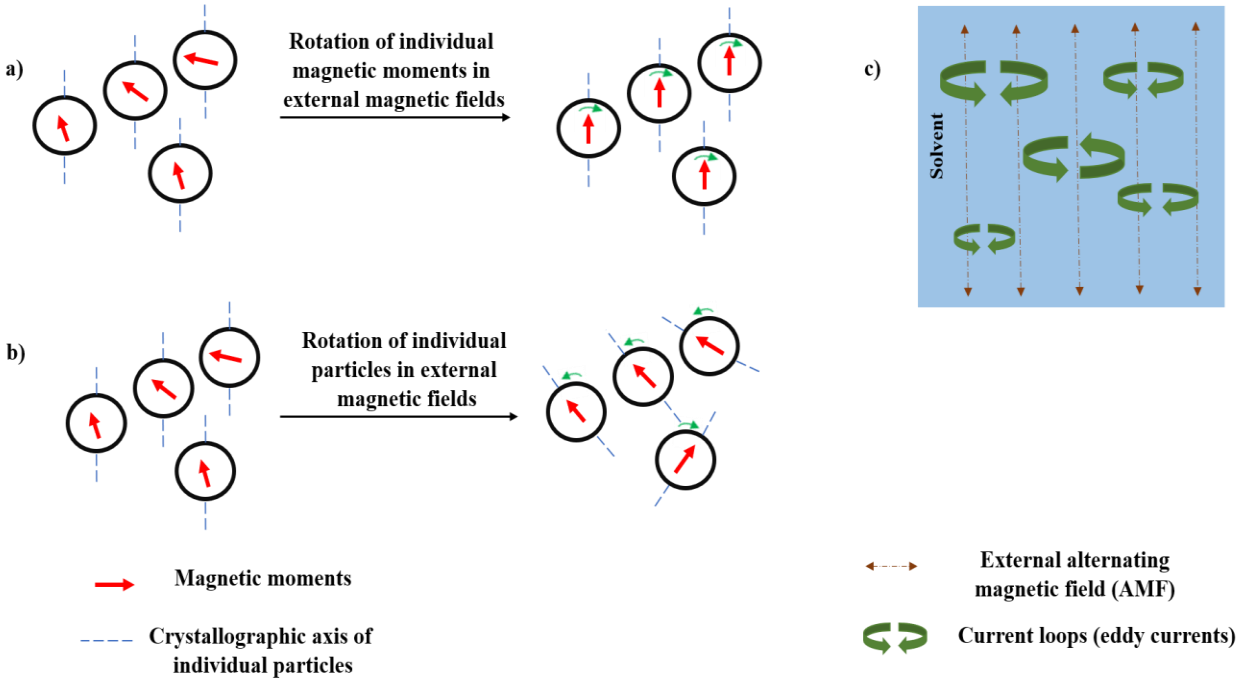

Figure 1.4 – Mechanisms for heat generation – a) Neels relaxation b) Browns relaxation and c) Eddy currents.

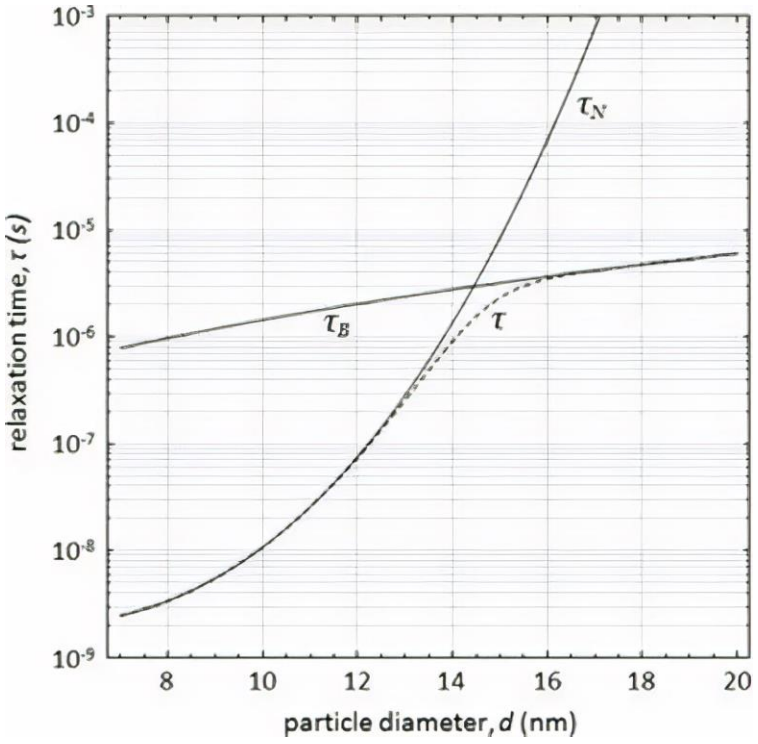

Figure 1.5 – Relaxation times for single-domain magnetite nanoparticles in an aqueous medium (K=25 kJ/m^3, T = 310 K, η=8.9*10^{-4} Pa s) (5).

1.6. Concept of Specific Absorption Rates of IONPs

Specific absorption rate (SAR) is a general term related with the amount of heat generated or dissipated by an ensemble of nanoparticles (5). The magnetic susceptibility of a ferro-fluid (ensemble of IONPs dispersed in a solvent) is a function of the frequency of the external alternating magnetic field (AMF) required for generation of heat from IONPs (35). The magnetic susceptibility of ferrofluids can be theoretically modelled by two components – 1) real part $\chi`(\omega)$ and 2) imaginary part $\chi``(\omega)$ (shown in Equation 4) (35). The real part of the magnetic susceptibility $\chi`(\omega)$ of the ferrofluid system increases with the frequency (f) of the external AMF up to the point ($f * \tau_N = 1$) when it matches the natural flipping frequency of the system (defined by the Neels relaxation time (τ_N)) i.e. the system remains in-phase with AMF (shown in Figure 1.6). Whereas, at frequencies higher than the Neels relaxation time (τ_N) of the system (out of phase with the AMF), the real part of the susceptibility drops, and the imaginary part increases (shown in Equation 5) (35). Heat generation from IONPs using AMF is dependent on the imaginary part of the susceptibility (shown in Figure 1.6). The value of the imaginary part is maximized when f

exceeds τ_N and fulfills the condition of $\omega*\tau_N = 1$ (shown in Equation 5) (35). It is at this point SAR values are maximized for a ferro-fluid system at specific anisotropy and temperature (shown in Equation 6). This is defined as the critical frequency of the system for maximizing SAR values (35). At values above the critical frequency, when $\omega*\tau_N > 1$, the imaginary part of the susceptibility drops thus decreasing SAR values (shown in Figure 1.6). In the equations discussed above, τ_N is used instead of τ_{eff} as it is assumed the average size of IONPs in the ferro-fluid system is very small (less than 20 nm), so contribution from Browns relaxation mechanism is neglected (discussed in Section 1.5). Thus, for effective generation of SAR values, one needs to predict the Neels relaxation time of the system. In practical scenarios, predicting the Neels relaxation time from theoretical models is not possible as value of anisotropy and size of a ferro-fluid system forms a distribution thus giving large deviations from theoretically predicted Neels relaxation time (shown in Equation 1) (35).

$$\chi(\omega) = \chi`(\omega) - i\chi``(\omega) \quad (4)$$

where $\chi(\omega)$ – complex function of the magnetic susceptibility

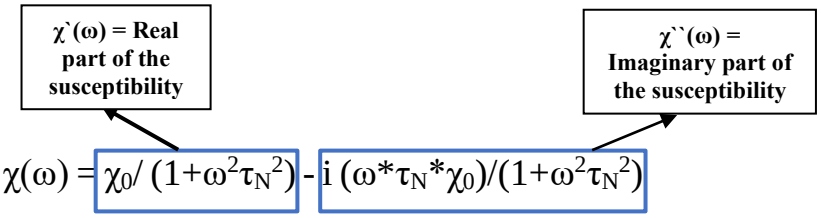

$$\chi(\omega) = \chi_0/(1+\omega^2\tau_N^2) - i(\omega*\tau_N*\chi_0)/(1+\omega^2\tau_N^2) \quad (5)$$

where $\omega = 2*\pi*f$; $\chi_0 = nm^2/3k_BT\mu_0$

where ω – angular frequency, n – particle number density, m – particle mass, μ_0 – magnetic permeability, k_B - Boltzmann constant, T – temperature.

$$SAR = \tfrac{1}{2}*(\omega*\chi_0*\mu_0*H^2) * (\omega\mathcal{C}_N/1+\omega^2\mathcal{C}_N^2) \quad (6)$$

where H – magnetic field amplitude, $\mathcal{C}_N$ – Neels relaxation time.

To control size and monodispersity, synthesis of IONPs in organic solvents via thermal decomposition is the preferred route (discussed in Section 1.2, Subsection 1.2.2). Therefore, to utilize superparamagnetic IONPs for biomedical applications, the nanoparticles need to be

efficiently transferred from organic to aqueous medium via phase transferring agents. The next section will include general function of phase transferring agents and specifically function of sodium citrate as a phase transferring agent which is primarily focused in this study.

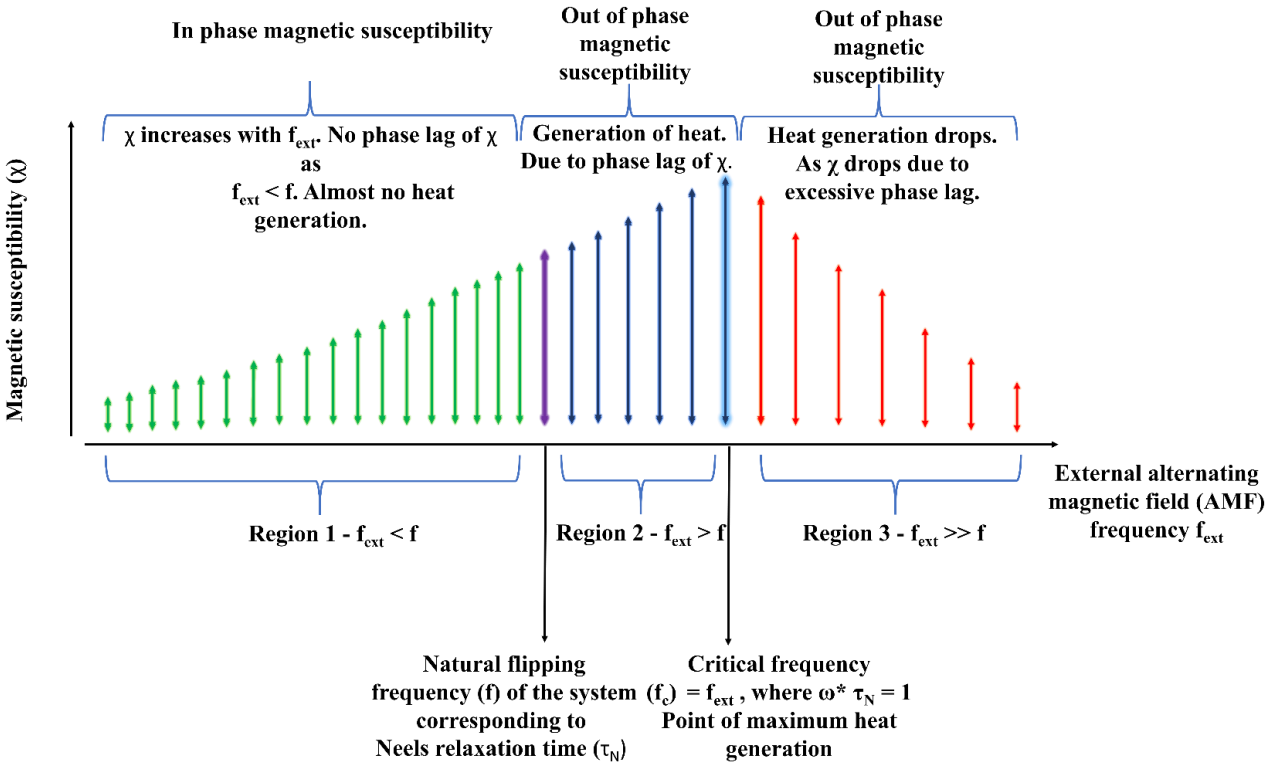

Figure 1.6 – Schematic showing heat generation from a ferro-fluid system as function of external magnetic field frequency (f_{ext}) and magnetic susceptibility (ω).

1.7. Phase Transferring Agent

Efficient phase transfer of monodisperse IONPs from organic to aqueous medium can be accomplished using different phase transferring agents (PTAs). In this section, general idea and working principle of phase transferring agents and function of a common PTA – sodium citrate in phase transfer process of IONPs are respectively discussed in the following subsections.

1.7.1. What is Phase Transferring Agent?

A phase transferring agent (PTA) is used with one reactant to make it react with a second reactant present in a different phase (36). PTAs are used to transfer salts, colloidal particles, and nanoparticles from one media to another (e.g., organic to aqueous media and vice versa) based on

specific applications (1). During organic synthesis of nanoparticles, the final product needs to be transferred to an aqueous media for biomedical applications (1). There are generally two possible mechanisms which can occur during a phase-transferring process which involves ligand-ligand interaction or exchange. In case of ligand-ligand interaction, the PTA chemically binds to the existing ligands on the nanoparticles thus helping in transfer to a different media whereas in ligand-ligand exchange, the PTA replaces the existing ligands on the nanoparticles during the phase transfer process. A schematic is shown in Figure 1.7. In previous works of Bandyopadhyay et al., a ligand-ligand exchange mechanism was shown during phase transfer of IONPs from organic to aqueous media using sodium citrate as PTA (37).

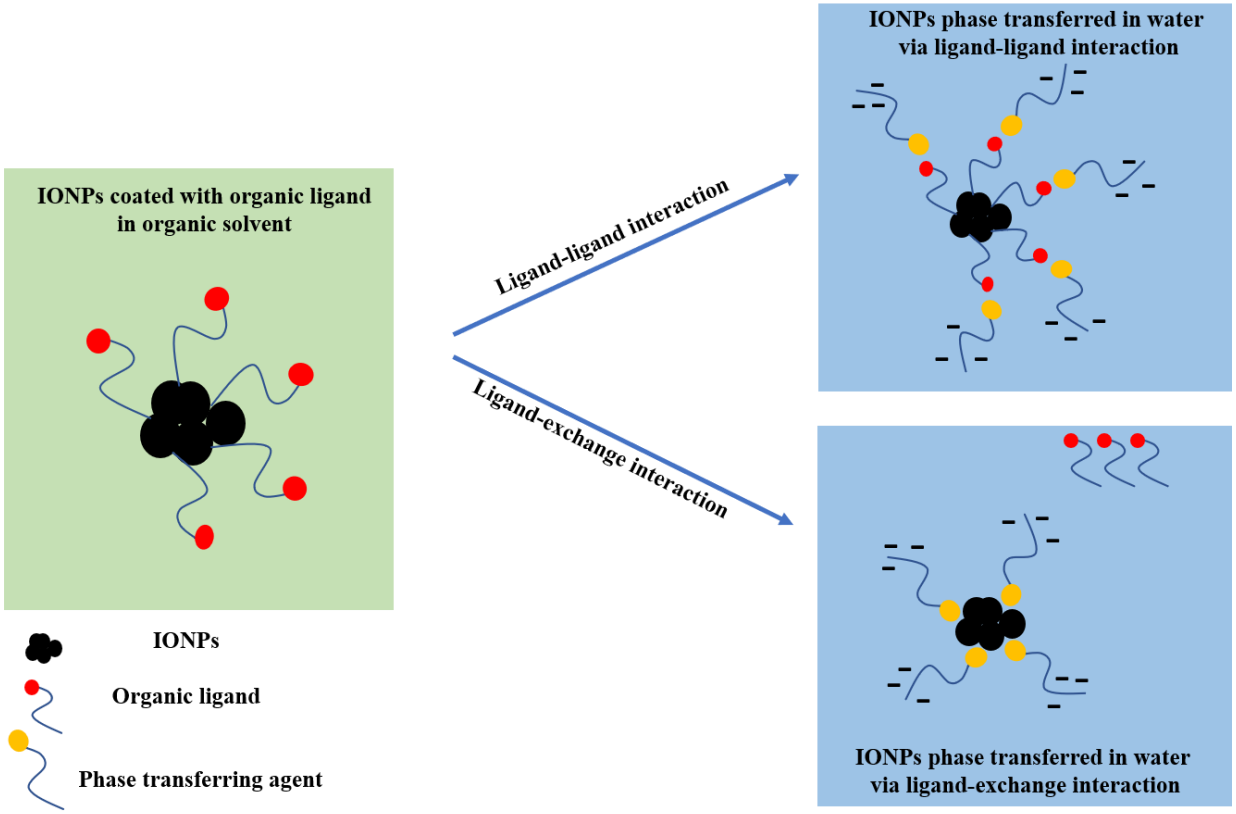

Figure 1.7 – Schematic showing the general phase transfer processes.

Phase transfer of IONPs using PTA in aqueous media, is commonly achieved by the process of electrostatic stabilization (37). The PTAs used in these processes are usually ionic compounds which chemically binds to the surface of IONPs and stabilizes them in water via electrostatic repulsion (37). This prevents agglomeration of IONPs and helps to keep the system stably

dispersed. Phase transferring of IONPs is important for increasing bio-circulation times of IONPs inside the human system, reducing toxicity levels and retaining superparamagnetic properties (38, 39). Ionic PTAs can be broadly classified into two types – 1) cationic and 2) anionic. Cationic PTAs Coulombically stabilizes the IONPs by giving positive surface charge whereas anionic PTAs stabilizes by negative surface charges (37). Previous studies have shown that cationic PTAs have shown more cytotoxicity as compared to their anionic counterparts (40-42). Biological cells have a potential difference across the interior and exterior parts of their cell membranes with a double lipid bilayer in between. The exterior of the membrane is positive, and the interior is negatively charged (43). Cationic surfactants show more active cellular uptake, reducing cell barrier potentials and increasing cytotoxic effects as compared to anionic counterparts (42). Thus, in this study, anionic PTA-sodium citrate will be used for phase transfer of IONPs. Phase transfer of IONPs via sodium citrate is discussed next.

1.7.2. Sodium Citrate as Phase Transferring Agent

The structure of sodium citrate consists of two symmetric carbonyl groups (C=O) and one asymmetric carbonyl group as shown in Figure 1.8. During functionalization of IONPs, the symmetric and the asymmetric C=O groups chemically interacts with the surface of IONPs thus dispersing the system in water (37). Successful functionalization of IONPs using sodium citrate is attributed to negative zeta potential values. The Na^+ counterions of sodium citrate is charge compensated by populations of negatively charged OH^- ions forming an electrostatic double layer. Thus, negative zeta potential values are observed for IONPs functionalized by sodium citrate (37). A general schematic of the phase transfer process is shown in Figure 1.9.

The phase transferred IONPs needs to be coated with a stimuli-responsive polymer for being utilized as efficient payload carriers for drug delivery. The following section will cover stimuli responsive hydrogel (3-D polymeric networks), different properties and synthesis techniques.

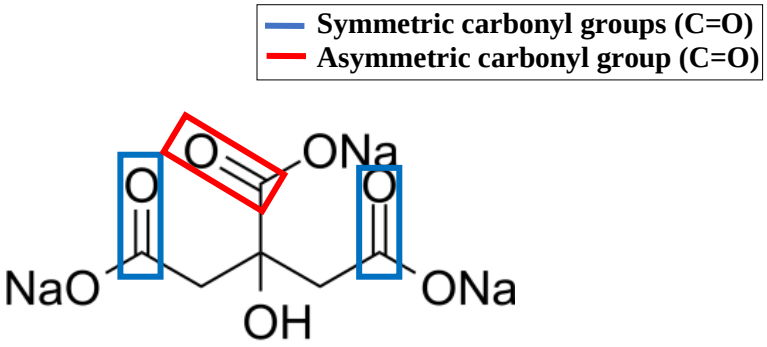

Figure 1.8 – Structure of sodium citrate (36).

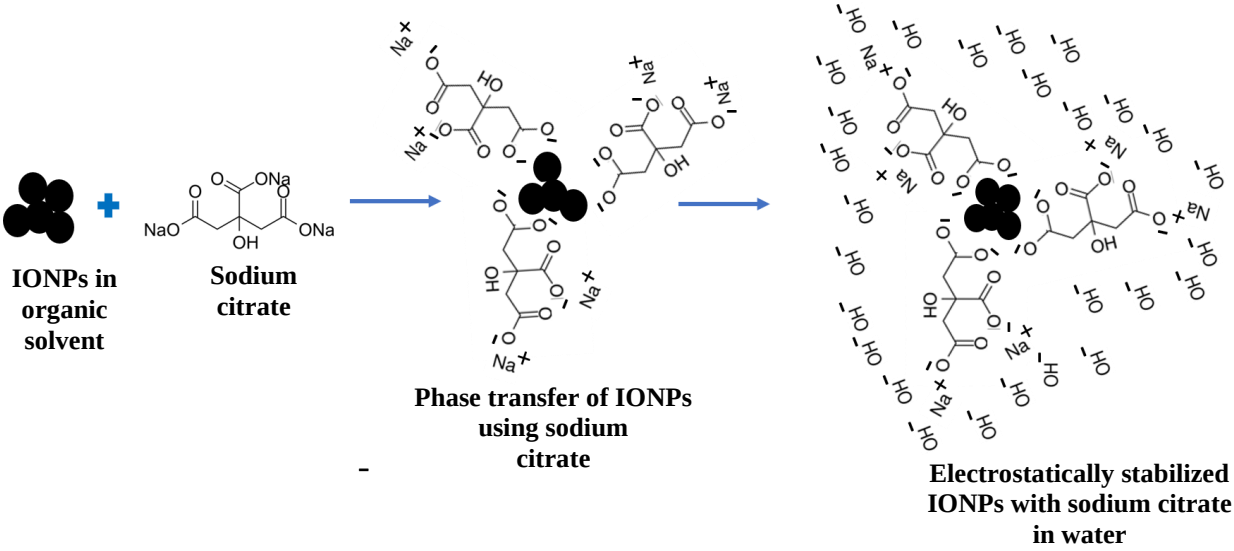

Figure 1.9 – Schematic showing the phase transfer of IONPs using sodium citrate in water.

1.8. Hydrogel

Hydrogels are 3-D polymeric networks dispersed in aqueous media (44). In simple terms, hydro means water and gel means a 3-D polymeric network. The most important property of hydrogel is large water holding capacities facilitated by the hydrophilic functional groups. Hydrogels can hold significant amounts of water, but the whole structure does not dissolve in water. This resistance to dissolution of the structure is mainly attributed to strong crosslinks between monomers forming the three-dimensional polymeric network (44). It is due to this water-retention capacity of hydrogel which makes its structure quite flexible and susceptible to different degrees of swelling and collapses based on various chemical and biological stimuli (shown in Figure 1.10) (45). Hydrogels

are defined as two or multi-component systems consisting of interlinked 3-D clusters of macromolecules with water phase in between (46). These structures are biocompatible and have flexibilities close to natural tissues. Thus, hydrogels have widely become popular over the past 50 years due to their applications in field of biomedicine (47, 48).

Hydrogels can be synthesized in various ways. The most general idea of hydrogel synthesis involves one step procedures like polymerization of single or multi-functional monomers or multi-step procedures involving synthesis of polymers and subsequently cross-linking them with a preferred cross-linking agent (45). Based on different types of synthesis procedures, the properties of hydrogels like cross-linking density, swelling capacity, biodegradability and mechanical strength can be tailored (45). The hydrogel used in this study is poly (N-isopropylacrylamide-acrylic acid) (pNIPAm-aac) and its properties will be discussed in next subsections.

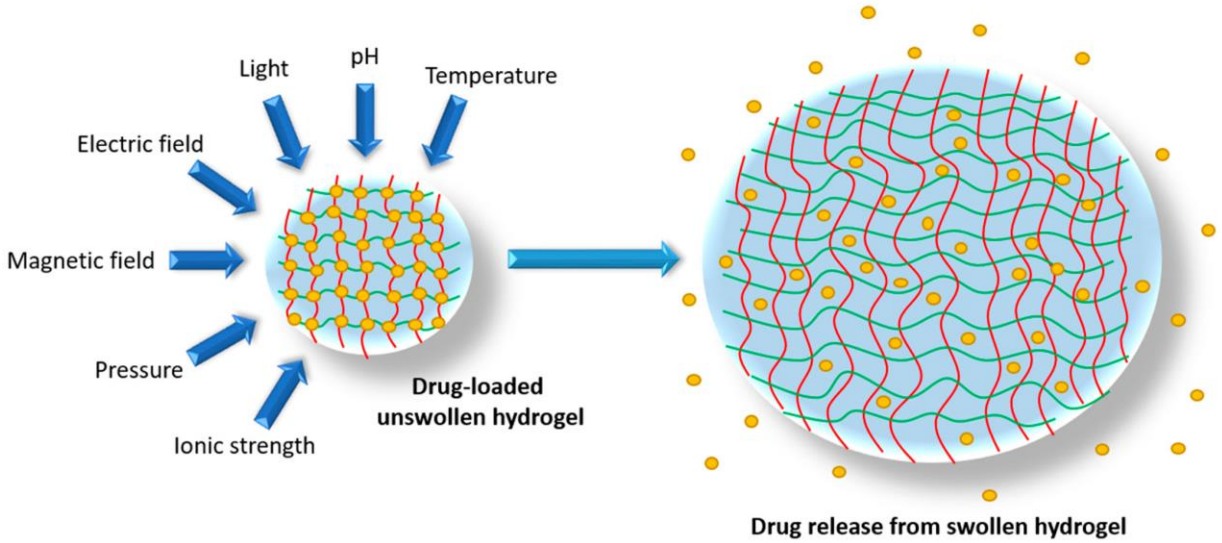

Figure 1.10 – Schematic of hydrogel showing drug release due to structural collapse as functions of multiple stimuli (45).

1.8.1. Poly (N-isopropylacrylamide-acrylic acid)

Poly (N-isopropylacrylamide-acrylic acid) (pNIPAm-aac) is a stimuli-responsive polymer first synthesized during the 1950s (46). One of the common ways to synthesis pNIPAm-aac is via the concept of radical polymerization, using monomers N-isopropylacrylamide (NIPAM), acrylic acid and N, N'methylene-bis-acrylamide (BIS). N-isopropylacrylamide (NIPAM) gives thermo-responsive properties to the final hydrogel structure, acrylic acid is used to give pH responsive

properties and BIS helps to form 3-D crosslinking polymeric networks.

1.8.1.1. Thermal Properties

pNIPAm is one of the most used and studied thermo-responsive hydrogels for biomedical applications due to its high biocompatibility. The solubility of pNIPAm varies inversely with temperature as compared to general salts (49). Thus, solubility of pNIPAm in water decreases with increase in temperature which starts changing the morphology of pNIPAm from globule to coiled state above a certain critical temperature (~ 32 °C) defined as volume phase transition temperature (VPTT) of the polymeric system (shown in Figure 1.11) (50). VPTT shows the change in volumetric dimensions of the hydrogel as function of temperature (51).

At temperatures lower than VPTT, pNIPAm-aac is dispersed in water in a globule state due to the formation of hydrogen bonds between the amide groups of the hydrogel and the water molecules. At temperatures above VPTT, due to outflow of bound water molecules from the polymeric network, the hydrogen bonds between the polymer and the water molecules break (51). This increases the net-entropy, lowering the total Gibb`s energy of the system (51). Thus, the process becomes entropically favorable at temperatures higher than VPTT (51). The VPTT of a system can be fine-tuned by changing the hydrophilic-lipophilic balance (HLB) of the polymeric network (51).

The VPTT of hydrogels is the most important factor for engineering hydrogel-based drug delivery systems. By general rule, increase in hydrophobic groups of the polymeric networks decreases the solubility of the polymeric networks in water, thus lowering its VPTT, whereas increasing hydrophilic groups (e.g., more ionic functional groups) increases the solubility, thus increasing its VPTT (51).

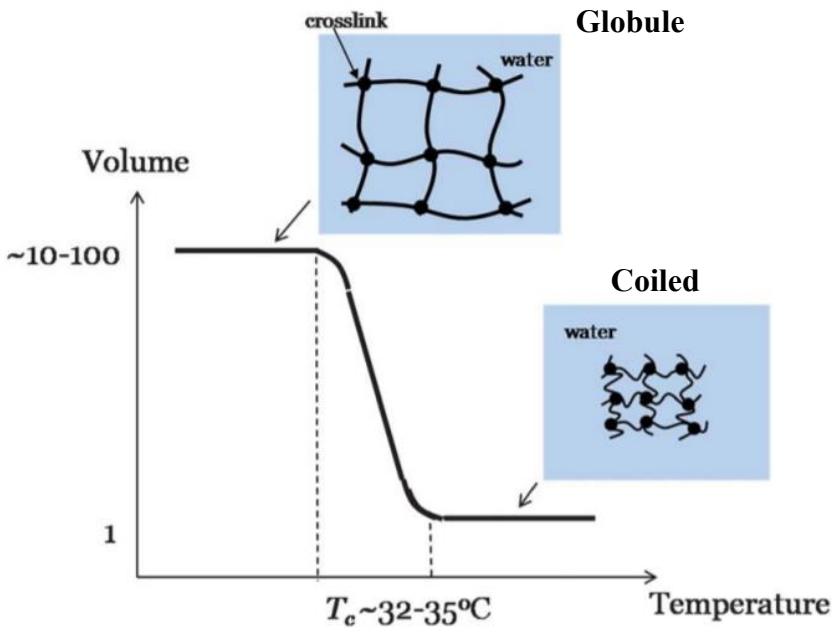

Figure 1.11 - Volume response of hydrogel as function of temperature (50).

1.8.1.2. pH Sensitive Properties

Hydrogel systems incorporated with specific acidic or basic groups can be made pH sensitive. Based on the pH-dependent ionization of the acidic and basic groups, collapse and swelling properties of the system can be controlled. Acidic groups dissociate at relatively higher pH as compared to basic groups and due to the electrostatic repulsion caused due to the ionization of these groups, a swelling effect of the system is seen whereas the same effect can be seen for basic groups at relatively lower pH. In some studies, it has been seen that pH responsive swelling/collapse caused due to basic groups is much less pronounced as compared acidic groups (52).

In this study, acidic group (acrylic acid) has been implemented in the pNIPAm system. The dissociation (pKa) value for acrylic acid is 4.2. At pH values above 4.2, deprotonation of the acid occurs causing a swelling effect whereas pH values below 4.2, acrylic acid does not dissociate, and a relative collapse of the system is observed (51). Hence, engineering pH sensitivity to hydrogel system can have good potential in the field of oncology. Previous studies have shown that the pH value of the surrounding environment in cancer tissues is mildly acidic (~ 6.4) as

compared to healthy tissues (7.2-7.5). Thus, environment-based pH responsivity can be utilized for producing advanced drug delivery systems (53).

1.8.1.3. Synthesis Routes

The most common polymerization concept used is radical polymerization (FRP) (54). FRP is a method in which polymerization proceeds with the formation of free radicals. The final polymeric product is formed by successive addition of free-radical building blocks. Generation of free radicals can be formed by initiator molecules or by application of external stimulus like ionizing radiation, electric discharge, or sonication (51). The free radical after being initiated continuously adds monomeric units, thereby growing the polymeric chain.

Some of the common synthesis techniques under free radical polymerization includes – 1) bulk polymerization 2) suspension polymerization 3) emulsion polymerization 4) dispersion polymerization and 5) precipitation polymerization (51). In this study, precipitation polymerization will be used in synthesis of pNIPAm-aac systems and is discussed in detail next.

1.8.1.3.1 Precipitation Polymerization

In precipitation polymerization, the main components involve a monomer, an initiator and a solvent which forms the continuous initial phase of the system. The initiator and the monomer remain soluble in the continuous phase. As the reaction is initiated via formation of free radical, the polymeric chain grows in length. Upon reaching a certain length, the polymeric chain collapses upon itself and precipitates from the continuous phase. The precipitated polymeric chain grows further by aggregation. On reaching a critical size, the polymeric particles are stabilized by imparted charge from the initiator. The final product formed is insoluble in the continuous phase. Thus, precipitation polymerization gives good control over particle sizes. Additionally, ionic surfactants are also commonly used for higher degree of electrostatic stabilization for synthesizing monodisperse systems of polymeric nanoparticles (51). A schematic showing the different phases of precipitation polymerization is shown in Figure 1.12. Synthesis of crosslinked functional polymers with uniform size, high water compatibility using precipitation polymerization was seen from previous study of Zhang et al (55).

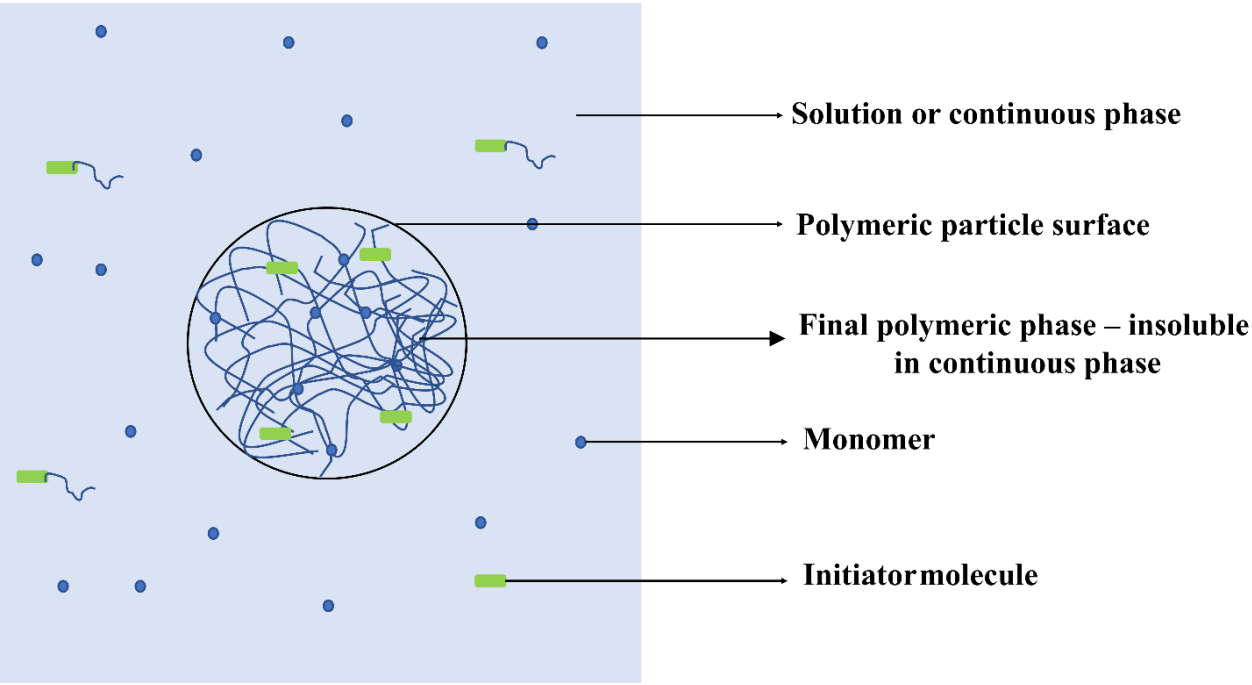

Figure 1.12 – Schematic showing the different phases of precipitation polymerization.(51)

Hydrogel discussed in this section, could be potentially utilized with different nanoparticle systems in order to synthesize hybrid nanoparticles which is discussed next. Henceforth, hybrid nanoparticles can show multi-functional properties like heat, pH, electrical and light responsivity which could have immense importance in biomedicine.

Hybrid Nanoparticles: Nanoparticles Polymeric Composites

Hybrid nanoparticle is a generic term used to describe a nanostructure composed of at least two distinguishable components. The structure can consist of two different organic nanoparticles, inorganic nanoparticles, or a combination of both organic and inorganic nanoparticles (56). This helps to overcome the limitations of single-component systems thus giving higher degrees of functionality to the nanostructure. E.g., hybrid inorganic nanostructures consisting of iron oxide nanoparticles coated with thermo-responsive polymers shows two different functionalities – heat sensing and superparamagnetism (57). Thus, different functionalities can be used in combination for many applications in advanced nano-drug delivery systems.

Some common hybrid nanostructures include – core-shell, yolk-shell, heterodimer, Janus, and dots on nanotube/nanorod (56). A schematic showing the different hybrid nano-architectures is shown

in Figure 1.13.

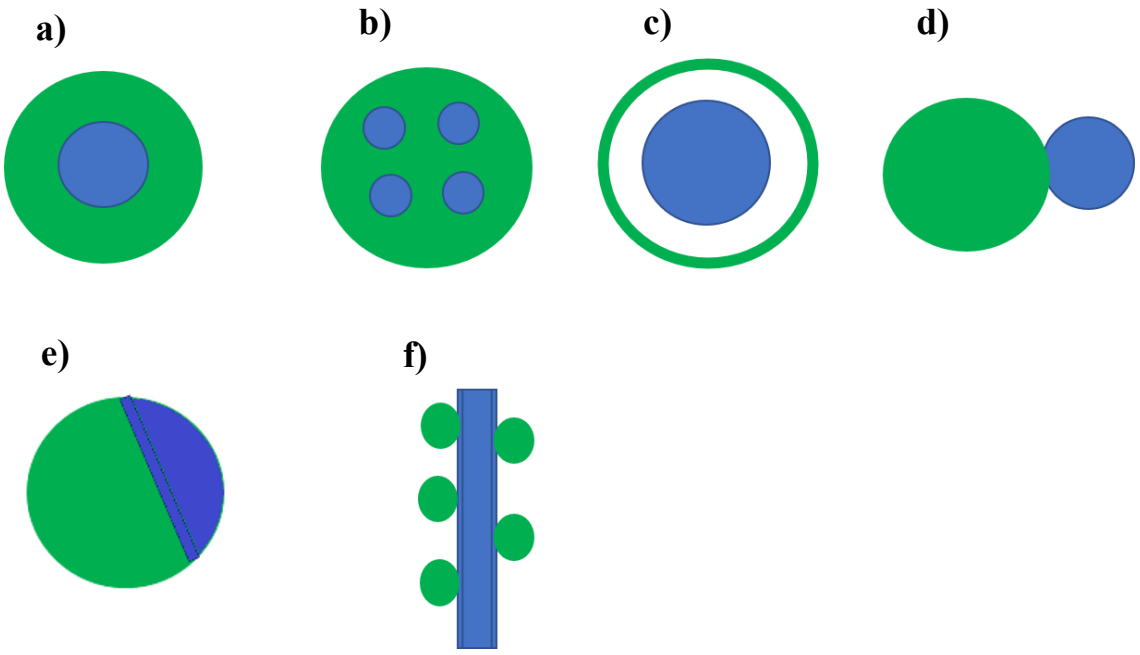

Figure 1.13 – Schematic showing different hybrid nano-architectures – a) single-core/single shell b) multiple core/single shell c) yolk-shell d) heterodimer e) Janus and f) dots on nanotube/nanorod (56).

In this work, focus will be given to synthesize hybrid NGs consisting of superparamagnetic IONPs and a thermo and pH-responsive polymer poly-N-isopropyl-acrylamide-acrylic acid (pNIPAm-aac). Hence, the thermal, pH and magnetic properties of the hybrid nanostructure will be utilized to synthesize multi-functional drug-delivery systems (DDS). Therefore, in the following section, the general pharmacokinetic properties and the common mathematical models required for understanding drug delivery mechanisms are discussed.

1.9. General Pharmacokinetic Requirements of Drug Delivery Systems

Drug delivery systems (DDSs) are pharmaceutical constructions which can achieve target-specific and controlled release of therapeutic agents in the human system. After incorporation of the DDS in the human system, the bioactive agents are released and transported across various biological barriers to reach the site of action. Considerable research has been conducted to understand the

effects of biological barriers in transport of biological ingredients (58). Despite, significant advancements, many drugs have undesirable toxic effects. Hence, future attempts should be made to generate better patient compliance effect by optimizing the number and frequency of doses required to maintain efficient therapeutic response. Therefore, it is necessary to develop DDS and understand them prior to use in the human system. DDSs control the drug release rate and drug absorption and ultimately the therapeutic effects of the drug. Theoretically, ideal DDSs ensure that the active drug is available at the site of action according to the need of patient for an intended duration. The drug concentration at the specific site should remain within the therapeutic window, that is, between minimal effective concentration (MEC) and minimal toxic concentration (MTC) (59). This concept is shown in Figure 1.14. In the following subsection, common mathematical models used to engineer DDS is discussed briefly.

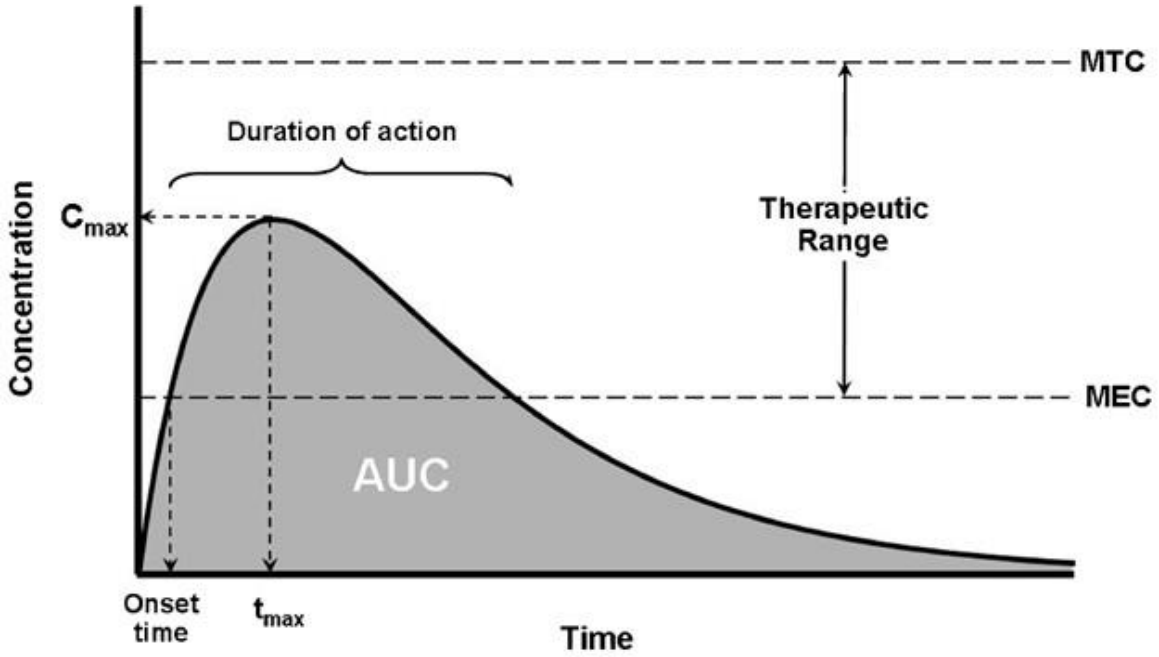

Figure 1.14 – Pharmacokinetic parameters showing released drug concentration as function of temperature. C_{max} – Maximum concentration of drug released, t_{max} – time to reach C_{max}, AUC – are under the curve, MTC – Maximum tolerated concentration, MEC – Minimum effective concentration (59).

1.9.1. Common Mathematical Models

Engineering and controlling release from drug-delivery systems is an essential prerequisite for efficient DDS. Therefore, quantitatively modelling of release dosages enable pharmacists and

engineers to work together with the aim of designing controlled drug delivery systems. It is possible to use mathematical tools that describe the dependence of release as function of time. Hence it is very useful to predict the release kinetics before implementing in real-time human biological systems. Analytical solutions have been used to design several simple and complex drug delivery systems. They allow the measurement of important physical parameters like drug diffusion coefficient, amount and type of active agents, polymer, and adjuvants as well as the size and shape of the system required to achieve desired drug release profiles (60).

Some common mathematical models which will be used in this study to fit drug release profiles are - zero-order model, first-order model, Higuchi model and Korsmeyer-Peppas model also known as power law model) (60). Details of each individual models are briefly discussed next.

1.9.1.1. Zero-Order Model

Zero order models are usually used to fit drug release profiles which varies linearly over time. Therapeutic systems exhibiting zero-order kinetics often show concentration-independent releases. A typical mathematical formulation for a zero-order model is shown in Equation 9 (60).

$$C_t = C_o + k_0 t \quad (9)$$

where C_t - amount of active agent released as a function of time, C_o - initial concentration of the active agent released and k_0 - zero-order constant.

A typical problem with zero-order kinetic system is rapid release of bioactive agents over short periods leading to alternating conditions of overexposure and underexposure. Therefore, frequent dosages are necessary to maintain effective concentration within the therapeutic range but compliance and control over the bioactive agent becomes difficult. Hence, systems can be made to control the release rate of the bioactive agent thus maintaining exposure conditions within the therapeutic range for prolonged period of time. This concept can be realized with active DDS structures by using a variety of materials ranging from mineral oil to complex formulations such as aqueous/alcoholic gels which can form a drug reservoir, thus maintaining adequate concentration of the bioactive agent inside the DDS matrix (60).

1.9.1.2. First-Order Model

First order models are generally used to describe concentration-dependent release profiles over time. In simple terms, for first-order release kinetics, the amount of active biomaterial released from the system at a specific instance is proportional to the amount remaining inside the matrix at that point (60). Hence, release profiles with first-order kinetics show non-linearity and gradually decreases as function of time. A typical mathematical formulation for a first-order model is shown in Equation 10 (60).

$$\log Q_1 = \log Q_o + (k_1 * t)/2.303 \quad (10)$$

where Q_1 - amount of active agent released at time t, Q_o - initial concentration of active agent in the drug matrix, k_1 - first order constant.

1.9.1.3. Higuchi Model

Higuchi model is used for systems containing high active material concentration (typically higher than the solubility concentration) in the matrix, matrix with porosity. It also fits very well when the concentration of the active material inside the matrix of the system is low and the release happens mainly through the pores of the matrix (60). In general, the simplified form of the Higuchi model linearly relates the fraction of drug released at specific time points as a function of square root of time. The mathematical formulation for Higuchi model is shown in Equation 11 (60).

$$f_1 = k_H \sqrt{t} \quad (11)$$

where f_1 - fraction of the drug released from the system at specific time points, k_H - release constant of Higuchi.

Some of the major drawbacks of the Higuchi model are – 1) it does not fit well with swelling, collapsing, and eroding polymeric structures and 2) the diffusivity of the active material should be constant ensuring maintenance of perfect sink conditions (60).

1.9.1.4. Korsmeyer-Peppas Model

Korsmeyer-Peppas model or power law is one of the most comprehensive models to describe drug release from polymeric systems (60). This model establishes an exponential relation between release and time. The mathematical formulation is shown in Equation 12. This model was specifically developed to understand drug release from 3D-polymeric networks like hydrogels (60). The power law is useful when the release mechanism of the system is not known, and more than one type of transport phenomenon is occurring (60). In simple terms, the power law is a generalization of all the individual models (discussed above) trying to combine independent effects of drug diffusion, relaxation, and transport (60).

$$M_i/M_\infty = Kt^n + b \quad (12)$$

where M_i - amount of drug released over time, M_∞ - amount of drug present at equilibrium, n - exponent of release (describes the release phenomenon), b - burst release.

The value of n in the power law model gives information about the release mechanism or combination of mechanisms involved in the system. The possible range of values for the power law model and their associated release mechanisms are shown in Table 1.2 (60). Fitting with mathematical models are important for producing efficient DDS as discussed in this section. Another important aspect which needs to be considered is suitability of bioactive agent/drug with the DDS interface. Therefore, proper drug selection is necessary for producing increased efficacy of DDS. In the next section, common drugs used with DDS are discussed.

Table 1.2 - Showing different release mechanisms based on different values of release exponent (n) in power law model (60).

Release mechanism model	Release exponent (n)
Fickian diffusion	0.43 - 0.5
Anomalous transport	0.50<n>1,0
Case I transport	0.85 - 1.0
Super Case II transport	0.85 - 1

1.10. Common Drugs for Drug Delivery Systems

Previously, studies have been performed where drugs with varying degrees of toxicity have been tested with different DDS. For real-time applications, selection of proper drug, specific to DDS properties is important and can be quite complicated. Appropriate drug selection can depend on several factors like DDS solvent environment, interaction between drug and DDS, toxicity, and therapeutic efficiencies and even mode of delivery in patients. Some available chemotherapeutic drugs include doxorubicin, epirubicin and valrubicin.

In this work a non-toxic, hydrophilic model protein – cytochrome C (cyt C) was chosen. The pNIPAm-aac (hydrogels) are highly soluble in water (discussed in Section 1.8) combined with the hydrophilicity of cyt C makes the loading process efficient. The non-toxicity of the drug also makes it suitable to work with it under laboratory conditions. The occurrence, and common applications of cyt C is briefly discussed below.

Cytochrome C

The cytochrome C complex (cyt C) is a small hemeprotein found loosely associated with the inner membrane of mitochondria in plants, animals and other unicellular organisms. Its main function is cell apoptosis. Cyt C is water-soluble, unlike other cytochromes (61). It is capable of undergoing oxidation and reduction as its iron atom converts between the ferrous and ferric forms due to presence of a free single electron in its chain (61). It has also been shown to have therapeutic

capabilities commonly being used as an anti-obesity drug for diet induced obesity (61).

In the next chapter, synthesis procedures for different samples used in this study and corresponding characterization techniques are discussed.

Chapter 2: MATERIALS AND METHODS

This chapter consists of three sections in which chemicals used for synthesis of different samples, synthesis methods of different samples and its corresponding characterization techniques are shown, respectively.

2.1. Materials

Iron chloride hexahydrate ($FeCl_3.6H_2O$), oleic acid (99 %), 1-octadecene (99 %), oleylamine (99 %), iron pentacarbonyl, ferrous chloride tetrahydrate and ferric chloride anhydrous, aqueous ammonia solution (25 wt % NH_3 in water), N-isopropylacrylamide (NIPAM), acrylic acid (d = 1.051 mg/mL), sodium dodecylsulphate (SDS), potassium persulphate (KPS), N-N`-methylenebis (acrylamide) (BIS), trisodium citrate dihydrate, acetone (99 %), hexane (99 %), toluene (99 %), isopropanol (99 %), cytochrome C (cyt C) were purchased from Sigma-Aldrich®. Iron oleate precursor was synthesized by using iron chloride hexahydrate ($FeCl_3.6H_2O$) and oleic acid. NIPAM was recrystallized to remove impurities and all other chemicals were used as received. Milli-Q (MQ) water (18.2 MΩ/cm at 25 ºC, filtered with pore size 0.22 µM) was used from MilliQ® Reference Water Purification System installed in the Ugelstad Laboratory.

2.2. Methods

In this section, different synthesis procedures used are shown. Methods involving synthesis of iron oleate precursor, derivation of IONPs from precursors, phase transfer of IONPs, synthesis of thermal and pH responsive hydrogel - Poly (N-isopropylacrylamide-acrylic acid) (pNIPAm-aac) and hybrid systems containing pNIPAm-aac and IONPs will be presented in the following subsections.

2.2.1. Synthesis of Iron Oleate

The iron-oleate complex was prepared using a previously reported protocol (62). $FeCl_3{\cdot}6H_2O$ (5.4 g) and sodium oleate (18.25 g) were dissolved in a mixture of solvents consisting of ethanol (40 mL), MQ water (30 mL) and hexane (70 mL), in a round bottom flask (250 mL). The final solution was refluxed at 70 °C for 4 hours under vigorous stirring at 1100 rpm. Two separate phases were formed as shown in Figure 2.1. A dark red phase containing iron oleate complex with organics and

a colourless aqueous phase. The product was transferred to a separator funnel and washed three times with MQ water.

The dark red phase containing iron oleate was collected in a round bottom flask (500 mL) and mounted in a Büchi R-210 Rotavapor System for further drying of the remaining organics. The rotavapor system contained Büchi V-491 heating bath and V-700 vacuum pump. The temperature of the heating bath was kept constant at 80 ºC and the pressure and rotation were slowly varied over a range from (250-75 mbar) and (400-100 rpm). The entire drying process lasted for 1 hour. Finally, a darkish brown viscous paste of iron oleate was obtained (shown in Figure 2.1) which was further utilized in synthesis of iron oxide nanoparticles (IONPs).

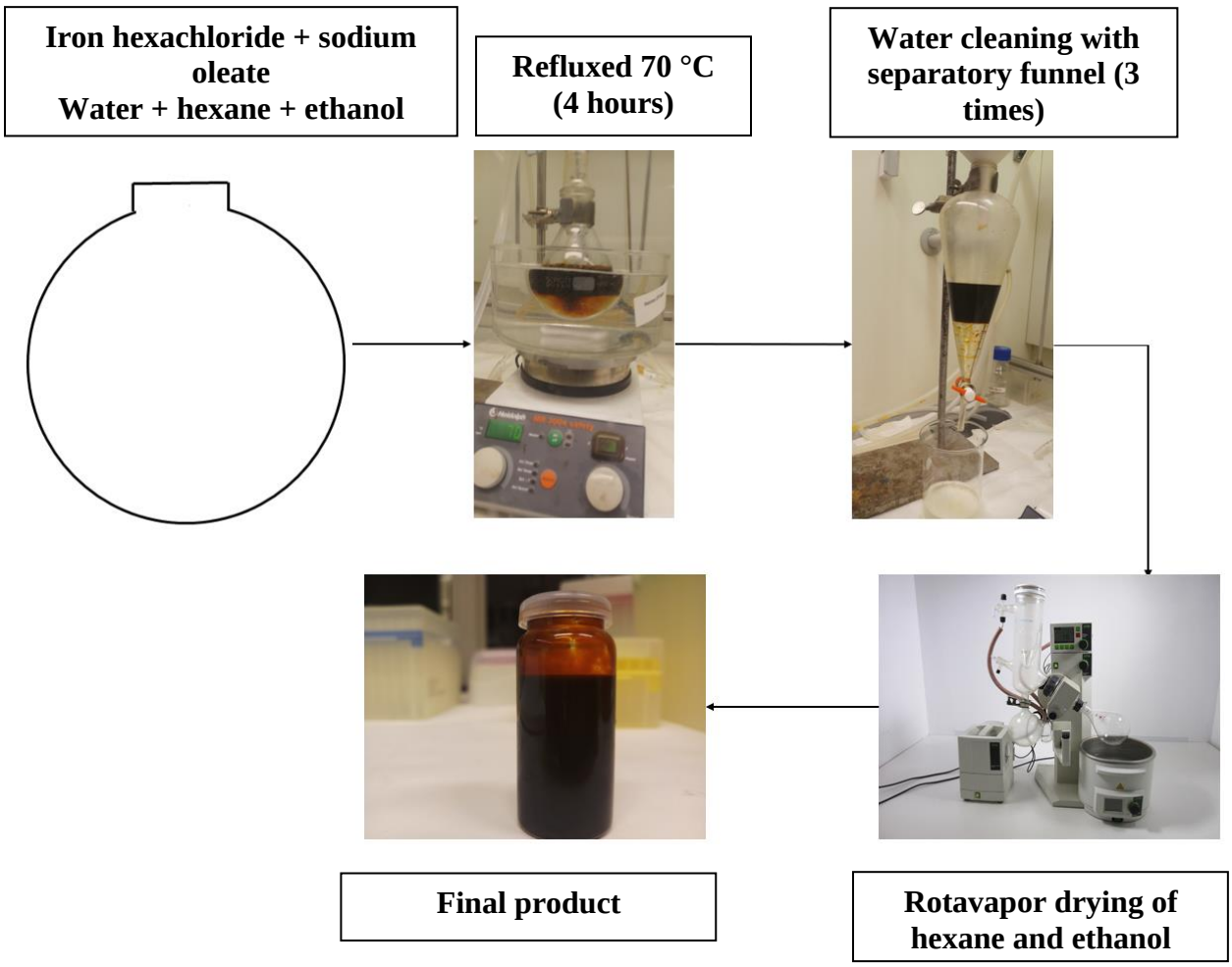

Figure 2.1 – Schematic showing synthesis of iron oleate.

2.2.2. Synthesis of IONPs using Iron Oleate

The synthesis protocol have been adapted from the previous works of Sharma et al. (63). In this method, iron oleate (1.65 g) was measured into a 3-necked round bottom flask (100 mL). Oleic acid (600 µL) and the solvent 1-octadecene were added to the flask. The top opening of the flask was connected to a conventional condenser whch was further connected to a standard schlenk line. The reaction was carried out in argon atmosphere. One opening of the 3-necked round bottom flask was blocked with a stop-cock and in the last opening a temperature sensor was placed to measure the change in temperature of the reaction mixture. The temperature sensor was connected to a microcontroller for examining and controlling the temperature profile during the reaction. A magnetic stirrer was used at 450 rpm for homogeneous temperature distribution in the system. The reactants were heated at a rate of 3 ºC/min up to 320 ºC. Then the temperature was kept constant at 320 ºC for 45 mins and finally cooled for 20 mins. The round-bottom flask was removed from the setup and the formed particles were moved for cleaning. For cleaning the particles, hexane (25 mL), isopropanol (50 mL) and acetone (25 mL) were added in the same solution and the particles were precipitated using a round neodymium-based magnet. The main function of isopropanol was to transfer the particles from 1-octadecene to hexane and acetone was used to precipitate out the particles from hexane. Further three times cleaning were performed using acetone and the final particles were dispersed in toluene (20 mL) by ultrasonication for 1 min. A schematic of the reaction procedure is shown in Figure 2.2. The IONPs obtained using this method will be termed as IONPs_oleate for the entire study.

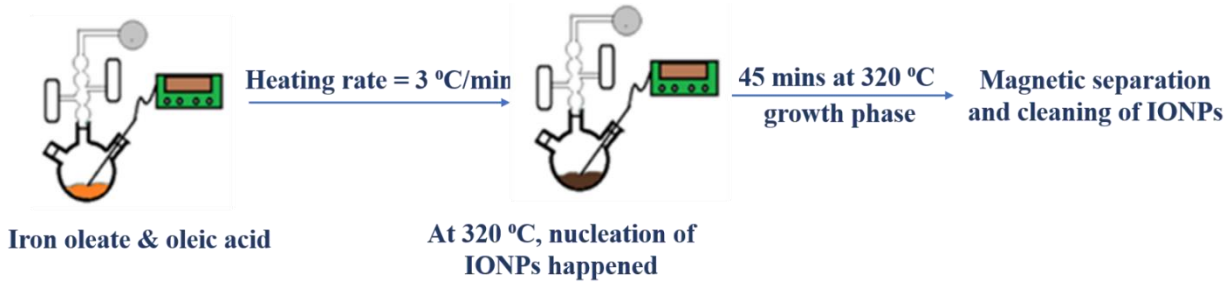

Figure 2.2 - Schematic showing synthesis of IONPs using iron oleate as precursor (IONPs_oleate).

2.2.3. Synthesis of IONPs using Iron Pentacarbonyl

The synthesis is based on the work by Singh et al. with some modifications (29). Oleylamine (740 uL) was heated in 1-octadecene (25 mL) in a three necked round bottom flask up to 120 ºC for 30 mins. Then the heating was further continued at a heating rate of 10ºC/min up to 180 ºC. The iron pentacarbonyl precursor was quickly injected at this point using a syringe (5 mL) and the reaction was continued at 180 ºC for further 20 mins. Then the reaction was naturally cooled to room temperature. Cleaning of the particles was performed in the exact same manner as in the case of IONPs derived from iron oleate (discussed in Subsection 2.2.2). The final particles were dispersed in hexane (20 mL) by ultrasonication for 1 min. A reaction schematic is shown in Figure 2.3. The IONPs derived using this method will be termed as IONPs_penta for the entire study.

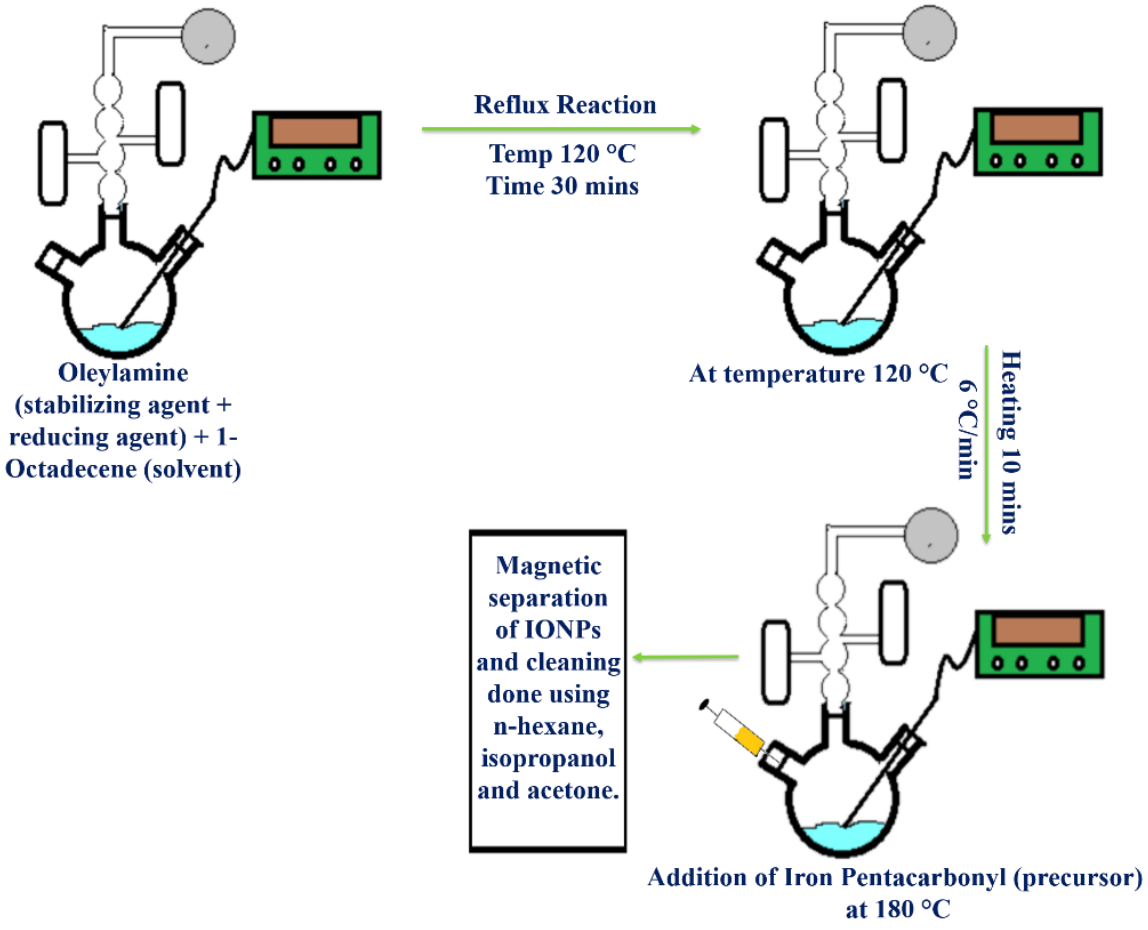

Figure 2.3 - Schematic showing synthesis of IONPs using iron pentacarbonyl as precursor (IONPs_penta).

2.2.4. Concentration test of IONPs

The concentration test for the obtained IONPs (discussed in Subsections 2.2.2 and 2.2.3) was performed to calculate particle yield (mg/ml), For the concentration test, 3 empty Eppendorf tubes were first weighed. A known volume (300 uL) of both the IONPs systems was taken out from their respective organic media (toluene in case of IONPs_oleate and hexane in case of IONPs_penta particles) and poured in the empty Eppendorf tubes. The tubes were dried at 70 ºC for 6 hours to evaporate the solvent. Lastly, the dried tubes were weighed and the concentration of IONPs was obtained by using Equation 13. The average value of concentration (mg/ml) obtained over three batches were taken and used further.

Concentration (mg/ml) = (Weight of tubes after drying – Weight of empty tubes) *3.3 (13)

2.2.5. Phase Transfer of IONPs

The as-synthesized IONPs were chemically engineered with sodium citrate for phase transfer from organic solvent to water for further study. The phase transferring process was taken and modified from previous works of Bandyopadhyay et al. (1). In the first step, IONPs (5 mg) were precipitated from their respective organic solvents. IONPs_oleate which was dispersed in toluene, methanol was used to precipitate the particles. In case of IONPs_penta, acetone and isopropanol were used in a ratio of 3:1 to precipitate from hexane.

The precipitated IONPs (5 mg) were cleaned three times with sodium citrate solution (10 mM) while being kept on the neodymium-based magnet. Finally, the cleaned IONPs were mixed with 10 mL sodium citrate solution and kept for ultrasonication for 2 hours at 65 °C.

The sodium citrate functionalized IONPs obtained were further cleaned three times with MQ water on a magnet and finally the phase transferred particles were re-dispersed in 5 mL MQ water for further use. A flowchart showing the phase transfer of IONPs with sodium citrate to transfer them from organic solvent to water is shown in Figure 2.4. The phase transferred IONPs (if the IONPs are derived from iron oleate) will be simply referred to as phase transferred IONPs_oleate particles and similarly for the phase transferred IONPs (if the IONPs are derived from iron pentacarbonyl) will be simply referred to as phase transferred IONPs_penta particles.

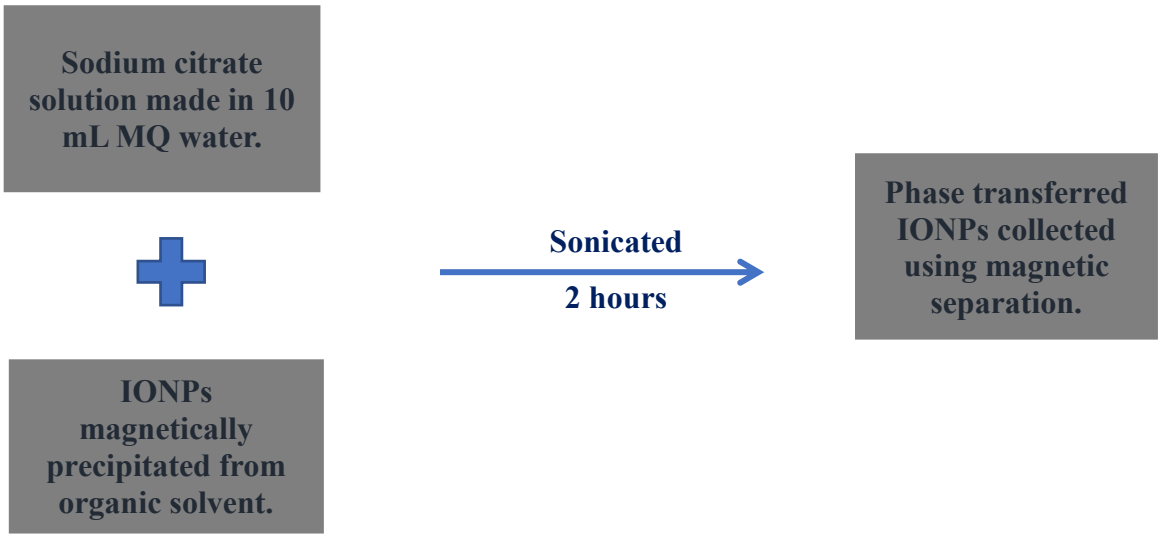

Figure 2.4 – Schematic showing the flowchart of phase transfer of IONPs with sodium citrate from organic to aqueous media.

2.2.6. Concentration Test of Phase Transferred IONPs

A similar technique was followed for the concentration test of phase transferred IONPs (as discussed in Subsection 2.2.4). For the concentration test, 3 empty Eppendorf tubes were first weighed. A known volume (1000 uL) of both the phase transferred IONPs systems was taken out from water and poured in the empty Eppendorf tubes. The tubes were dried at 70 ºC for 6 hours to evaporate the solvent. Lastly, the dried tubes were weighed, and the concentration of particles were obtained using Equation 13. The average value of concentration (mg/ml) obtained over three batches were taken and used further.

2.2.7. Recrystallization of N-isopropyl acrylamide

N-isopropyl acrylamide (NIPAM) was recrystallized for removal of impurities which could inhibit the radical polymerization reaction. The protocol was modified from the one reported by Bandyopadhyay et al. (1). In the recrystallization process, the NIPAM monomer (5 g) was dissolved in n-hexane (50 mL) at 110 °C in a glass flask equipped with a water condenser, and the reaction was made to run for 2 hours. Thereafter, the flask was directly put into an ice bath for 30 mins for rapid recrystallization. The solution was then filtered by using φ-70 mm filter paper

circles yielding the pure monomer. After drying, the purified NIPAM was stored at −21 °C to prevent absorption of moisture. An image of the final product is shown in Figure 2.5.

Figure 2.5 – Image of recrystallized NIPAM.

2.2.8. Synthesis of pNIPAm-aac nanogels

pNIPAm-aac nanogels (NGs) were synthesized using free radical polymerization. The experimental procedure was taken from Bandyopadhyay et al. (1). A molar composition of 85 % NIPAM, 10 % acrylic acid and 5% BIS was used. NIPAM (181 mg) and BIS (14.8 mg) were put directly in the round bottom flask under nitrogen atmosphere. In parallel, an SDS solution (4.2 mM) was prepared in MQ water (10 mL). The as-prepared SDS solution was added to the round bottom flask containing the reactants and left to stir under nitrogen flow for 30 mins. The acrylic acid solution (126 μL, 1.46 M) was added 5 mins before addition of the KPS (400 μL, 207.2 mM) which functions as an initiator for the polymerization reaction. MQ water was used as solvent for both acrylic acid and KPS. The reaction was allowed to run for further 2 hours. The formed NGs solution was poured into a prewashed dialysis tube (MWCO14 kDa) and dialyzed overnight to remove unreacted residual reactants. Finally, the dialyzed NGs were freeze dried using a freeze drier. A reaction schematic for the synthesis of NGs is shown in Figure 2.6. The pNIPAm-aac nanogels will be abbreviated as bare NGs/NGs for the entire study.

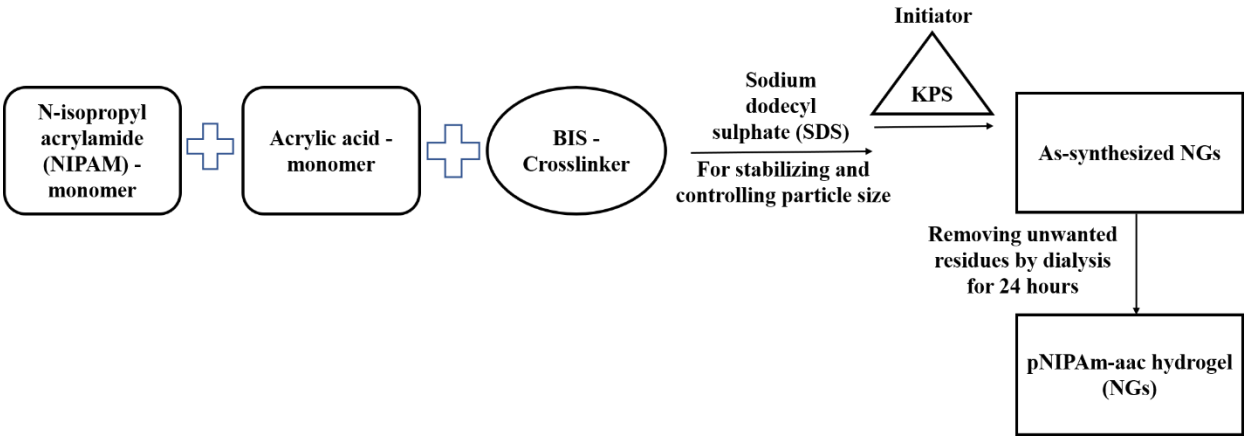

Figure 2.6 – Reaction schematic showing the steps for synthesis of pNIPAm-aac hydrogel (NGs).

2.2.9. Synthesis of Hybrid Systems

NGs systems containing phase transferred IONPs will be referred to as hybrid NGs for the entire study. Three different methodologies – insitu, post and addition were employed for synthesis of hybrid NGs as discussed next.

2.2.9.1. Synthesis of Hybrid Systems using In-situ Technique

An in-situ method was used to synthesize pNIPAm-aac nanogels (NGs) with phase transferred IONPs. The samples will be referred to as NGs_insitu. The phase transferred IONPs were added during the synthesis of NGs. This method is modified from the works of Bandyopadhyay et al. (1). A similar approach was followed (discussed in Subsection 2.2.6) but the only difference was the addition of phase transferred IONPs with SDS. A molar composition of 85 % NIPAM, 10 % acrylic acid and 5 % BIS was used. NIPAM (181 mg) and BIS (14.8 mg) were put directly in the round bottom flask under nitrogen atmosphere. Different amounts of phase transferred IONPs were added with SDS solution (10 ml, 4.2 mM), and the solution was left to stir under nitrogen flow for 30 min. Prior to addition of the initiator KPS solution (400 µL, 103.6 mM), acrylic acid (126 µL, 1.46 M) was added into the solution. MQ water was used as solvent for both KPS and acrylic acid. The reaction was allowed to run for further 2 hours. A flowchart of the in-situ technique is shown in Figure 2.7. The formed NGs_insitu solution was dialyzed and freeze dried. The NGs_insitu particles were magnetically separated and cleaned with MQ water two times to get the magnetic bottom product. The two intermediate cleaning steps with MQ water were performed with further efforts to remove bare NGs (non-magnetic part) from the magnetically collected bottom product.

The magnetic bottom product was then analyzed to understand the interaction of phase transferred IONPs with NGs. A flowchart of the magnetic separation procedure implemented is shown in Figure 2.8. The samples separated in this manner will be referred to as magnetically separated NGs_insitu particles.

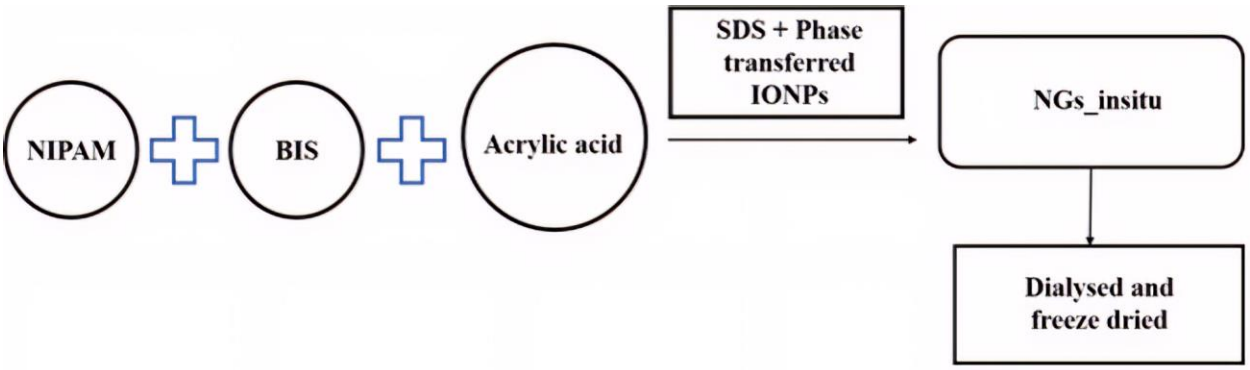

Figure 2.7 – Flowchart showing the steps for synthesis of NGs_insitu systems.

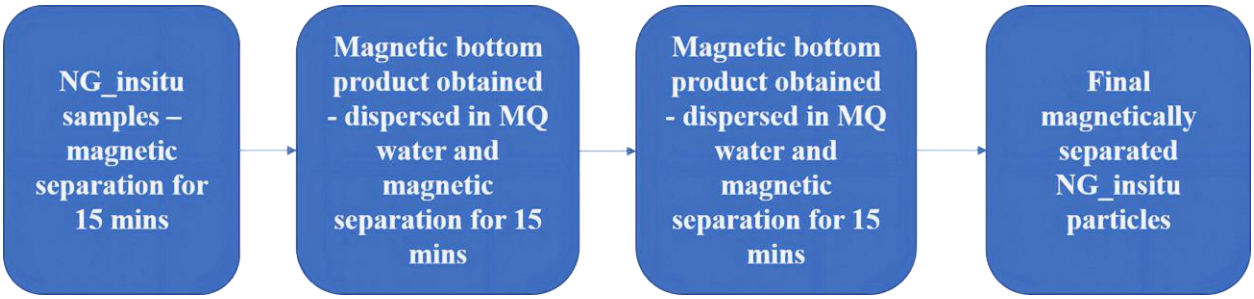

Figure 2.8 – Flowchart showing the magnetic separation and cleaning steps to obtain magnetically separated NGs_insitu systems.

2.2.9.2. Synthesis of Hybrid Systems using Post Technique

A post technique was used to synthesize pNIPAm-aac (NGs) with phase transferred IONPs. The samples prepared using this route will be abbreviated NGs_post for the entire study. The post coating protocol have been adapted and modified from the previous works of Bandyopadhyay et al. (1). In this process, the major difference with insitu technique is the addition of the phase transferred IONPs after synthesis of NGs. The bare NGs were first prepared using the same

protocol (discussed in Subsection 2.2.8). The freeze dried bare NGs obtained were mixed with known amount of phase transferred IONPs (centrifuged out from aqueous media at 14,500 rpm for 10 mins) and stirred for 2 hours at 500 rpm. After 2 hours, the as-obtained NGs_post particles were freeze dried to form powder. A flowchart of the post-coating technique is shown in Figure 2.9. The NGs_post particles were also magnetically separated following a similar protocol as used in case of magnetically separated NGs_insitu particles. The samples in this case will be referred to as magnetically separated NGs_post particles.

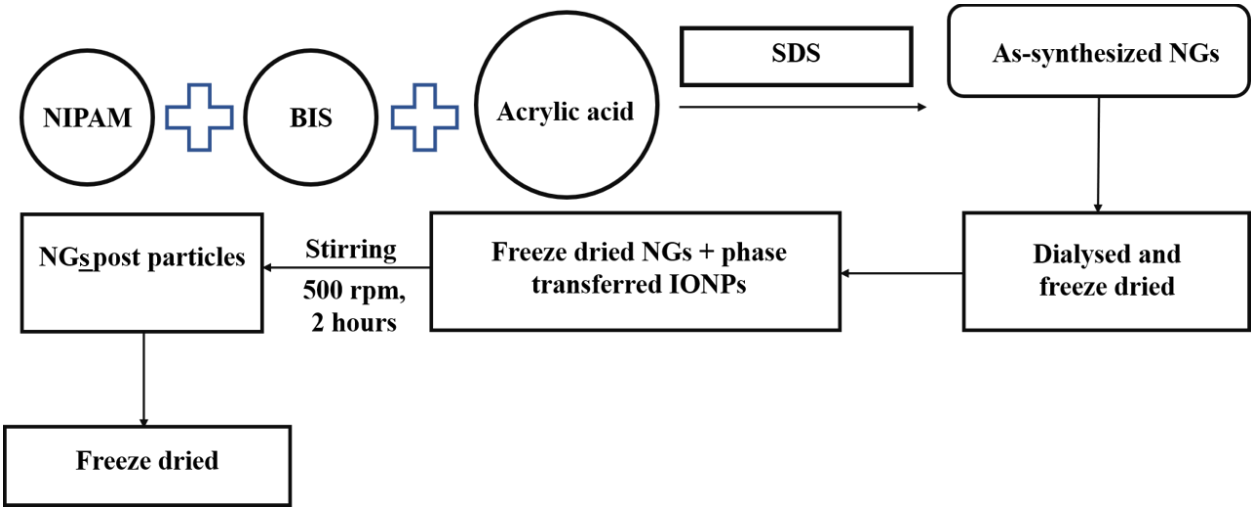

Figure 2.9 - Flowchart showing the steps for synthesis of NGs_post systems.

2.2.9.3. Synthesis of Hybrid Systems using Addition Technique

An intermediate hybrid system was synthesized by addition technique to understand how temperature and stirring effect interaction of phase transferred IONPs with NGs. First, a similar protocol was followed (discussed in Subsection 2.2.8) to prepare bare NGs. In this process, known amount of phase transferred IONPs were added with NGs before dialysis. The system was then dialyzed for 24 hours and freeze dried. A flowchart of the addition technique is shown in Figure 2.10. The samples obtained using this method will be abbreviated as NGs_added for the entire study. The NGs_added particles were also magnetically separated following a similar protocol as used in case of magnetically separated NGs_insitu and post particles. The samples in this case will

be referred to as magnetically separated NGs_added particles. The different systems and their variations synthesized and discussed overall in this section is presented in Table 2.1.

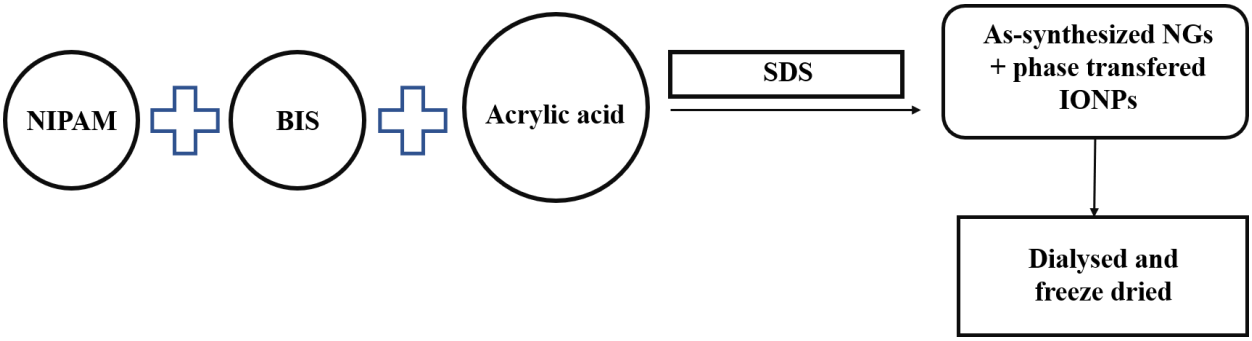

Figure 2.10 - Flowchart showing the steps for synthesis of NGs_added systems.

Table 2.1 - Different particles and their variations synthesized with different techniques.

Particles and their variations	**Technique used (in brief)**
IONPs_oleate	Thermal decomposition of iron oleate precursor.
IONPs_penta	Thermal decomposition of iron pentacarbonyl precursor.
Phase transferred IONPs_oleate	Phase transfer using sodium citrate – to transfer IONPs_oleate from organic media to water.
Phase transferred IONPs_penta	Phase transfer using sodium citrate – to transfer IONPs_penta from organic media to water.
NGs	Free radical polymerization
NGs_insitu	Free radical polymerization with phase transferred IONPs incorporated during the process (in-situ technique).
NGs_insitu magnetically separated	Magnetic separation of magnetic part from NGs_insitu systems.
NGs_post	Free radical polymerization with phase transferred IONPs incorporated after the process and stirred. (post technique).
NGs_post magnetically separated	Magnetic separation of magnetic part from NGs_post systems.
NGs_added	Free radical polymerization with phase transferred IONPs added after the process without stirring. (added technique).
NGs_added magnetically separated	Magnetic separation of magnetic part from NGs_added systems.

2.2.10. Loading of Drug – Cytochrome C

Two common loading approaches involve -1) incorporation of the drug in the system at the point of synthesis (in-situ technique) and 2) addition of the drug in the system after synthesis (post-technique). The absorption of the drug in the hydrogel matrix can be achieved by a breathing in technique (64). A schematic of the breathing in mechanism is shown in Figure 2.11.

In this study, post breathing in mechanism has been implemented to load the hydrogel with cytochrome C (cyt C). Utilizing the high-water holding property of pNIPAm-aac hydrogels, the hydrogels swell in aqueous media (discussed in Chapter 1, Section 1.8). Cyt C dissolved in the aqueous medium then gets taken in by the nanogels and the structure gets loaded with the drug.
The optimized loading protocol has been directly taken from the previous works of Bandyopadhyay et al. (1). For effective loading of hydrogel samples, freeze-dried hydrogel (1.67 mg) was mixed with water (1 mL) containing cyt C (0.5 mg) in a glass vial (6 mL). Another parallel glass vial was prepared containing similar weights of hydrogel and cyt C. The two vials were kept on shaking for 2 hours and the two vials were mixed to form a 2 mL solution of the loaded hydrogel. The solution was then dialyzed for 24 hours to remove unloaded cyt C and the final sample was then taken for further release studies. A general flowchart of the loading protocol is shown in Figure 2.12.

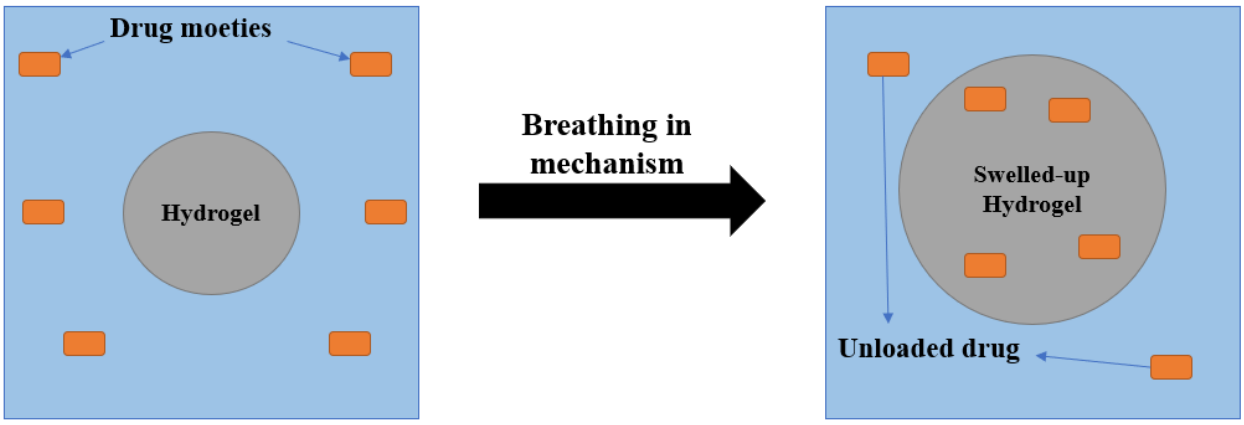

Figure 2.11 – Schematic showing the general breathing in drug loading technique.(65)

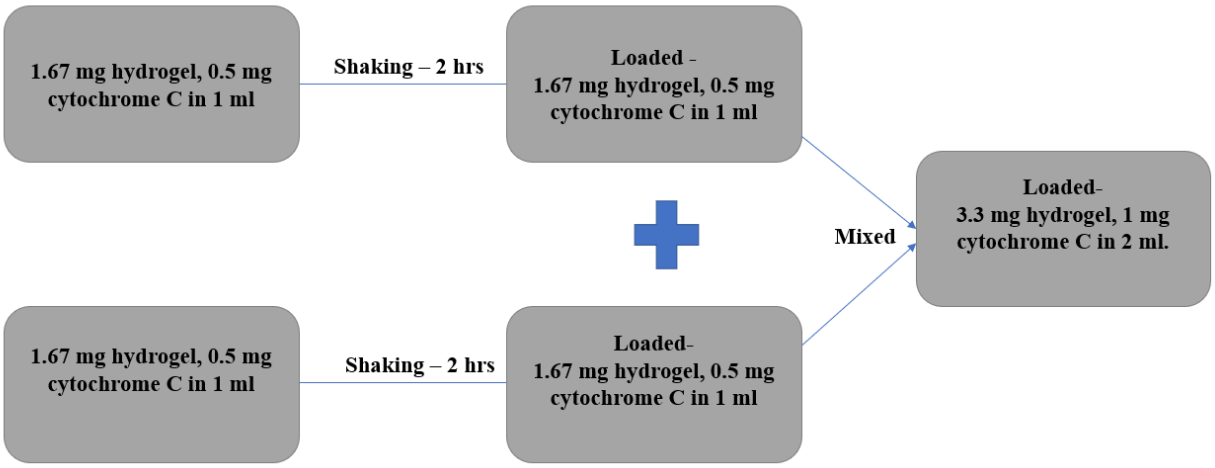

Figure 2.12 – Flowchart showing the loading protocol.

2.3. Characterization

2.3.1. X-ray Diffraction

Crystallographic structures of IONPs were investigated by X-ray powder diffraction (XRD) using a Bruker D8 Advance Da-Vinci equipped with a LynxEye detector working in Bragg–Brentano geometry. Diffraction patterns were recorded with CuKα radiation (λ = 1.5406 Å), a step size of 2Θ = 0.0138 ° and an integration time of 0.75 s using a variable divergent slit.

2.3.2. High Resolution Transmission Electron Microscopy

High resolution transmission electron microscopy (HRTEM) images were taken using the JEOL 2100 transmission electron microscope operating at 200 kV. The samples were diluted with their respective solvents and drops of the diluted samples (~ 20 uL) were put on a Formvar carbon-coated copper grid. Imaging was performed on IONPs samples. The size and polydispersity index were analyzed from the obtained HRTEM images using ImageJ software. The size analysis was performed manually for 200 particles. The images were taken and segmented in four equal parts. From each part, 50 particles were chosen manually and analyzed. This was done to proportionately select particles over the entire image.

2.3.3. Dynamic Light Scattering

Malvern Zetasizer Nano ZS© was used to measure the particle size and zeta potential of phase transferred IONPs, NGs, NGs_insitu, NGs_post and NGs_added systems at different conditions. The variation of these conditions was performed by changing the temperature and pH of the system. For NG samples, the temperature was varied from 25 to 60 ºC and its effect on sample size was studied. The samples were also studied at acidic conditions of pH = 3.5. For phase transferred IONPs, the size and zeta potential values were also observed at 25, 45 and 60 ºC, respectively. The solvent used for all the samples was MQ water. All values were generated in triplicates and the average was taken.

2.3.4. Vibrating Sample Magnetometry

Magnetic measurements of IONPs, phase transferred IONPs and NGs systems were carried out using MicroMag™ 3900 vibrating sample magnetometer (VSM). MicroMag™ 3900 was operated at room temperature with maximum applied magnetic fields of 1 T and the magnetization of the samples were recorded. The magnetization data obtained as a function of applied field was normalized by the mass of the sample used for comparative study.

2.3.5. Modular System for measuring Magnetic Susceptibility

A magnetic susceptibility meter (MFK1) commonly called kappabridges, was used to measure the variation of magnetic susceptibility as a function of temperature (-196 – 0 °C). The device was maintained at default settings of AC magnetic field strength 200 A/m and 976 Hz. Susceptibility data obtained for IONPs as function of temperature was mass normalized for comparative study.

2.3.6. UV-visible Spectroscopy

UV-vis spectroscopy was used for studying the loading and release of cyt C from NGs, NGs_insitu, NGs_post and NGs_added samples. Analysis of the loading and release studies were carried out using Shimadu© UV-vis recording spectrophotometer, model no. UV-2401PC. For loading and release studies, the relative decrease in intensity for cyt C absorbance peak in the range 409-411nm was observed over time.

2.3.7. Volume Phase Transition Temperature Calculations

The calculation of the volume phase transition temperature (VPTT) for hydrogels was devised based on its swelling and collapse behavior. The study of swelling and collapse behavior of general hydrogel systems is based on variation of specific spectroscopic parameters (for e.g., – optical density) as function of temperature (66). Real time hydrogel systems are not completely monodispersed thus differently sized particles will collapse at their own unique VPTT. This results in a range of temperatures along the collapsing or swelling curve, thus making it difficult to comment on a single temperature defining the VPTT of the entire system. Hence, VPTT in our system was defined as the temperature at which the ratio of the collapsed and swelled hydrogels was equal (67). Figure 2.13 shows a general example of utilization of spectroscopic parameters to calculate VPTT.

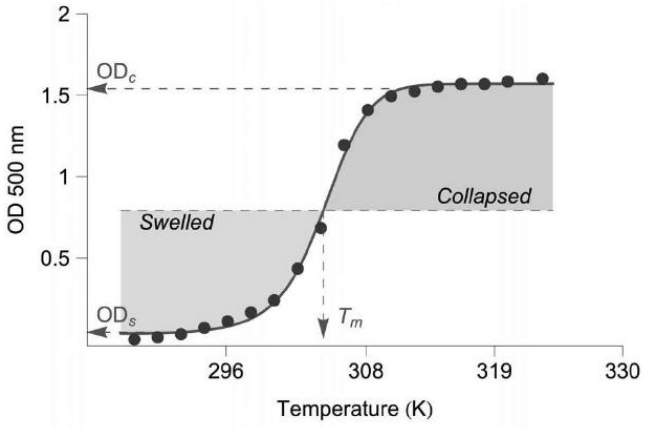

Figure 2.13 - Change in optical density as a function of temperature for determination of VPTT

Thus, the above-mentioned definition of calculating VPTT is devised based on the swelling and collapse behavior of the hydrogel (68). In this study, the variation in hydrodynamic diameter of the nanogel systems was studied as function of temperature (25–60 ºC) using Malvern Zetasizer Nano ZS©. The nanogel systems were heated from 25–60 ºC and conversely cooled in the same temperature range. Thus, heating, and cooling curves were obtained for the systems. The temperature change was done in steps of 5 ºC. Hydrodynamic sizes of the nanogel systems were obtained at each step. A spectroscopic parameter (α) was introduced to define the change in hydrodynamic sizes of the nanogel systems (shown in Equation 14). The value (α) showed

normalized volumetric collapses of the systems. The calculated α values were then plotted as function of temperature in Sigma Plot® and was fitted with a five parameter Gaussian curve as shown in Equation 15. Based on the fitting parameters obtained from the Gaussian curves, a Matlab® code was used to replot the curves between 25 and 60 ºC as shown in Figure 2.14 (69).

$$\alpha = (D/D_0)^3 \quad (14)$$

where D – hydrodynamic diameter at specific temperature point, D_0 – hydrodynamic diameter at 25 ºC.

$$y = y_o + a/1 + e^{-[x - x_o b]}{}^c \quad (15)$$

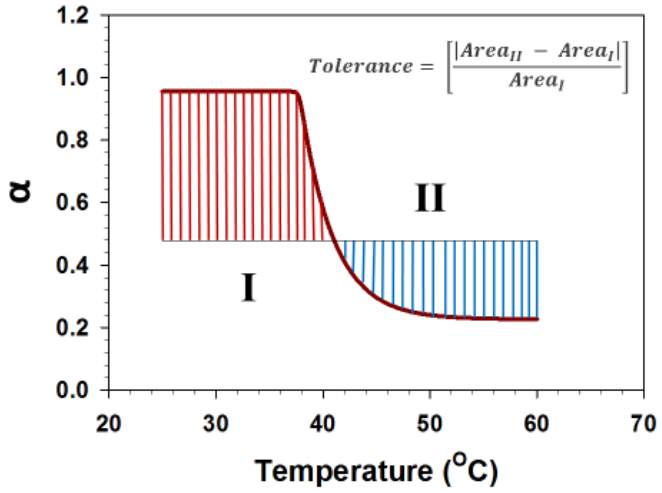

Figure 2.14 - Schematic depicting area equalization for VPTT calculations

The code then divides the curve into two parts and calculates the area under the curve using Simpson's 1/3rd rule. A mean temperature is chosen to start the calculation. A tolerance value is set defining the preciseness of VPTT calculation. The number of iterations defined the resolution of the code on the curve. If the relative difference of the areas of the collapsed and swelled states do not fall under the mentioned tolerance value, the code loops itself unless the value of relative difference in area goes below the tolerance value. The number of iterations and tolerance have been fixed at 1000 and 0.001 respectively for all calculations of VPTT. Hence VPTT values were obtained from the heating and cooling curves and an average value was reported

2.3.8. Release Study of Cytochrome C

For the release study of cytochrome C (cyt C), the loaded hydrogel systems (2 mL) were taken, and additional water (3 mL) was added to dilute the samples before UV-visible spectroscopy was conducted using a UV-vis spectrophotometer. This dilution was done to bring down the absorbance intensity of cyt C within instrumental limits. In this case, the decrease in concentration of cyt C inside the dialysis tube was examined over time. The release of cyt C was studied based on the decrease of absorbance peak in the spectral range 409-411 nm over a period of 20 hours. The release setup was maintained at different conditions of 40 ºC, 45 ºC with acidic pH conditions (3.5) based on specific experiments performed. A typical setup of dialysis for drug release study is shown in Figure 2.15. The sink condition for the release of cyt C was maintained by MQ water (2 litres) in the beaker. The molecular weight of cyt C is ~ 12000 Da (70). The dialysis membrane used in the release setup had a cut off (14000 Da) higher than the molecular weight of cyt C which allowed released drug from hydrogel systems to diffuse out from the membrane into the sink.

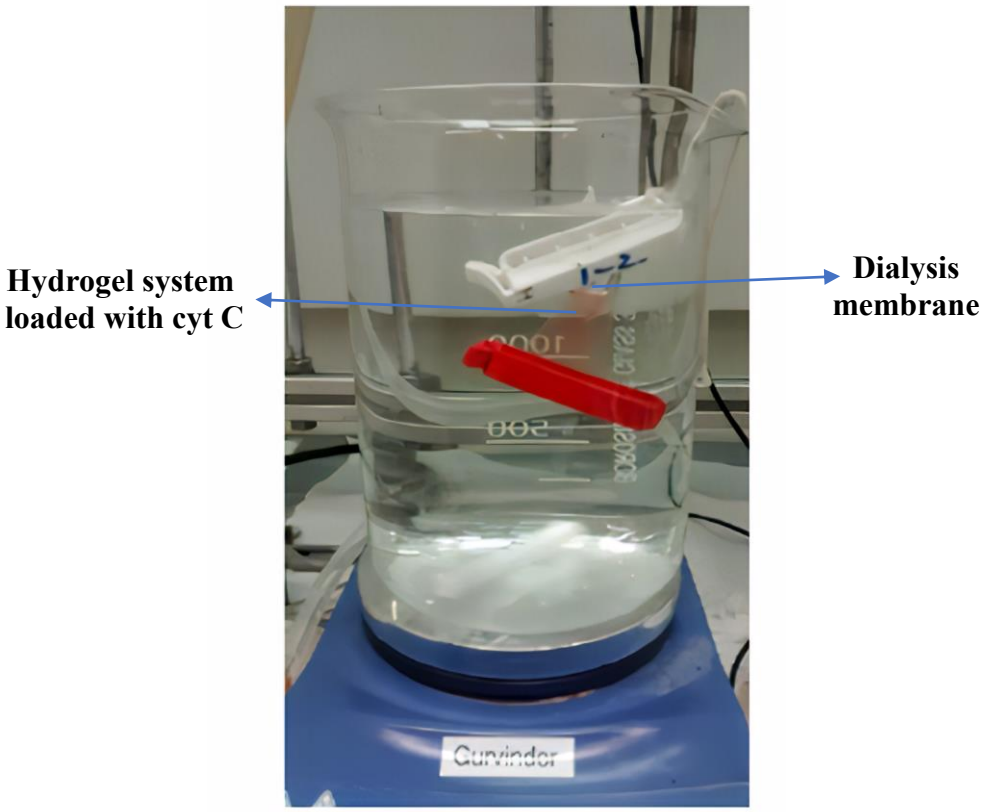

Figure 2.15 – Dialysis setup for release of cytochrome C.

2.3.9. Magnetherm

Magnetherm is designed for studying heating properties of magnetic nanoparticles. An image of different components of the device is shown in Figure 2.16. The magnetherm device consists of four parts: 1) Function generator – for producing discrete electrical frequencies, 2) power amplifier – for amplifying the electrical frequencies to produce higher voltages 3) magnetherm unit - consisting of a solenoid coil and a capacitor which utilizes the voltage and frequency produced to generate AMF. The magnetherm unit also serves as the sample holder for exposing the sample to AMF and 4) water bath – which is connected to the magnetherm unit to mitigate any heat generated from the magnetic coils (inside the magnetherm unit). A rough schematic of the connections of the magnetherm device is shown in Figure 2.17. Before running measurements, the AMF condition defining the magnetic field frequency and amplitude was set by changing the capacitance and solenoid in the magnetherm unit. The system can operate with solenoid coils of 2 different turns (9 and 18) with 3 different capacitor values, thus giving options for running the instrument at 6 possible frequencies and magnetic field conditions. The six different frequency and their corresponding magnetic field values are shown in Table 2.2.

Heat production studies were performed from phase transferred IONPs on exposure to different AMF conditions using the therm setup. Phase transferred particles (10 mg) were dispersed in MQ water (1 ml) for the experimental runs. Therefore, background heating effects from MQ water without the particles also needed to be checked (baseline temperature correction), on exposure to AMF conditions. Increase in temperature was seen from MQ water without the particles due to formation of eddy currents which is common at high AMF frequencies in radio-frequency range (discussed in Chapter 1, Section 1.5) (5, 71). Three baseline runs were done at each AMF condition. Parallelly, the experimental runs were performed for phase transferred IONPs_oleate particles dispersed in MQ water. Each individual baseline was subtracted from the temperature profile of the particles. Therefore, three datasets of time vs temperature profiles were obtained. The average of the datasets at each time point is presented further in this study. The experimental runs were conducted for period of 1 hour and the change in temperature was recorded each second with precision of 0.01 ºC. The heat generated from magnetic nanoparticles was quantified using specific absorption rates (SARs) (discussed in Chapter 1, Section 1.6). SAR values were calculated

directly from provided manufacturers software by inputting obtained average temperature profiles as function of time.

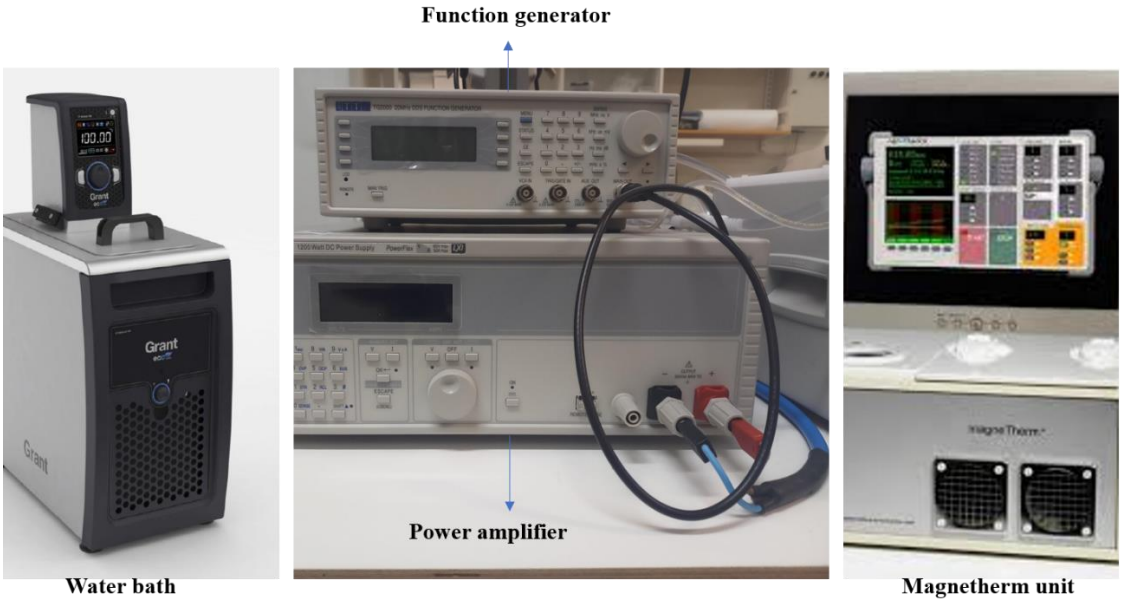

Figure 2.16 – Image of different components of Magnetherm device.

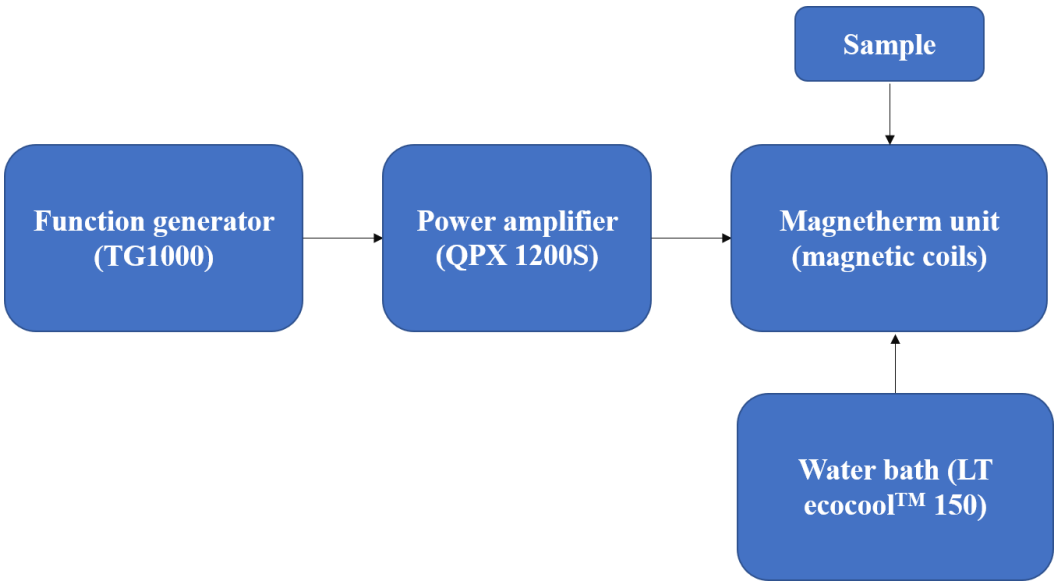

Figure 2.17 – Rough schematic of the connections of magnetherm device.

Table 2.2 – Showing different frequency values with its corresponding magnetic fields.

No of AMF conditions	Coil turn	Capacitor value (nF)	Nominal frequency (kHz)	Maximum magnetic field value (mT)
1	9	200	162.2	25
2	9	88	243.4	21
3	9	6.2	930.3	12
4	18	200	102.7	30
5	18	88	154.1	21
6	18	6.2	587.3	12

2.3.10. Release Study of Cytochrome C: with Magnetherm Setup

Cytochrome C (cyt C) was loaded in hydrogel systems using same procedure (discussed in Section 2.2, Subsection 2.2.10). In this setup, hydrogel systems loaded cyt C (2 mL) were put in a dialysis tube and the tube was connected to a sample holding shaft as shown in Figure 2.18 – a). The tube with the sample holding shaft was put inside a water jacket which functioned as sink in this setup as shown in Figure 2.18 – b). Heated water from water bath was circulated outside the walls of the jacket using flow tubes to maintain temperature of the sink. The sink in this setup was much smaller in volume as compared to sink (discussed in Subsection 2.3.8). Henceforth, the water inside the jacket was rotated using an external pump to maintain constant sink conditions. The tube, holding shaft and jacket was placed inside magnetic coils and the release study was performed as shown in Figure 2.18 – c). The shaft was slowly rotated using a stepper motor to account for uniform diffusion of cyt C from the membrane into the sink. The study was performed for total time of 10 hours for different hydrogel systems. The release in this case was also recorded using UV-vis spectrophotometer. Release data were collected every hour. After every hour, the dialysis tube was taken out and the decrease in concentration of cyt C was seen based on decrease of its equivalent absorbance peak in the range 409-411 nm. Release studies were performed with and without alternating magnetic fields (AMFs). The cut off for the dialysis membrane in this setup was 20000 Da. In the following chapter, results obtained in this work are presented.

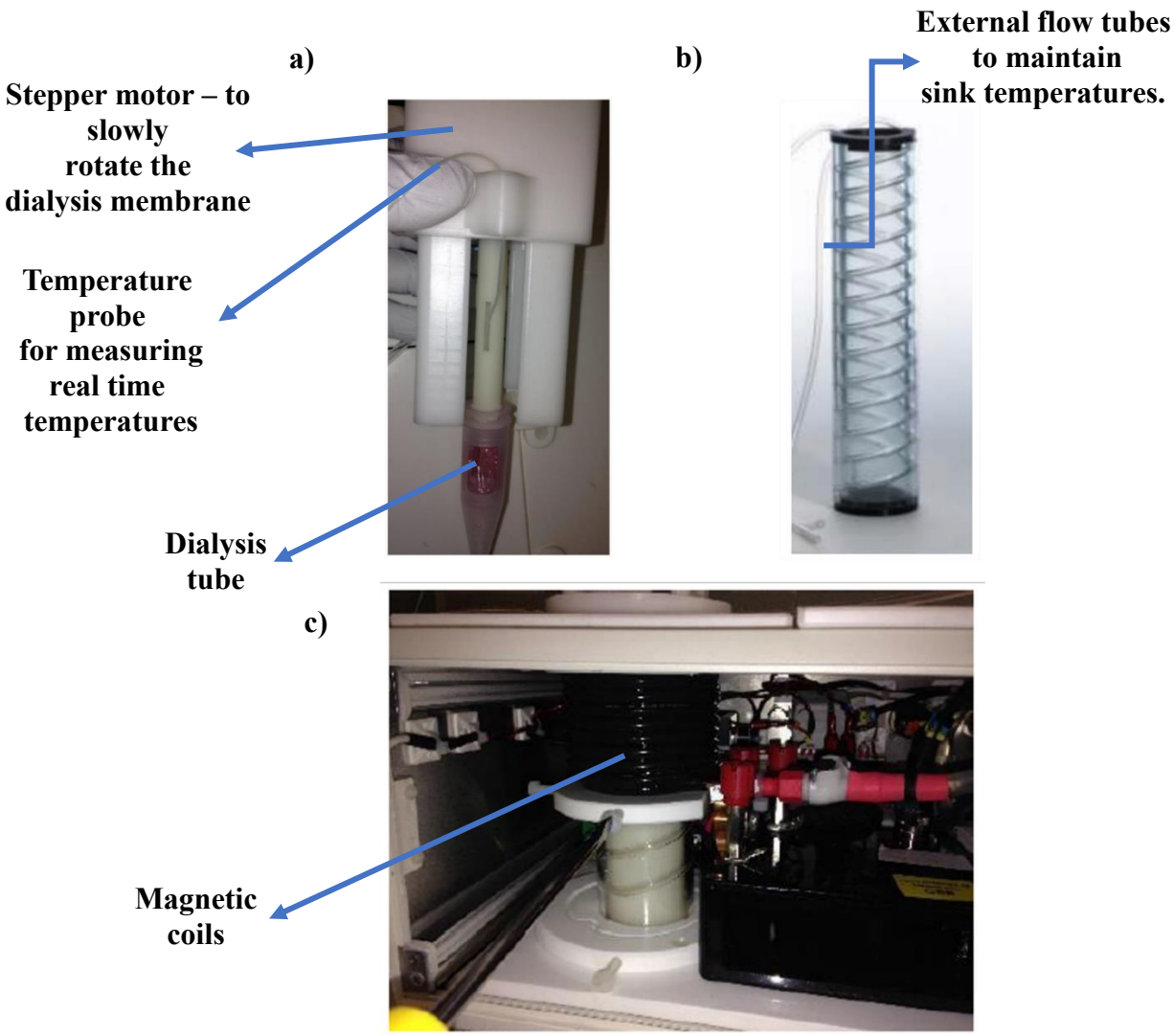

Figure 2.18 – a) Image showing dialysis tube connected to shaft. b) Image showing water jacket which functions as sink. c) Image showing the tube, shaft and water jacket placed inside magnetic coils.

Chapter 3: Results

This chapter will first start with size, crystal structure and magnetic characterization of two types of IONPs – 1) IONPs_oleate and 2) IONPs_penta obtained from thermal decomposition of precursors iron oleate and iron pentacarbonyl, respectively. In the next section, the properties of phase transferred IONPs_oleate and IONPs_penta particles will be shown. The following section will involve characterization of bare NGs. Thereafter, the different hybrid NGs systems will be presented and compared. Lastly, the loading and release of cytochrome C under different conditions of elevated temperatures, acidic pH, and external alternating magnetic fields (AMFs) will be presented.

3.1. Iron Oxide Nanoparticles

In this section, characterization of IONPs synthesized by thermal decomposition methods are presented. The entire section is divided in three subsections. Firstly, images obtained from HRTEM is presented. Secondly, crystallographic, and magnetic characterization of IONPs systems using XRD and VSM is shown. In the last subsection, IONPs yield (mg/mL) obtained from concentration test are shown.

3.1.1. Size Characterization of Iron Oxide Nanoparticles

The HRTEM images of IONPs_oleate and IONPs_penta particles are shown in Figure 3.1- a) and b) respectively. The average size for IONPs_oleate particles was 16 ± 2 nm and IONPs_penta particles was 8 ± 1 nm with polydispersity index (PDI) of (~ 0.1) in both cases. For calculation of PDI, the formula used is shown in Equation 16 (72).

$$\text{PDI} = (\text{Standard deviation}/\text{Mean size}) \quad (16)$$

The size distribution of IONPs systems is shown in Figure 3.1- c) and d) respectively.

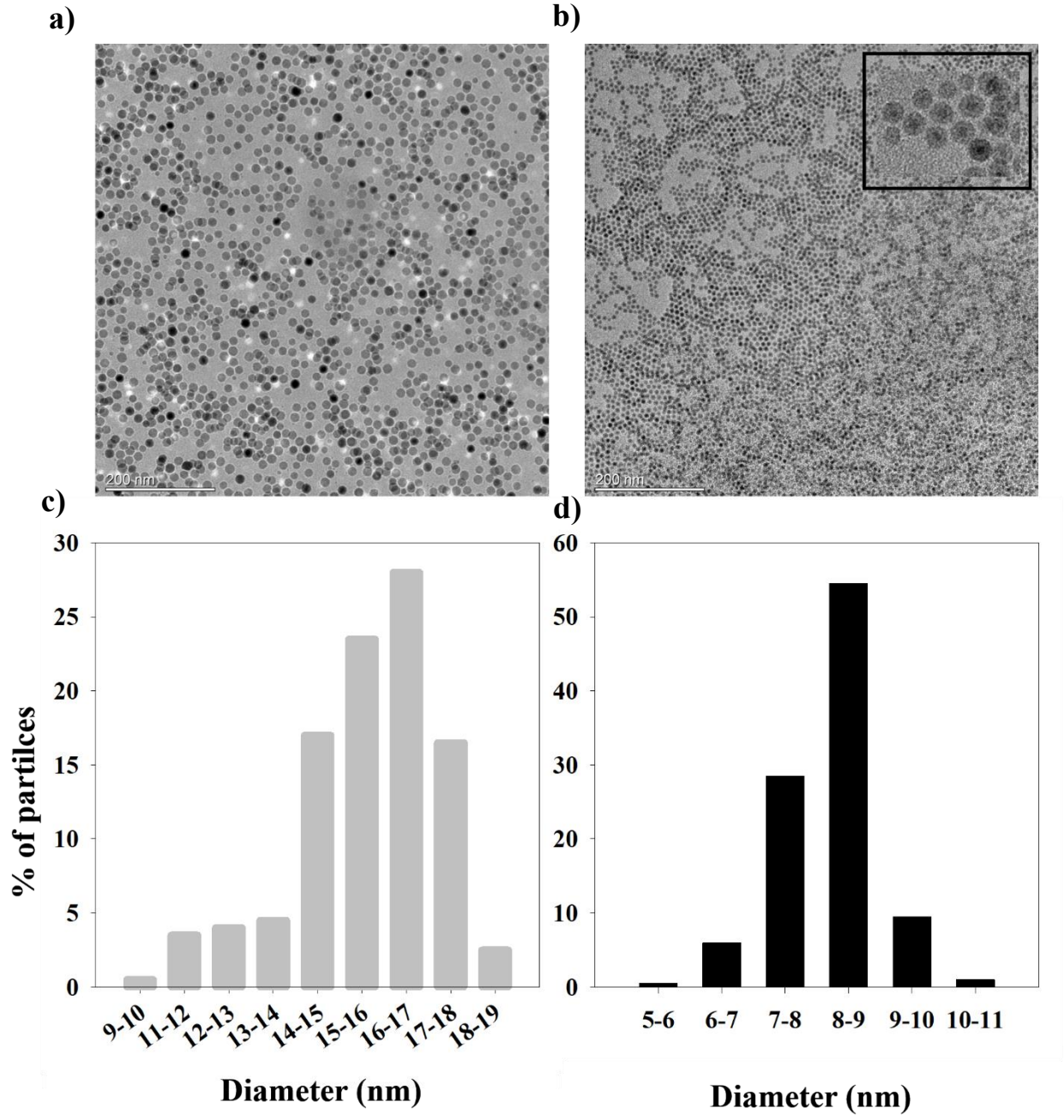

Figure 3.1 – a) and b) HRTEM image of IONPs_oleate and IONPs_penta particles. The scale bar is 200 nm in both the images[1] . c) and d) Particle size distribution of IONPs_oleate and IONPs_penta particles, respectively.

[1]Courtesy – Anuvansh Sharma, PhD

3.1.2. Crystallographic and Magnetic Characterization of Iron Oxide Nanoparticles

The XRD pattern of IONPs_oleate and IONPs_penta particles is shown in Figure 3.2 – a) and b) respectively. IONPs_oleate particles exhibited characteristic peaks at 2θ values – 30 °, 35 °, 43 °, 62 ° which represents inverse cubic spinel structure of magnetite (63). The above-mentioned 2θ values correspond to lattice planes - (220), (311), (400) and (440) respectively as matched with crystallographic database **(COD-1539747 Fe_3O_4)** using DIFFRAC.EVA software. Similarly, for IONPs_penta particles characteristic peaks of magnetite phase was seen at 2θ values – 35 ° and 43 ° corresponding to lattice planes - (311) and (400) matched with crystallographic database **(COD-1539747 Fe_3O_4)** using DIFFRAC.EVA software.

The magnetic hysteresis (M-H loops) of IONPs_oleate and IONPs_penta particles are shown in Figure 3.2 – c). The maximum applied magnetic field was 1 T. Both systems showed superparamagnetism at room temperature with zero hysteresis losses. The measured saturation magnetization of IONPs_oleate was 74.3 emu/g and that of IONPs_penta particles was 21.9 emu/g. Figure 3.2 – d) shows the magnetic susceptibility of IONPs_oleate and IONPs_penta particles as function of temperature. The temperature point where the magnetic susceptibility value maximizes shows the blocking temperature (T_B) of the system (73). From Figure 3.2 – d) the T_B for IONPs_oleate and IONP_penta systems were obtained at -190 ºC (83 K) and -38.7 ºC (234.3 K) respectively.

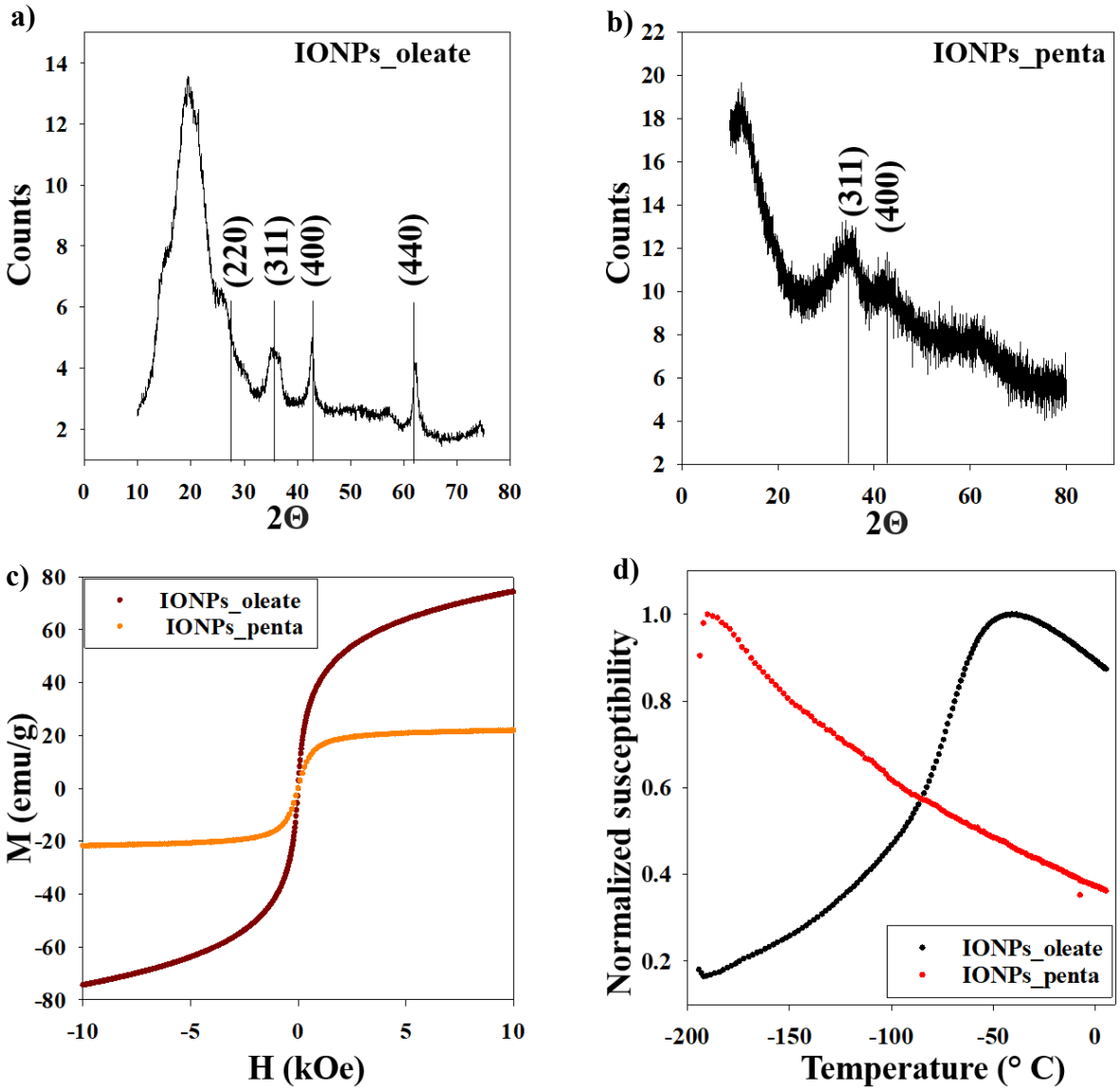

Figure 3.2 - a) and b) XRD pattern showing crystallographic data of IONPs_oleate (matched with **(COD-1539747 Fe_3O_4)**) and IONPs_penta particles (matched with **(COD-1539747 Fe_3O_4))**, respectively. c) Magnetic hysteresis (M-H loops) of IONPs_oleate and IONPs_penta particles using VSM at room temperature. d) Magnetic susceptibility measurements of IONPs_oleate and IONPs_penta particles as function of temperature using magneto-susceptibility meter.

3.1.3. Concentration Test of Iron Oxide Nanoparticles

The concentration obtained for as-synthesized IONPs_oleate and IONPs_penta particles was 11.0 ± 3.7 mg/mL and 15.7 ± 0.9 mg/mL respectively as shown in Table 3.1.

The IONPs_oleate and penta particles were dispersed in 20 mL of toluene and hexane, respectively (discussed in chapter 2, section 2.2.2 and 2.2.3). The obtained concentration values were used to take out a predetermined amount of IONPs (5 mg) from their respective organic solvents which was further used for the phase transfer process as discussed in the upcoming part.

Table 3.1 – Shows the concentration values obtained for IONPs_oleate and IONPs_penta particles, respectively.

Particles	**Volume of dispersed IONPs used (uL)**	**Weight of empty Eppendorf tubes (mg)**	**Weight of Eppendorf tubes after drying (mg) at 70 ºC for 6 hours**	**Concentration (mg/ml)**	**Average concentration (mg/ml)**
	300	999.8	1010.0	10.2	
IONPs_oleate	300	994.5	1006.2	11.7	11.0 ± 3.7
	300	1002.5	1013.5	11.0	
	300	987.9	992.3	14.7	
IONPs_penta	300	992.6	997.5	16.3	15.7 ± 0.9
	300	1008.4	1013.2	16.0	

3.2. Phase Transferred Iron Oxide Nanoparticles (IONPs)

The as-synthesized IONPs were phase transferred using sodium citrate to transfer from organic to aqueous media. This section is divided in five subsections. Firstly, the hydrodynamic sizes and zeta potentials of the phase transferred IONPs obtained using DLS technique are presented. The repeatability of the process is also shown. Secondly, stability studies of the particles over time, different temperatures, and pH conditions are shown followed by concentration study of the obtained phase transferred IONPs. Thereafter, magnetic characterization of phase transferred IONPs are presented using VSM. Lastly, heat production from phase transferred IONPs on exposure to AMF under different field conditions is studied using Magnetherm setup.

3.2.1. Hydrodynamic Size and Zeta Potential Measurements using Dynamic Light Scattering

The hydrodynamic sizes and zeta potential of phase transferred IONPs_penta and IONPs_oleate particles are shown in Figure 3.3 - a), b), c) and d). A series of 12 and 10 experiments respectively were performed to phase transfer IONPs_oleate and IONPs_penta particles. The average hydrodynamic size and zeta potential for IONPs_oleate particles obtained over 12 experiments was 236 ± 32 nm and -50 ± 2 mV, respectively whereas for IONPs_penta particles obtained over 10 experiments was 355 ± 37 nm and -41 ± 7 mV.

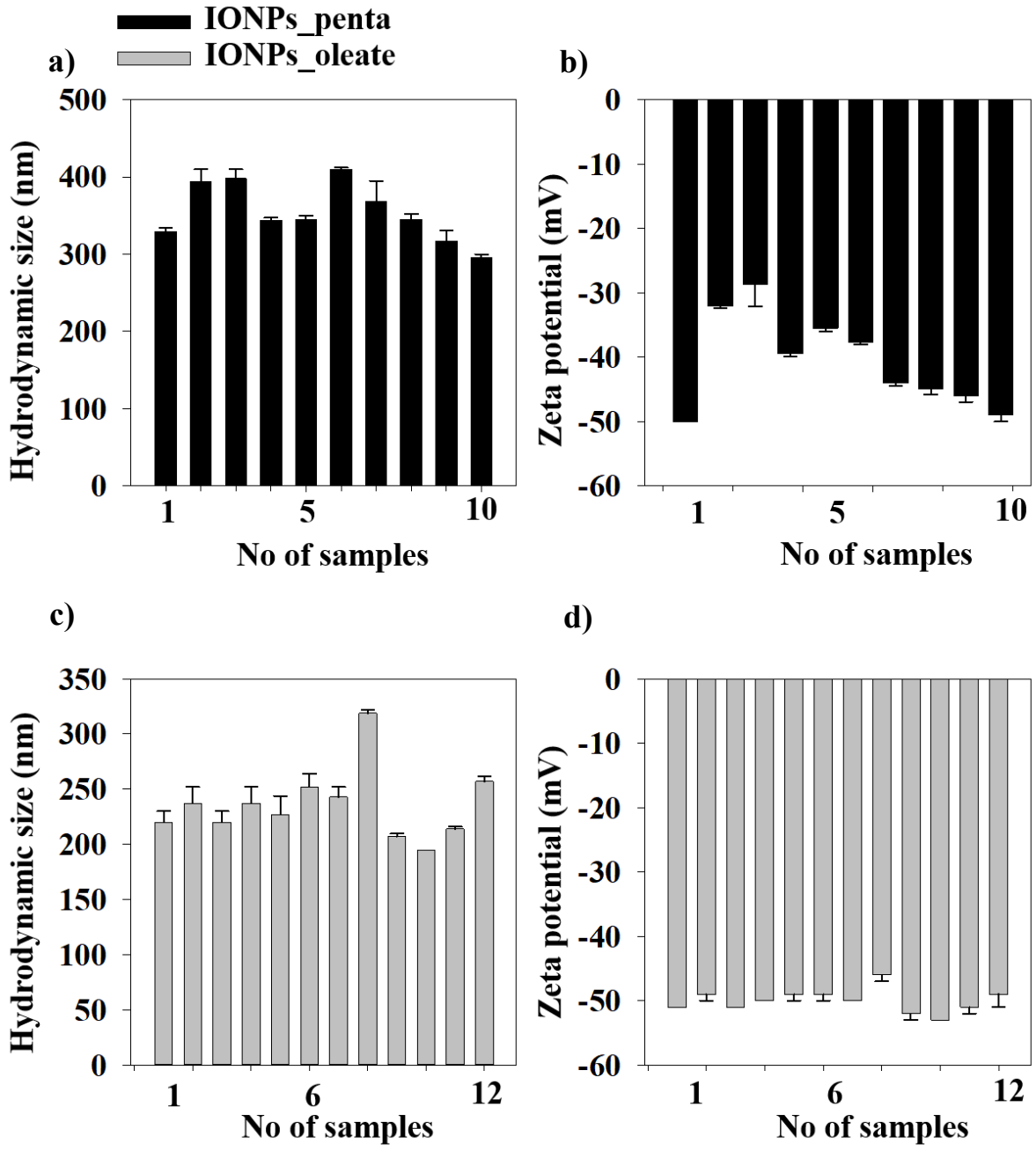

Figure 3.3 – a) and b) Hydrodynamic sizes (nm) and zeta potentials (mV) of phase transferred IONPs_penta particles. c) and d) Hydrodynamic sizes (nm) and zeta potentials (mV) of phase transferred IONPs_oleate particles.

3.2.2. Stability Study of Phase Transferred IONPs

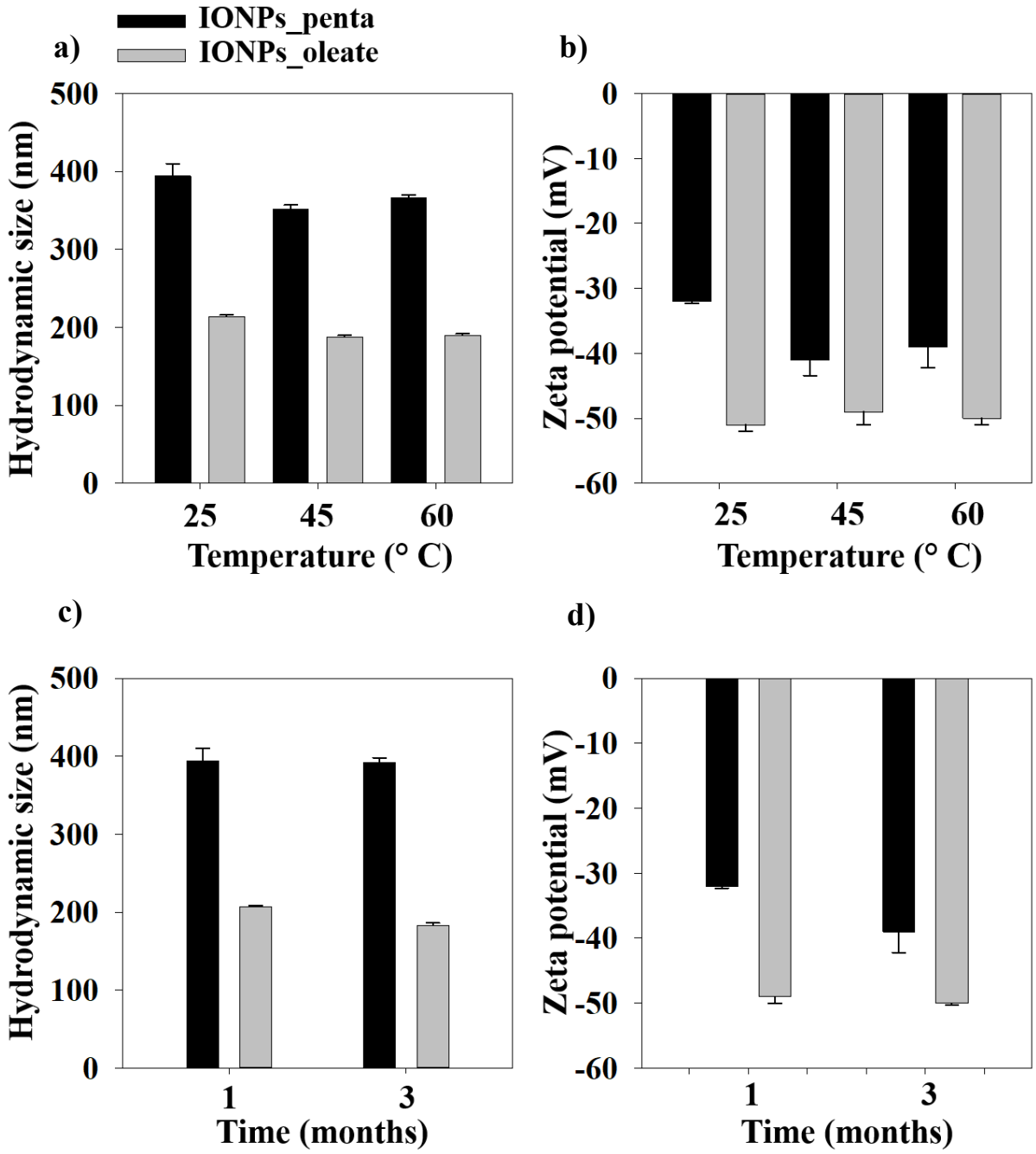

Figure 3.4 – a) and b) Hydrodynamic sizes (nm) and zeta potential (mV) of IONPs_oleate and IONPs_penta particles at temperatures 25 ºC, 45 ºC and 60 ºC respectively. c) and d) Hydrodynamic sizes and zeta potentials of IONPs_oleate and IONPs_penta particles for a time period of 2 months.

The stability of phase transferred IONPs_oleate and IONPs_penta particles at elevated temperatures of 45 ºC and 60 ºC was studied by measuring hydrodynamic sizes and zeta potentials as shown in Figure 3.4 – a) and b), respectively. The stability of the phase transferred IONPs over a period of two months is shown in Figure 3.4 – c) and d).

Hydrodynamic sizes and zeta potentials were measured at different pH values for both phase transferred IONPs_oleate and penta particles as shown in Figure 3.5 – a) and b). The phase transferred IONPs_oleate particles were stable in the pH range (~ 3.5 – 7) and the IONPs_penta particles were stable in the range (~ 4 – 7). At more acidic pH conditions, less than ~ 3.5 for IONPs_oleate and ~ 4 for IONPs_penta particles, the hydrodynamic sizes increased above 500 nm correspondingly lowering the zeta potential values, thus decreasing the stability of the systems, in turn showing agglomeration effects.

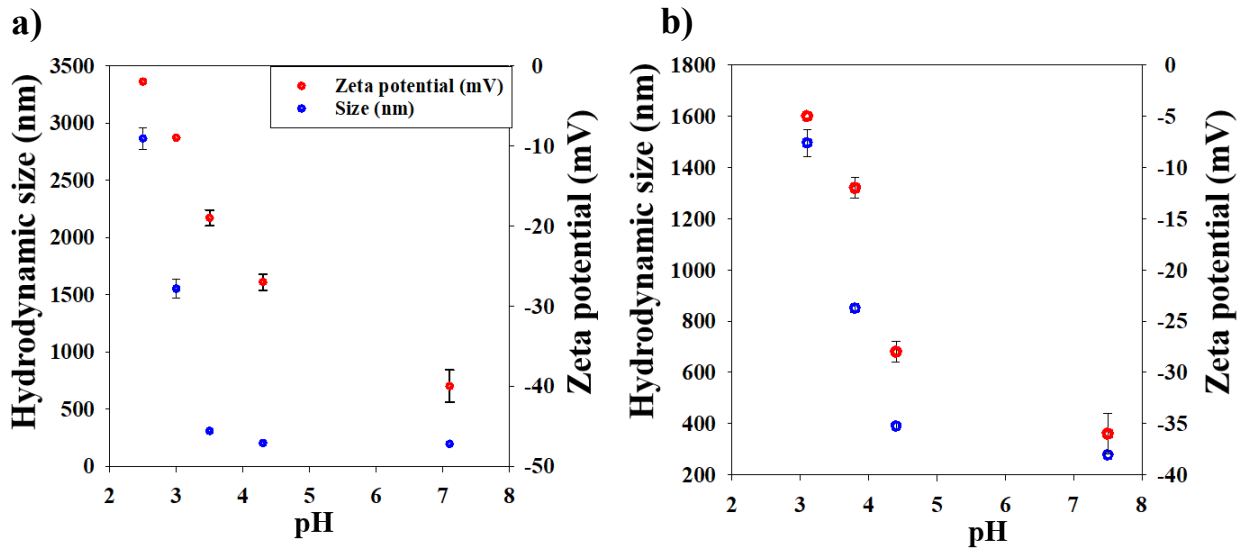

Figure 3.5 – a) Hydrodynamic size (nm) and zeta potential (mV) of phase transferred IONPs_oleate particles at different pH conditions. b) Hydrodynamic size (nm) and zeta potential (mV) of phase transferred IONPs_penta particles at different pH conditions.

3.2.3. Concentration Test of Phase Transferred IONPs

The as-synthesized IONPs were phase transferred using sodium citrate to transfer them from organic to aqueous media. The concentration values obtained for phase transferred IONPs_oleate and IONPs_penta particles was 0.8 ± 0.1 mg/mL and 0.5 ± 0.1 mg/mL respectively as shown in

Table 3.2.

The obtained concentration values for both the systems were used to take out predetermined amounts of phase transferred IONPs from aqueous media which was further used with pNIPAm-aac nanogels (NGs) to synthesize hybrid NGs.

Table 3.2 – Shows the concentration values obtained for phase transferred IONPs_oleate and IONPs_penta particles, respectively.

Particles	**Volume of dispersed IONPs used (uL)**	**Weight of empty Eppendorf tubes (mg)**	**Weight of Eppendorf tubes after drying (mg) at 70 ºC for 6 hours**	**Concentration (mg/ml)**	**Average concentration (mg/ml)**
	1000	999.2	1000.0	0.8	
Phase transferred IONPs_oleate	1000	987.6	988.4	0.8	0.8 ± 0.1
	1000	1002.2	1002.9	0.7	
	1000	999.8	1000.2	0.7	
Phase transferred IONPs_penta	1000	992.5	993.1	0.9	0.5 ± 0.1
	1000	1000.4	1001.0	0.6	

3.2.4. Magnetic Characterization of Phase Transferred IONPs

The magnetic hysteresis of phase transferred IONPs_oleate and penta particles are shown in Figure 3.6 – a) and b) respectively. The maximum external applied magnetic field was 1 T. Both phase transferred systems were superparamagnetic at room temperature with close to zero hysteresis losses. The measured saturation magnetization (Ms) of IONPs_oleate particles was 26.1 emu/g and that of IONPs_penta was 0.6 emu/g.

Due to relatively low Ms values of phase transferred IONPs_penta particles, the oleate system was chosen for study on exposure to different AMF conditions as presented next.

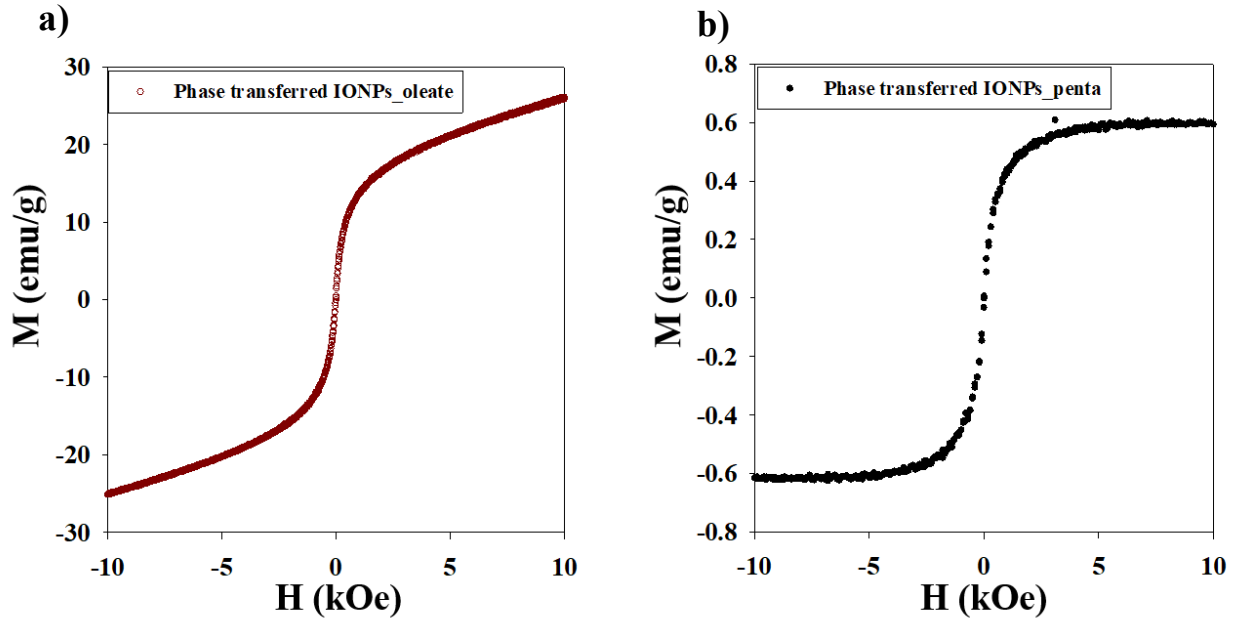

Figure 3.6 - a) Magnetic hysteresis (M vs H) of phase transferred IONPs_oleate particles at room temperature. b) Magnetic hysteresis (M vs H) of phase transferred IONPs_penta particles.

3.2.5. Heat production from Phase Transferred IONPs with Alternating Magnetic Field

The average change in temperature (° C) for phase transferred IONPs_oleate particles as function of time under five different external AMF conditions are shown in Figure 3.7 - a), b), c), d) and e) respectively. The error in temperature at each time point is shown by the shaded black region while the average temperature values are shown by white lines. The temperature profiles obtained were used to calculate specific absorption rates (SAR) (W/g) at different AMF conditions. The SAR values with error bars at different AMF conditions is shown in Figure 3.7 – f).

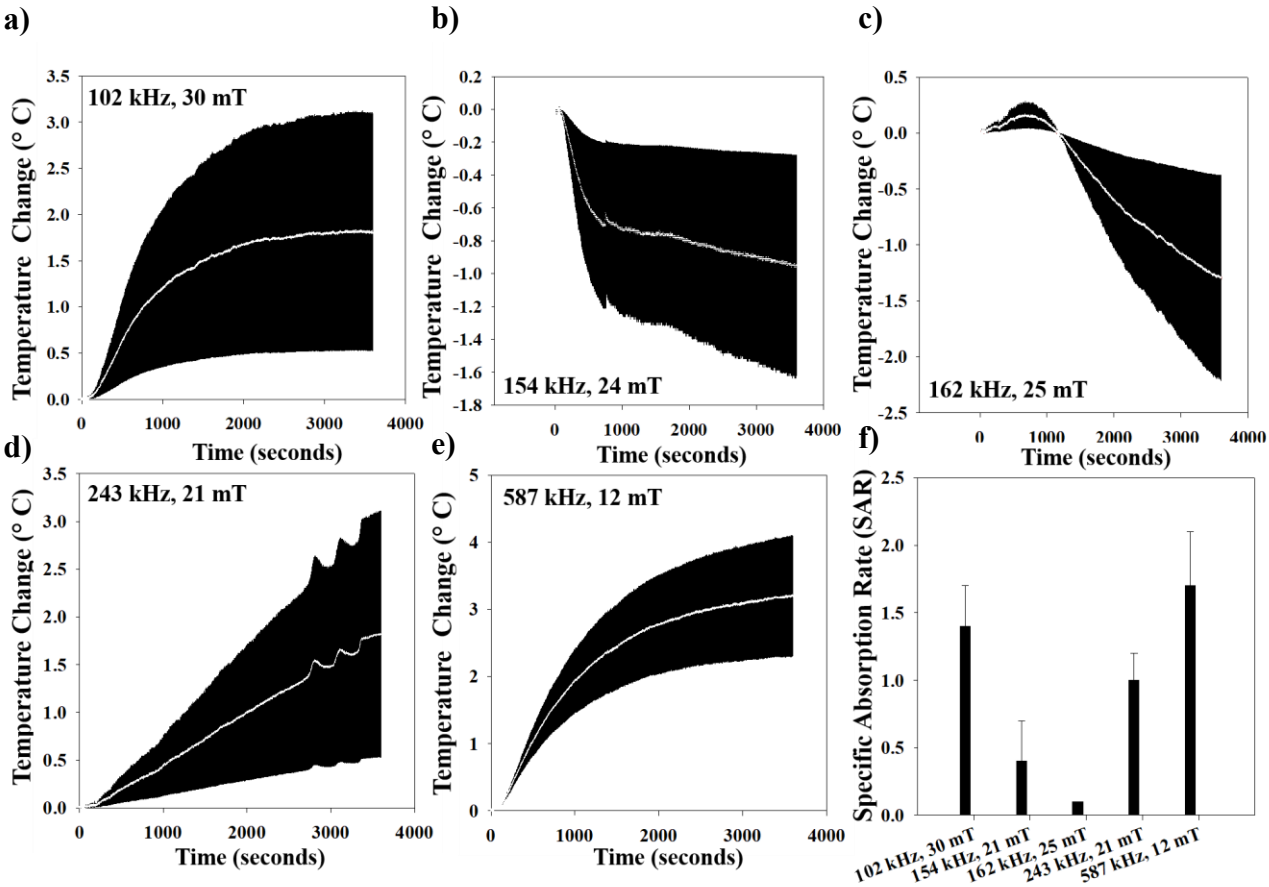

Figure 3.7 - a), b), c), d) and e) Temperature change as function of time under different AMF conditions for phase transferred IONPs_oleate particles. The shaded regions (shown in black) show the error in temperature produced. f) Specific absorption rates (SAR) (W/g) for phase transferred IONPs_oleate particles at different AMF conditions.

In Figure 3.8 – a) and b) a comparison of the temperature progression vs time and SARs for magnetite (Fe_3O_4) nanoparticles (NPs) and phase transferred IONPs_oleate particles are shown, respectively. The experimental runs in Figure 3.8 – a) is shown up to 10 mins. Both the experiments were performed at AMF condition (587 kHz, 12 mT).

The temperature and pH based physico-chemical properties of bare NGs is discussed in upcoming section 3.3. It is important to understand the properties of bare NGs which was further utilized in synthesizing hybrid NGs (containing phase transferred IONPs).

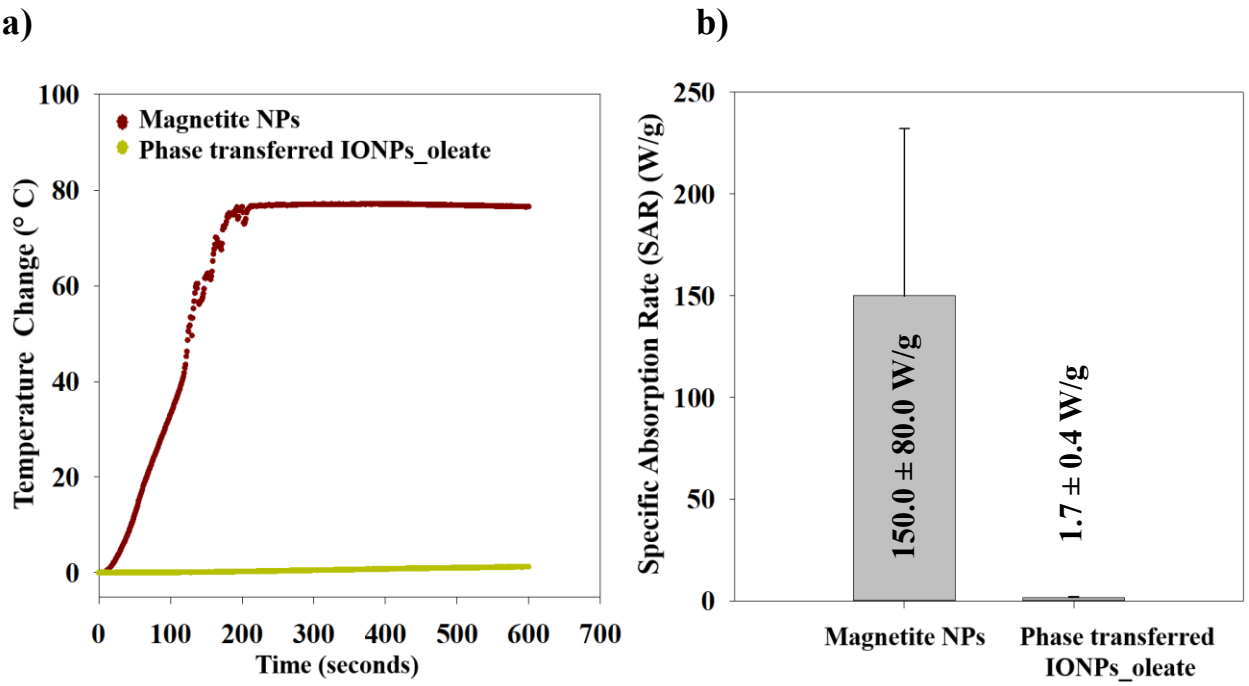

Figure 3.8 - a) Comparative study of temperature change (° C) as function of time (seconds) between magnetite NPs and phase transferred IONPs_oleate particles. The experimental run was performed at optimized AMF condition (587 kHz, 12 mT). b) Comparison of specific absorption rates (SAR) (W/g) of magnetite NPs and phase transferred IONPs_oleate particles.

3.3. N-isopropyl Acrylamide-Acrylic Acid Nanogels

The NGs were used with phase transferred IONPs to synthesize hybrid NGs to investigate thermal, pH and magnetic properties for drug delivery applications. This section is divided in three subsections. The first subsection will start with presenting amount of NGs obtained per batch. The second and third subsections will involve study of thermal and pH-responsive properties of NGs using DLS.

3.3.1. Synthesized Amounts

Seven batches of NGs were synthesized. The NGs amount obtained per batch is shown in Table 3.3. The average NGs yield obtained was 156.9 ± 9.8 mg. Samples from these batches were further taken for characterization to understand different properties as discussed in the upcoming parts.

Table 3.3 – NGs amounts obtained per batch.

No of batches	Obtained amounts (mg)	Average amount (mg)
1	143.4	156.9 ± 9.8
2	165.2	
3	152.0	
4	156.0	
5	162.4	
6	170.8	
7	148.2	

3.3.2. Thermo-responsive Properties

The hydrodynamic sizes at 25 °C and 45 °C for seven batches of NGs is shown in Figure 3.9 – a). All the NGs batches showed collapse in size when the temperature was increased from 25 °C to 45 °C. The average size of NGs for seven batches at 25 °C and 45 °C was 250 ± 20 nm and 93 ± 2 nm, respectively. NGs from batch 1 was taken and the collapse in hydrodynamic diameter was studied as function of temperature. The diameter of NGs were recorded at different temperatures using DLS during heating and cooling cycles. The obtained diameters at different temperature points were used to calculate normalized volumetric collapses of NGs using Equation 17.

$$\alpha = (D/D_0)^3 \quad (17)$$

where D – hydrodynamic diameter at specific temperature, D_0 – hydrodynamic diameter at 25 ^oC.

The parameter (α) representing volumetric collapse of NGs was plotted as function of temperature as shown in Figure 3.9 - b). The heating and cooling dataset of temperature vs normalized volumetric collapses (α) was fitted with a five parameter Gaussian curve. The R^2 values obtained for both fitted heating and cooling datapoints was ~ 0.99, which showed good fitting (shown in Table 3.5). The fitted curves were replotted using a Matlab® code to calculate the Volume Phase

Transition Temperature (VPTT) of NGs systems (discussed in detail in Chapter 2, Section 2.3.7). The calculated VPTT of NGs is shown in Table 3.6.

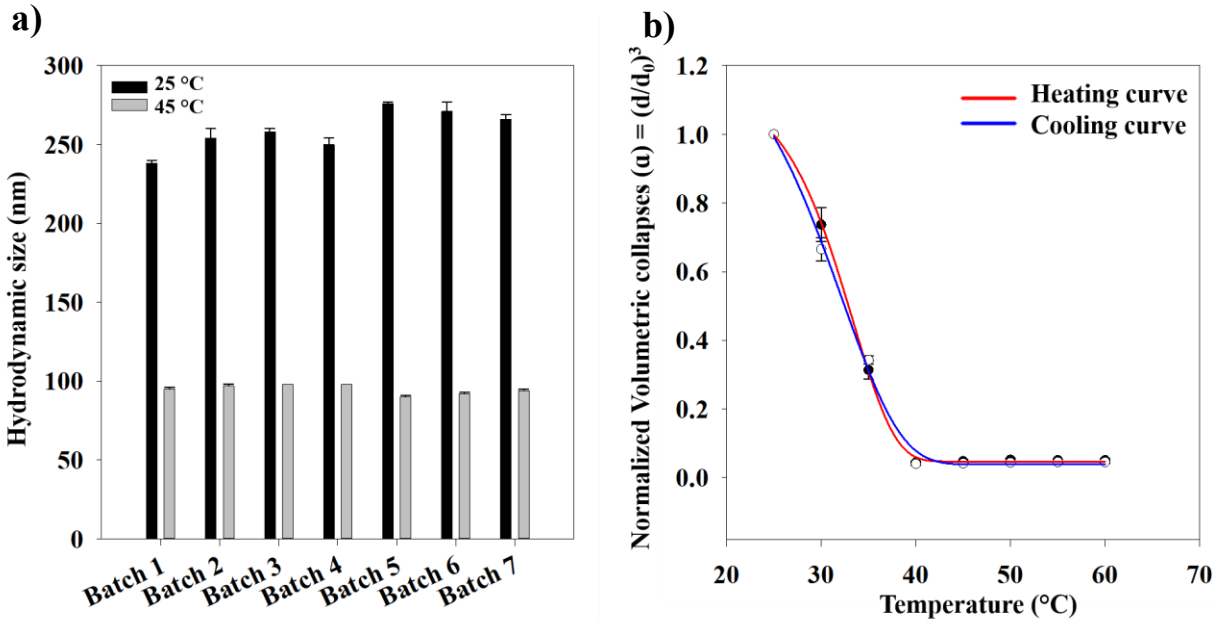

Figure 3.9 - a) Shows the hydrodynamic sizes (nm) of seven batches of NGs at 25 °C and 45 °C, respectively using DLS. b) Shows the volumetric collapse (VCE) of NGs as function of temperature (25 – 60 °C) during consecutive cycles of heating and cooling.

3.3.3. pH-responsive Properties

The combined effect of temperature and pH on hydrodynamic size of NGs is shown in Figure 3.10. NGs from batch 1 was taken to understand pH-responsive properties. Sizes of NGs at two different pH conditions (4.2 and 3.5) were obtained at specific temperatures of 25 °C, 40 °C and 45 °C.

The NGs was later utilized with phase transferred IONPs for synthesizing hybrid NGs which is shown in next section.

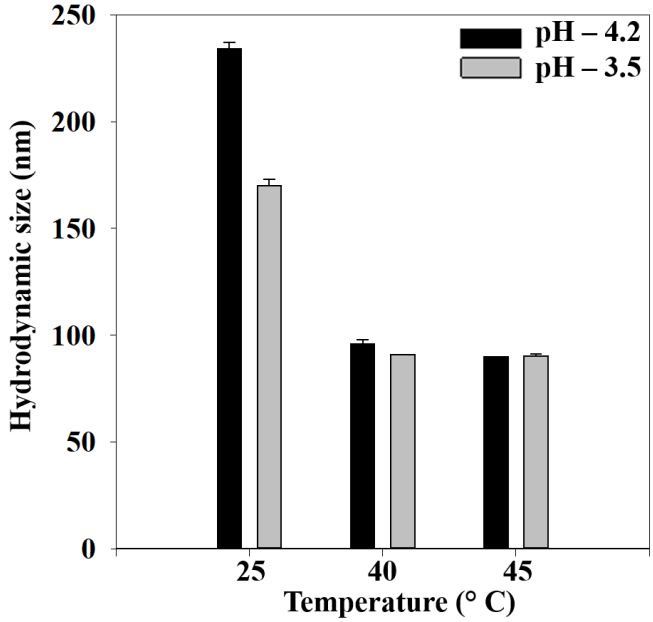

Figure 3.10 – Hydrodynamic sizes of NGs at specific temperatures of 25 °C, 40 °C and 45 °C at pH – 4.2 and 3.5, respectively measured using DLS.

3.4. Hybrid NGs: NGs with Phase Transferred IONPs

Phase transferred IONPs was used with pNIPAm-aac (NGs) nanogels to synthesize multi-functional hybrid NGs with thermal, pH and magnetic properties. This section is divided into two subsections. Firstly thermal, pH and magnetic properties of NGs with phase transferred IONPs_oleate particles will be shown and similarly the second subsection will cover NGs with phase transferred IONPs_penta particles.

3.4.1. NGs with Phase Transferred IONPs_oleate Particles

NGs with phase transferred IONPs_oleate particles were synthesized using three different techniques – 1) in-situ, 2) post, 3) addition (discussed in Chapter 2, Section 2.2.9). The hybrid NGs obtained from these techniques is referred to as NGs_insitu, NGs_post and NGs_added, respectively. Firstly, amount of hybrid NGs obtained with different techniques will be presented. Next, thermal, pH and magnetic properties of hybrid NGs will be understood. Lastly, the hybrid NGs were separated magnetically (with a neodymium magnet) to collect the magnetic bottom product (discussed in Chapter 2, Section 2.2.9). The bottom product was analyzed to understand

the interaction between NGs, and phase transferred IONPs. The magnetically separated samples is referred to as NGs_insitu magnetically separated, NGs_post magnetically separated and NGs_added magnetically separated, respectively.

3.4.1.1. Synthesized Amounts

The different amounts of phase transferred particles used for in-situ, post and addition techniques are shown in Table 3.4. The obtained amounts of hybrid NGs per batch is also included in Table 3.4. Hybrid NGs containing the highest amount of phase transferred particles (4 mg) synthesized using three different techniques were later characterized to understand its thermal, pH and magnetic properties.

Table 3.4 – Hybrid NGs amount obtained per batch.

Hybrid NGs	Amount of phase transferred IONPs_oleate used (mg)	Obtained amount (mg)
NGs_insitu	0.8	175.3
	1.0	163.2
	1.3	152.7
	2.0	158.0
	3.0	167.4
	4.0	170.8
NGs_post	4.0	145.2
NGs_added	4.0	162.0

3.4.1.2. Thermo-responsive Properties

The thermo-responsive properties of hybrid NGs synthesized using in-situ, post and added techniques, respectively is shown in Figure 3.11 and Figure 3.12, respectively. Figure 3.11 - a) shows the hydrodynamic sizes of NGs_insitu particles at 25 ºC and 45 ºC, as function of different masses of phase transferred IONPs_oleate used. The first point on the x-axis (0 mg) in Figure 3.11 - a) stands for hydrodynamic size of bare NGs (without phase transferred IONPs) (discussed in Section 3.3). The hydrodynamic size of bare NGs was replotted to compare with hybrid NGs. The

highest mass of phase transferred IONPs_oleate particles used to synthesize NGs_insitu system was 4 mg. Same amount of phase transferred particles (4 mg) was chosen to synthesize hybrid NGs using post and added techniques. Henceforth, comparison of hydrodynamic sizes of NGs_insitu, NGs_post and NGs_added particles obtained from three different techniques at 25 ºC and 45 ºC is shown in Figure 3.11 – b).

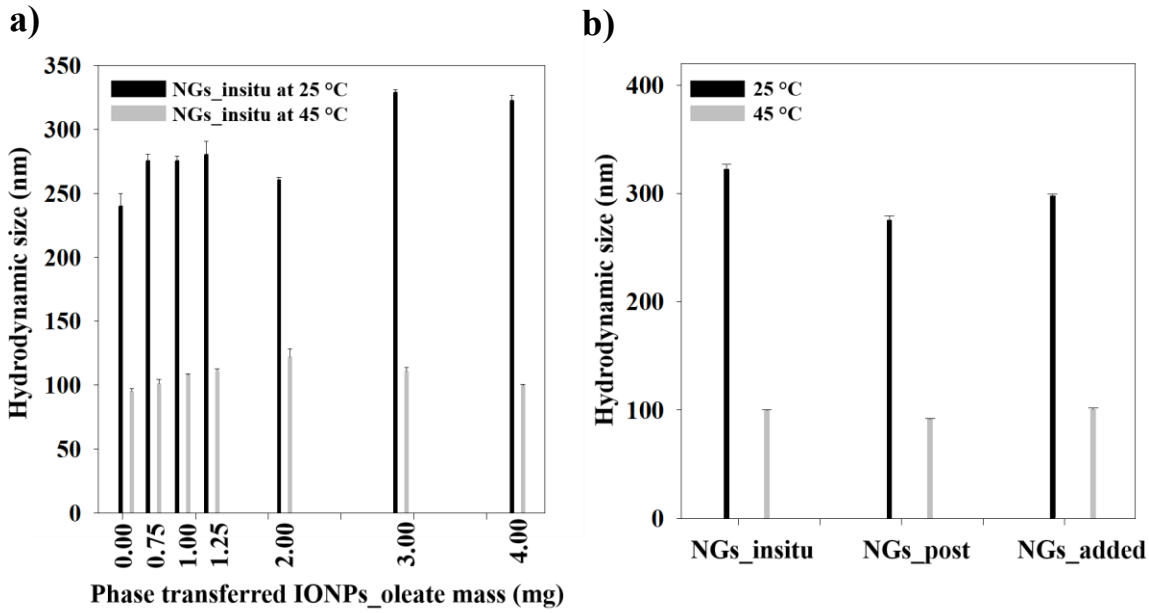

Figure 3.11 a) – Hydrodynamic sizes (nm) of NGs_insitu particles at 25 ºC and 45 ºC, respectively with different amounts (mg) of phase transferred IONPs_oleate. b) Hydrodynamic sizes (nm) of NGs_insitu, NGs_post and NGs_added particles with phase transferred IONPs_oleate (4 mg) at 25 ºC and 45 ºC, respectively.

The comparison of the volumetric collapse efficiencies VCE (%) at 45 ºC for bare NGs, NGs_insitu, NGs_post and NGs_added systems, respectively is shown in Figure 3.12 a). The VCE (%) of the nanogel systems at 45 ºC is calculated using Equation 18.

$$VCE\ (\%) = [1 - (D_{45}/D_{25})^3] * 100 \quad (18)$$

where D_{45} = Hydrodynamic diameter at 45 ºC, D_{25} = Hydrodynamic diameter at 25 ºC.

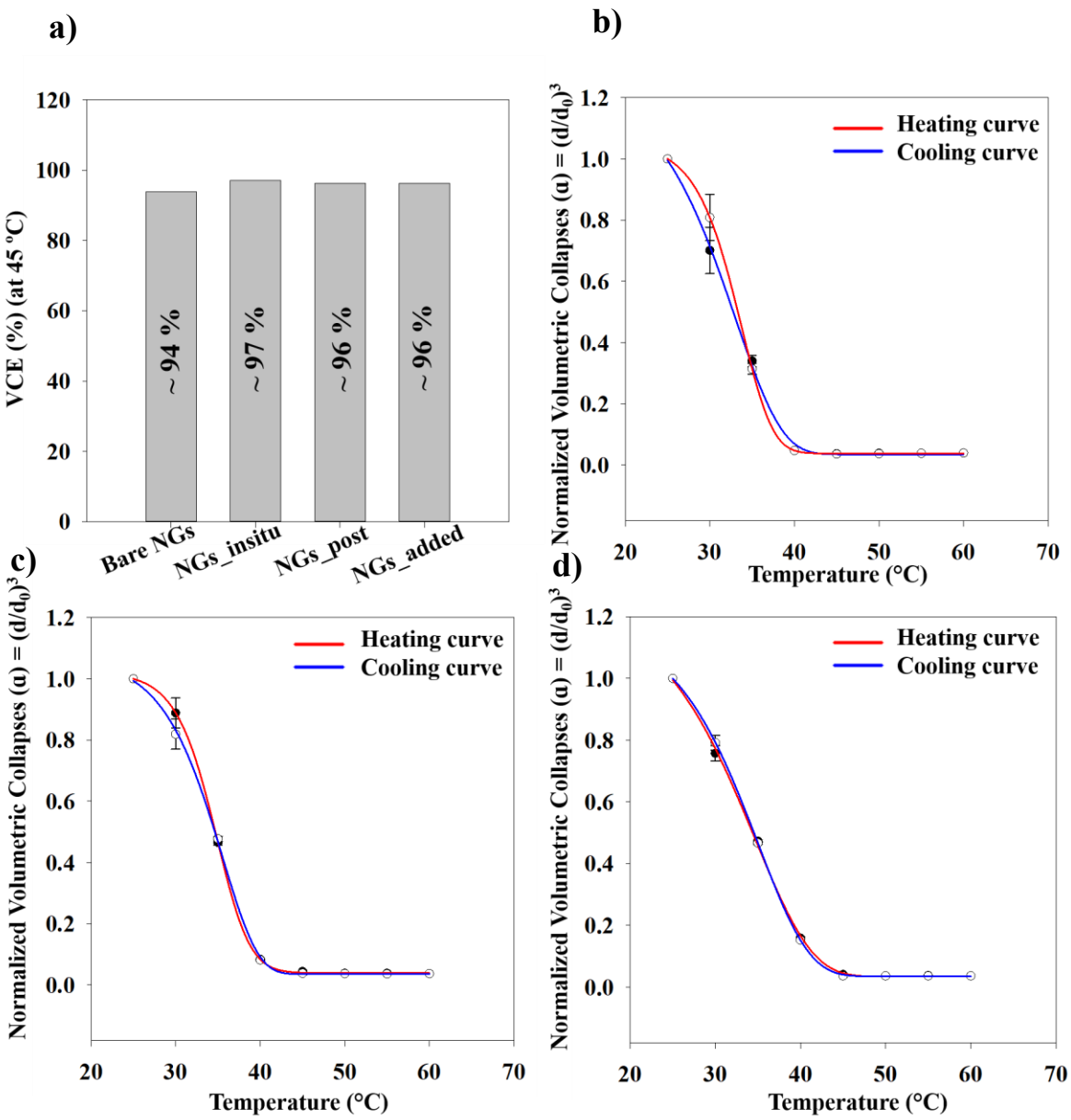

Figure 3.12 a) – Comparison of the volumetric collapse efficiencies VCE (%) at 45 ºC for bare NGs, NGs_insitu, NGs_post and NGs_added particles (with phase transferred IONPs_oleate (4 mg)). b), c) and d) Normalized volumetric collapses of NGs_insitu, NGs_post and NGs_added particles (with phase transferred IONPs_oleate (4 mg)) as function of temperature (25 – 60 °C) during consecutive cycles of heating and cooling.

The normalized volumetric collapse of NGs_insitu, NGs_post and NGs_added systems containing phase transferred IONPs_oleate (4 mg) as function of temperature (25 – 60 ºC) is shown in Figure 3.12 – b), c) and d), respectively. The hydrodynamic diameters obtained using DLS were used to calculate volumetric collapses as function of temperature using Equation 17. The heating and cooling dataset of temperature vs normalized volumetric collapses (α) was fitted with a five

parameter Gaussian curve to calculate VPTT of hybrid NGs systems. All the R^2 values obtained for fitted heating and cooling datapoints for three hybrid NGs was ~ 0.99 (shown in Table 3.5). The calculated VPTTs of hybrid NGs is shown in Table 3.6.

3.4.1.3. pH-responsive Properties

The combined effect of temperature and pH on hydrodynamic size (nm) of NGs_insitu and NGs_post systems are shown in Figure 3.13 – a) and b), respectively. Sizes of NGs_insitu particles at two different pH conditions (4.8 and 3.5) were obtained at specific temperatures of 25 °C and 40 °C. Likewise, for NGs_post particles the sizes were also obtained at specific temperatures of 25 ºC and 40 ºC maintaining pH conditions (4.5 and 3.5). At more acidic pH (3.5), the hydrodynamic sizes were smaller and hence collapse of hybrid NGs was higher. The magnetic properties of hybrid NGs is shown next which can be employed for different biomedical applications.

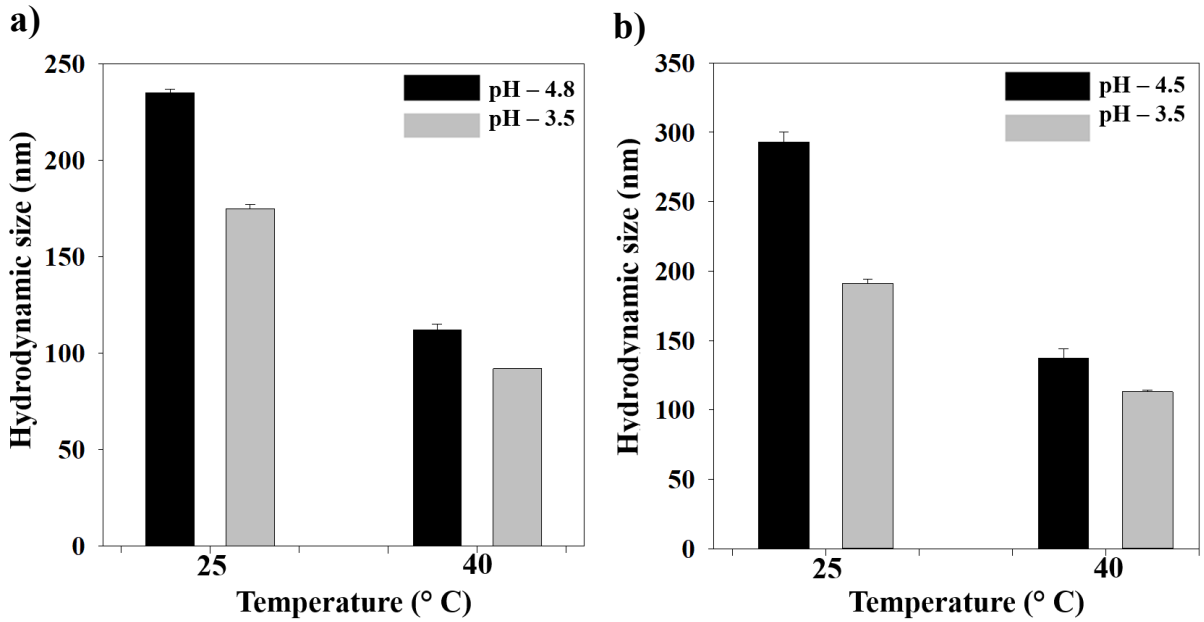

Figure 3.13 a) – Hydrodynamic sizes of NGs_insitu particles at specific temperatures of 25 °C and 40 °C at pH – 4.8 and 3.5, respectively. b) Shows the hydrodynamic sizes of NGs_post particles at specific temperatures of 25 °C and 40 °C at pH – 4.5 and 3.5, respectively.

3.4.1.4. Magnetic Properties

The magnetic hysteresis of NGs_insitu, NGs_post and NGs_added particles is shown in Figure 3.14 – a). The maximum external applied magnetic field was 1 T. All the hybrid NGs were superparamagnetic at room temperature. The measured saturation magnetization of NGs_insitu, NGs_post and NGs_added particles was 0.03 emu/g, 0.06 emu/g and 0.01 emu/g, respectively. The saturation magnetizations (emu/g) for NGs_insitu systems as function of mass of phase transferred IONPs_oleate particles used is shown in Figure 3.14 – b). The saturation magnetizations increased with increase in mass of phase transferred particles.

In the upcoming part, the magnetic part from hybrid NGs was separated magnetically (using a neodymium magnet) and its thermo-responsive properties was studied.

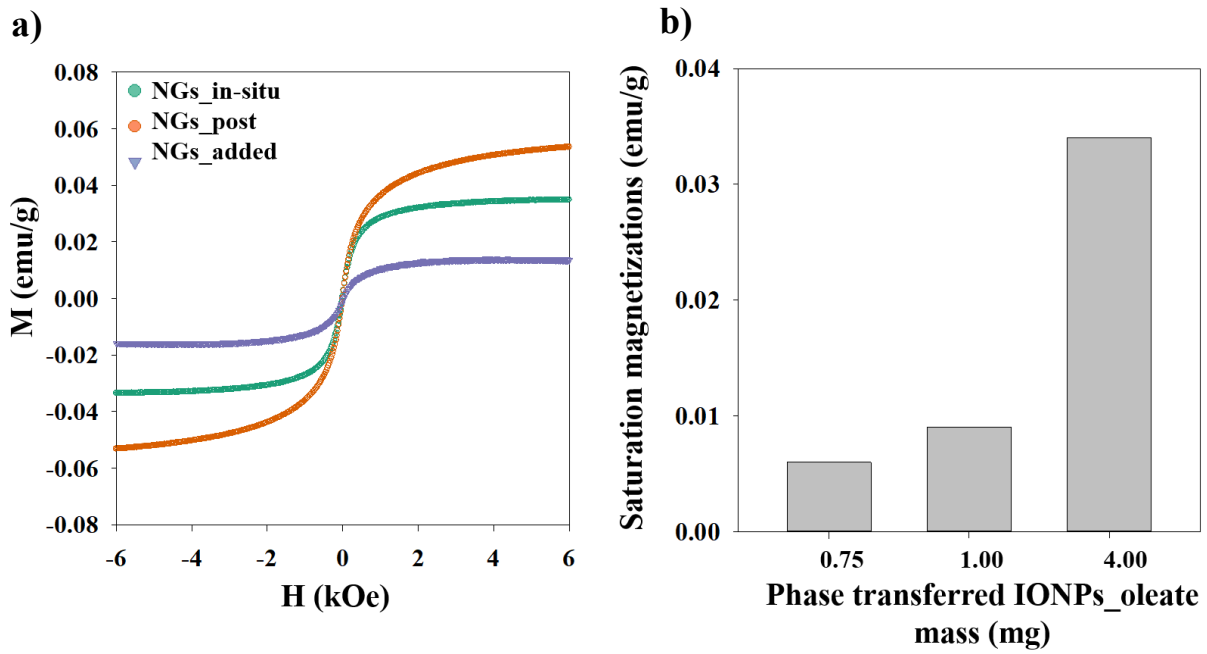

Figure 3.14 a) – Magnetic hysteresis (M vs H) of NGs_insitu, NGs_post and NGs_added particles containing phase transferred IONPs_oleate (4 mg) at room temperature. b) Saturation magnetizations (emu/gm) of NGs_insitu particles as function of mass of phase transferred IONPs_oleate (mg) used.

3.4.1.5. Magnetically Separated Hybrid NGs

The hybrid NGs were separated magnetically and its thermo-responsive properties were studied. The separated hybrid NGs is referred to as NGs_post, NGs_insitu and NGs_added magnetically

separated particles. The hydrodynamic sizes for NGs_post, NGs_insitu and NGs_added magnetically separated particles at specific temperatures (25 ºC, 45 ºC and 60 ºC) is shown in Figure 3.15.

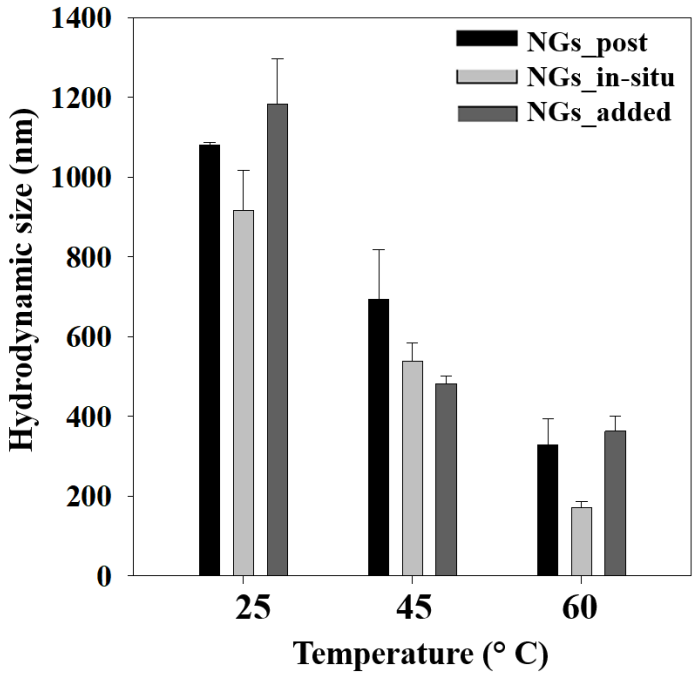

Figure 3.15 – Hydrodynamic sizes (nm) at 25 ºC, 45 ºC and 60 ºC respectively for NGs_post, NGs_insitu and NGs_added magnetically separated particles.

Table 3.5 – R^2-values showing fitting of heating and cooling data points with five-parameter sigmoidal curve.

NGs systems	Heating Datapoints – R^2	Cooling Datapoints – R^2
Bare NGs	~ 0.99	~ 0.99
NGs_insitu	~ 0.99	~ 0.99
NGs_post	~ 0.99	~ 0.99
NGs_added	~ 0.99	~ 0.99

Table 3.6 – Calculated VPTTs of bare NGs, hybrid NGs and hybrid NGs magnetically separated particles.

NGs systems	Volume Phase Transition Temperature (VPTT) (º C)
Bare NGs	35.9 ± 0.3
NGs_insitu	36.8 ± 0.2
NGs_post	35.7 ± 0.2
NGs_added	37.6 ± 0.1

3.4.2. NGs with Phase Transferred IONPs_penta Particles

The phase transferred IONPs_penta particles were also used with NGs to synthesize hybrid NGs. The hybrid NGs were synthesized using insitu and post technique. The different amounts of phase transferred particles used for synthesis of hybrid NGs using insitu and post techniques are shown in Table 3.7. The obtained amounts of hybrid NGs per batch is also included in Table 3.7. Hybrid NGs containing the highest amount of phase transferred particles (4 mg) synthesized using different techniques were later characterized to understand it thermal and magnetic properties.

Table 3.7 - Hybrid NGs amount (mg) obtained per batch.

Hybrid NGs	Amount of phase transferred IONPs_oleate used (mg)	Obtained amount (mg)
	1.0	156.2
NGs_insitu	1.3	155.9
	1.5	156.0
	4.0	168.7
NGs_post	4.0	149.4

3.4.2.1. Thermo-responsive Properties

The thermo-responsive properties of hybrid NGs synthesized using in-situ and post techniques, is shown in Figure 3.16. Figure 3.16 - a) shows the hydrodynamic sizes of NGs_insitu particles at 25 ºC and 45 ºC, as function of different masses (mg) of phase transferred IONPs_penta particles. The hydrodynamic size of bare NGs is also plotted with NGs_insitu systems for comparison as shown in Figure 3.16 – a). The hydrodynamic sizes (nm) of NGs_insitu and NG_post systems containing phase transferred particles (4 mg) at 25 ºC and 45 ºC respectively is shown in Figure 3.16 – c).

The volumetric collapse efficiency (VCE) (%) at 45 ºC for NGs_insitu and NGs_post systems is shown in Figure 3.16 – d). The VCE (%) of the particles at 45 ºC is calculated using Equation 18. The collapse of NGs_insitu system containing phase transferred particles (4 mg) as function of temperature (25 – 60 ºC) is shown in Figure 3.16 – b). The hydrodynamic diameters obtained using DLS were used to calculate normalized volumetric collapses as function of temperature using Equation 17 and in turn VPTT of the systems (discussed similarly in Subsection 3.3.2). The calculated VPTT of NGs_insitu system is shown in Table 3.9.

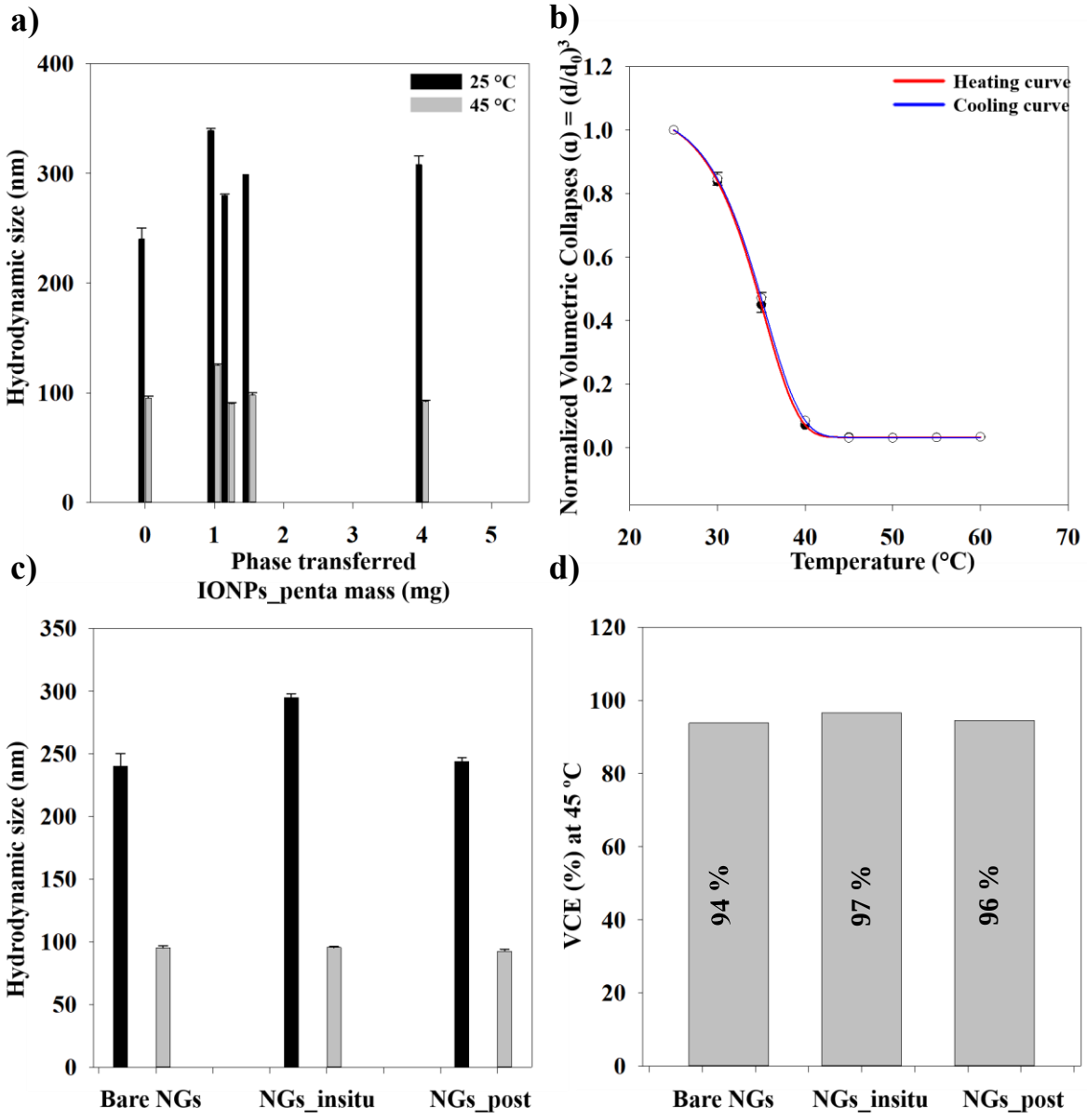

Figure 3.16 a) – Hydrodynamic sizes of NGs_insitu particles at 25 ºC and 45 ºC, respectively with different amounts of phase transferred IONPs_penta particles. b) Normalized volumetric collapses of NGs_insitu particles (with phase transferred IONPs_penta (4 mg)) as function of temperature (25 – 60 °C) during consecutive cycles of heating and cooling. c) Comparison of the hydrodynamic sizes of bare NGs, NGs_insitu and NGs_post particles with phase transferred IONPs_penta (4 mg) at 25 ºC and 45 ºC, respectively. d) Comparison of the volumetric collapse efficiencies (VCE) (%) at 45 ºC for bare NGs, NGs_insitu, NGs_post particles (with phase transferred IONPs_penta (4 mg)).

Table 3.8 – R^2-values showing fitting of heating and cooling data points with five-parameter sigmoidal curve.

NGs systems	Heating Datapoints – R^2	Cooling Datapoints – R^2
Bare NGs	~ 0.99	~ 0.99
NGs_insitu	~ 0.99	~ 0.99

Table 3.9 – Calculated VPTTs of bare NGs, NGs_insitu particles

NGs systems	Volume Phase Transition Temperature (VPTT) (º C)
Bare NGs	35.9 ± 0.3
NGs_insitu	36.8 ± 0.1

3.4.2.2. Magnetic Properties

The magnetic hysteresis of NGs_insitu particles is shown in Figure 3.17. The maximum external applied magnetic field was 1 T. The measured saturation magnetization of the system was 0.0013 emu/g.

The obtained hybrid NGs was further utilized as drug-delivery systems (DDS). In the following section, loading and release of model protein, Cytochrome C (cyt C) from hybrid NGs is studied. The effect of physico-chemical properties of hybrid NGs on release mechanisms is investigated.

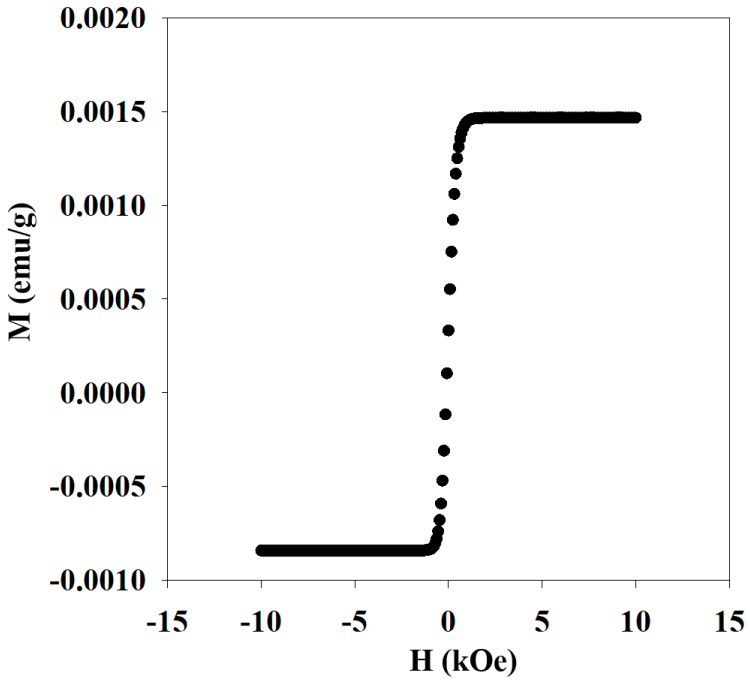

Figure 3.17 - Hysteresis (M vs H) loop of NGs_insitu particles containing phase transferred IONPs_penta (4 mg) particles at room temperature.

3.5. Release Study of Cytochrome C

The hybrid NGs were loaded with a model drug, cyt C. The release studies were performed for period of 20 hours at 40 ºC and acidic pH (3.5) and the release of cyt C was detected using UV-Vis spectroscopy. This section is divided into two subsections. Firstly, loading (L.E) and encapsulation efficiencies (E.E) of cyt C with bare and hybrid NGs systems (NGs_insitu, NGs_post and NGs_added) are presented. In the second subsection, the release of cyt C at condition 40 °C and 3.5 pH is shown.

3.5.1. Release of Cytochrome C

The calculated loading and encapsulation efficiencies (L.E and E.E) for different hybrid NGs systems containing phase transferred IONPs_oleate particles is shown in Table 3.10. The highest L.E and E.E was seen for bare NGs and the lowest values were obtained for NGs_added system. The standard deviation in L.E and E.E values shown in Table 3.10 for NGs and NGs_insitu systems was calculated over 4 samples.

Table 3.10 - Loading and encapsulation efficiencies (L.E and E.E) of NGs and hybrid NGs systems.

Samples	Loading efficiency (L.E) (%)	Encapsulation efficiency (E.E) (ug/mg)
NGs	85 ± 12	255 ± 36
NGs_insitu	70 ± 10	212 ± 30
NG_post	91	276
NG_added	68	206

The release of cyt C from bare NGs, NGs_insitu, NGs_post and NGs_added systems as function of time (hours) is shown in Figure 3.18. The release condition was maintained at 40 ºC and 3.5 pH. From Figure 3.18, the highest amount of cyt C at the end of ~ 20 hours was released from NGs_post system (~ 59 %) and the lowest amount released was seen from NGs_added system (~ 34%). It should be noted that for bare NGs systems, the release data is shown up to 10 hours. The L.E for the batches of NGs, NGs_insitu, NGs_post and NGs_added systems (for which the release studies are shown) was 87 %, 80 %, 91 % and 68 % respectively.

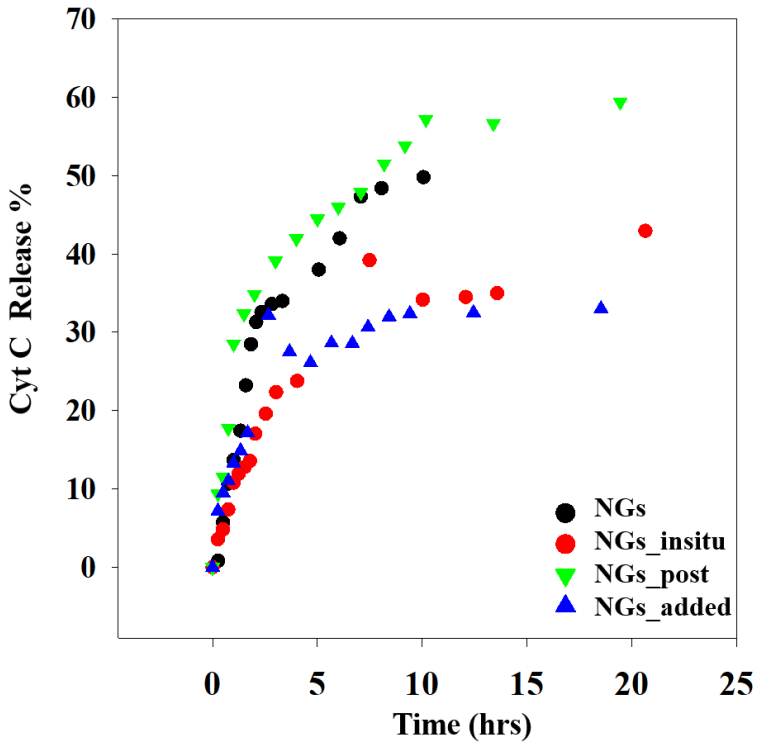

Figure 3.18 – Cytochrome C release (%) as function of time for bare NGs, NGs_insitu, NGs_post and NGs_added systems.

In next section, release of cyt C from hybrid NGs is studied on exposure to alternating magnetic field (AMF) and the real time temperature of the system was constantly monitored.

3.6. Release Study of Cytochrome C: with Alternating Magnetic Field

The release of cytochrome C from hybrid NGs containing phase transferred IONPs_oleate particles were performed on exposure to alternating magnetic field (AMF) while the temperature of the system was monitored real time. The magnetherm setup was utilized to perform this study (discussed in Chapter 2, Section 2.3, Subsection 2.3.10). The release studies were performed for period of 10 hours. This section is divided in two subsections. In the first subsection, two different conditions in which release study was performed is shown. In the second part, the release of cytochrome C from hybrid NGs is presented with the optimized release conditions.

3.6.1. Dynamic Release Conditions

Release study of cyt C was performed at dynamic temperature conditions. The real-time temperature at which the NGs systems were exposed varied as function of time, which was recorded with a fibre optic probe (shown in Chapter 2, Subsection 2.3.10, Figure 2.18 – a)). Dynamic temperature profile was recorded for 1 hour. The average and standard deviation (shaded region) of obtained temperature profiles were taken for five runs (shown in Figure 3.19 – a)), thus showing the dynamic condition was repeatable. Release of cyt C from NGs systems were performed on exposure to above stated dynamic condition. Temperature profiles for 1 hour will be referred to as 1 cycle for the entire study. The total duration of release study was performed for 10 cycles (i.e., 10 hours). This dynamic condition will be referred to as TP_WMF (temperature profile without magnetic field).

Similarly, dynamic temperature profile with AMF was also recorded for 1 hour. The average and standard deviation of obtained temperature profiles were taken for five runs (shown in Figure 3.19 – b)) thus showing that this dynamic condition was also repeatable. Release of cyt C was also performed for 10 cycles under this condition. The dynamic condition in this case will be referred to as TP_MF (temperature profile with magnetic field).

Lastly, comparison of TP_WMF and TP_MF conditions is shown in Figure 3.19 – c). The average

temperature values from both profiles were fitted with five parameter sigmoidal curve and compared. The overall temperature points for condition TP_WMF was comparatively higher as compared to TP_MF. The obtained R^2 values from both fitted TP_MF and TP_WMF profiles was ~ 0.99. The standard deviation of the temperature profiles overlapped but still differences were prominent between the two profiles especially at temperatures above 35 ºC as seen from Figure 3.19 – a) and b) respectively.

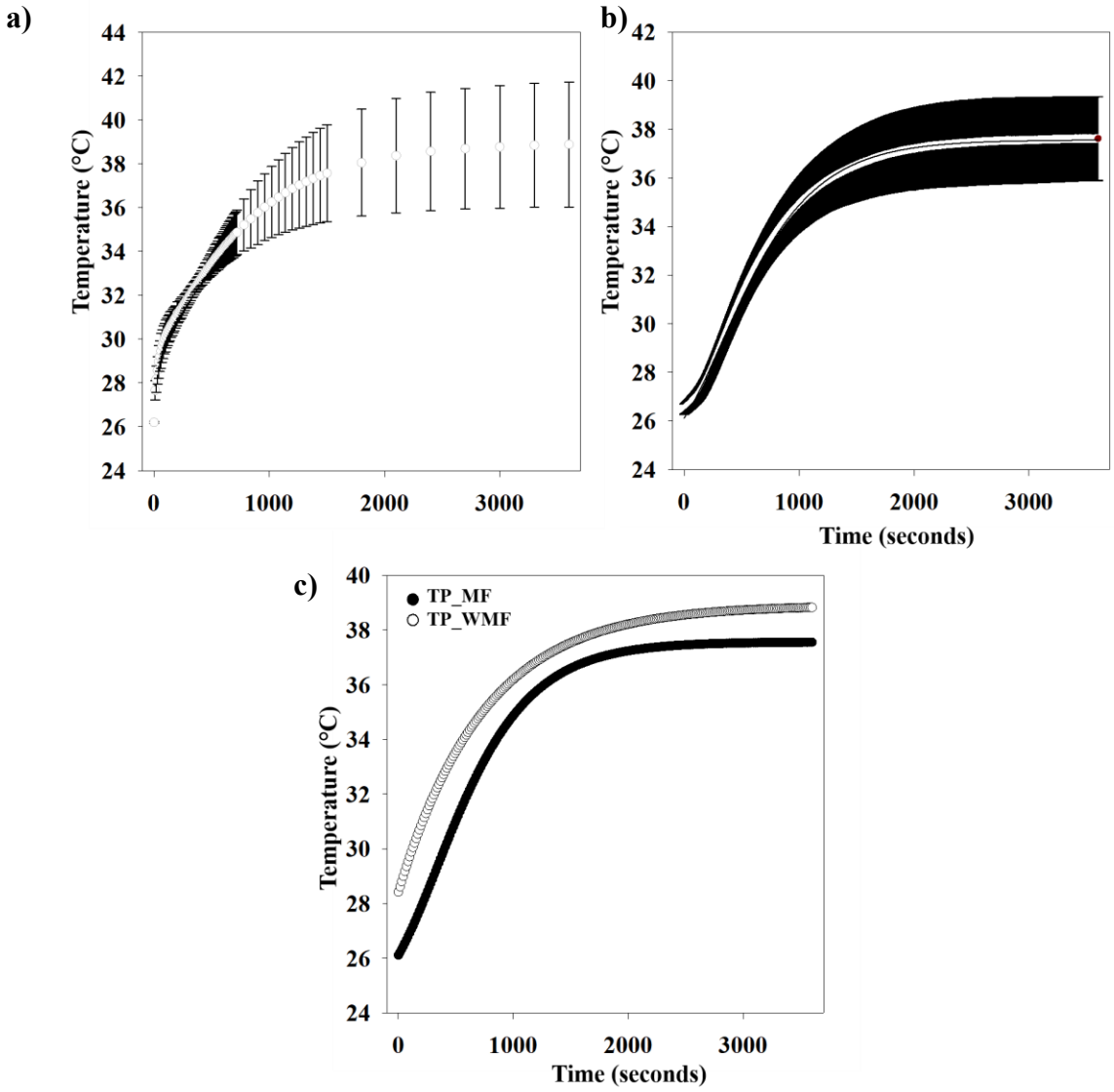

Figure 3.19 – a) Temperature profile without AMF as function of time used as release condition (TP_WMF). b) Temperature profile with AMF as function of time used as release condition (TP_MF)); shaded region shows standard deviation in temperature c) Fitted average values of TP_WMF and TP_MF with five parameter sigmoidal curve.

3.6.2. Release of Cytochrome C: With Alternating Magnetic Field

The release study of cyt C was performed at dynamic conditions – TP_WMF and TP_MF to understand the effect of AMF. For condition TP_MF, the magnetic field amplitude and frequency used was 12 mT and 587 kHz, respectively. The field parameters were optimized with phase transferred IONPs_oleate particles (shown in Section 3.2, Subsection 3.2.5). NGs and hybrid NGs systems were exposed to TP_WMF and TP_MF for 10 cycles. Each cycle lasted for 1 hour. Therefore, the release studies were performed for period of 10 hours. The release of cyt C was analyzed using UV-vis after each cycle. The release (%) as function of number of exposed cycles at condition TP_MF is shown in Figure 3.20 – b). For release study, bare NGs and hybrid NGs systems (with phase transferred IONPs_oleate particles) were used. Another system was introduced to understand the effect of increasing amounts of phase transferred IONPs_oleate particles on release of cyt C. In this system, known amount of phase transferred IONPs_oleate particles (10 mg) was simply added to bare NGs system already loaded with cyt C and release was performed under condition - TP_MF. The details of this system is attached in Appendix B. This system is referred to as Loaded NGs_added. From Figure 3.20 – b) under condition TP_MF, maximum and minimum release (%) of cyt C was observed from bare NGs (~ 72%) and Loaded NGs_added (~ 25 %) after exposure for 10 cycles. In this study, all the systems had loading efficiencies (L.E) 77 ± 1 %. In Figure 3.20 – a), the release of cyt C from NGs_insitu systems were shown at two different conditions - TP_MF and TP_WMF to understand the effect of AMF on release profiles.

In upcoming Chapter 4, the results presented in this chapter will be discussed in detail.

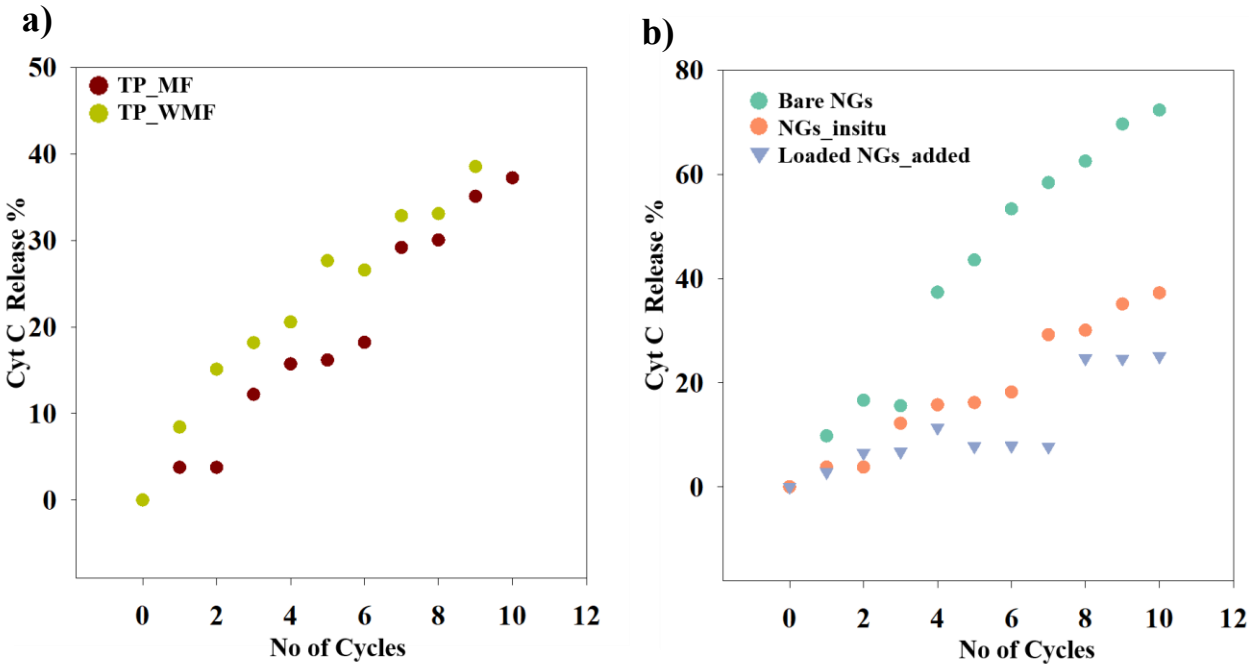

Figure 3.20 – a) Comparison of cyt C release (%) from NGs_insitu particles at two different conditions TP_MF and TP_WMF for 10 cycles. b) Release of cytochrome C (%) from bare NGs, NGs_insitu and Loaded NGs_added systems on exposure to condition TP_MF for 10 cycles.

Chapter 4: Discussion

In this chapter, the results will be discussed in the same chronological order as presented in Chapter 3. In the first section, size, crystallographic, and magnetic properties of iron oxide nanoparticles (IONPs) will be discussed. The second, third and fourth sections will involve detailed discussion on properties of phase transferred IONPs, bare NGs and hybrid NGs, respectively. In fifth section, release profiles of cytochrome C (cyt C) from NGs systems under different conditions of elevated temperatures and acidic pH will be fitted with conventional drug delivery models and analyzed. Lastly, release of cyt C from bare and hybrid NGs on exposure to external AMF conditions will be discussed.

4.1. Iron Oxide Nanoparticles

The properties of IONPs_oleate and IONPs_penta particles derived from two different precursors – 1) iron oleate and 2) iron pentacarbonyl will be discussed in this section. This section is divided in two subsections. The obtained sizes imaged using High Resolution Transmission Electron Microscopy (HRTEM) and crystallographic and magnetic properties of IONPs are discussed accordingly in each subsection.

4.1.1. Size Characterization of Iron Oxide Nanoparticles

The average sizes of IONPs_oleate particles (16 ± 2 nm) was larger as compared to IONPs_penta particles (8 ± 1 nm) (shown in Figure 3.1 - a) and b)). The size ranges obtained for both the systems was in accordance with previous work done by other research groups (29, 63). The formula used for calculating polydispersity index (PDI) was taken from previous works of Pusey et al. in which the PDI scale is defined between values 0-1 (72). Small value on the PDI scale corresponds to high monodispersity of the system. The PDI obtained for both the systems was ~ 0.1. Henceforth, both systems showed monodispersity which is an important criterion for applications in biomedicine relating to magnetically controlled drug release, magnetic detection and magnetic resonance imaging (MRI) due to homogeneous structural and magnetic properties of the IONPs systems (74).

4.1.2. Crystallographic and Magnetic Characterization of Iron Oxide Nanoparticles

IONPs_oleate particles exhibited characteristic peaks which showed dominant inverse cubic spinel structure of magnetite (75). There might also be presence of tetragonal maghemite phase (Fe_2O_3) occurring from oxidation of magnetite phase (Fe_3O_4) due to air exposure (63, 75). But only XRD is not enough to distinguish between the mentioned phases due to their close crystallographic structures. Also, the enhanced peak broadening effect seen due to small size of nanoparticles (< 20 nm) makes it even more difficult to quantify percentages of magnetite and maghemite phases (63). The broad peak at 2θ value – 19.8° is due to presence of organic ligand oleic acid which is used as stabilizing agent to control particle growth and aggregation (discussed in Chapter 1, Section 1.2, Subsection 1.2.2) (63, 76) .

IONPs_penta particles also showed presence of magnetite phase. But due to much smaller size of IONPs_penta particles (8 ± 1 nm) as compared to IONPs_oleate particles (16 ± 2 nm), the peak broadening effect was more pronounced. IONPs_penta particles formed core-shell structures as shown in a magnified image in Figure 3.1 – b). This was also seen in previous works done by research groups and it had also been studied that the core consisted of iron whereas the shell was composed of iron oxide (29, 77). It has been previously reported that IONPs_penta particles are more amorphous as compared to IONPs_oleate particles (29, 76). Henceforth, it may be due to amorphous nature of IONPs_penta particles as well as smaller size as compared to IONPs_oleate particles, the other standard diffraction peaks of magnetite at 30° and 62° were not detected. There might be presence of some maghemite phase due to air exposed oxidation of its outside shell, but it is difficult to understand using only XRD technique (29, 77).

The saturation magnetization (Ms) seen for IONPs_oleate particles (74.3 emu/g) was ~ 3.4 times higher as compared to IONPs_penta particles (21.9 emu/g) (shown in Figure 3.2 – c)). The obtained magnetization values for IONPs_penta systems were in close range with previous works performed by Singh et al (29). The lower magnetization value obtained for IONPs_penta particles is mainly due to two reasons – 1) nanoscale Kirkendall effect at room temperature and 2) small size and amorphous nature of core-shell IONPs_penta particles (29, 77). Kirkendall effect involves depletion and diffusion of iron core from the core-shell structures of IONPs_penta particles due to oxidation at room temperature. The Fe atoms from the core has higher outward rate of diffusion

as compared to inward diffusion rate of oxygen thus giving rise to unbalanced interfacial diffusion of Fe and O atoms. This gives rise to hollow or yolk-type structures. The transition from core-shell to hollow yolk-type structures had been previously studied to occur within 30 days (29). In amorphous IONPs_penta particles, the atomic magnetic moments have disordered orientation arising from random arrangement of atoms in the crystal structure. Also, at small sizes (less than 10 nm), the magnetic domains become non-existent which contributes to random alignment of magnetic moments (discussed in Chapter 1, Section 1.4, Subsection 1.4.2) (29, 77). It is due to both above-mentioned factors, the magneto-crystalline anisotropy (energy required to rotate the individual magnetic moments) reduces. Hence, less energy is required to thermally misalign the magnetic moments. Therefore, at room temperature (25 °C), the external applied field (1 T) (used during VSM characterization) was insufficient to completely overcome the thermal energy related disorderliness in magnetic moments and align all the moments in the field direction (77). It is for these reasons, that the saturation magnetization of IONPs_penta was significantly lower as compared to IONPs_oleate particles at room temperature.

In temperature vs susceptibility plot (shown in Figure 3.2 – d)), the observed T_B values for IONPs_penta particles (83 K) was much lower as compared to IONPs_oleate particles (234.3 K). This can again be attributed to low magneto-crystalline or magnetic anisotropic energy of IONPs_penta particles arising due to its smaller size and amorphous nature. The obtained T_B values for both the systems were higher as compared to previous work done by other research groups (29). It should be pointed out that T_B values are conventionally obtained from temperature vs magnetization plots. Therefore, T_B value shifts are seen in our study. Also, the susceptibility measurements were done at AC magnetic field conditions of 976 kHz which needs to be considered as it causes increase in T_B values (78).

In this section, crystallographic and magnetic properties of IONPs are discussed which are essential for surface engineering of IONPs for further applications in field of biomedicine. The IONPs were then phase transferred using sodium citrate to transfer from organic to aqueous media which will be discussed in next section.

4.2. Phase Transferred Iron Oxide Nanoparticles

This section is divided in four subsections. In the first subsection, properties of phase transferred particles in terms of hydrodynamic sizes and zeta potentials are discussed. In second and third subsections, stability of these particles under different conditions and magnetic properties are discussed, respectively. Lastly, heat production from phase transferred IONPs under different AMF conditions in terms of specific absorption rates (SARs) will be understood.

4.2.1. Hydrodynamic Size and Zeta Potential Measurements using Dynamic Light Scattering

The IONPs were successfully phase transferred from organic to aqueous media using sodium citrate. The carbonyl groups (C=O) of sodium citrate ionically interacts with the surface of IONPs resulting in the phase transfer process (63). The stabilization of phase transferred IONPs_oleate and IONPs_penta particles in water was seen by negative zeta potential values as shown in Figure 3.3 – b) and d) respectively. This is due to Na^+ counterions of sodium citrate which is charge compensated by populations of negatively charged OH^- ions of water forming an electrostatic double layer. Hence, the particles get electrostatically stabilized in water (37, 63). Batches of 10 and 12 experiments were performed to phase transfer IONPs_oleate and IONPs_penta particles, respectively which was used further in the study. The average hydrodynamic sizes and zeta potentials of IONPs_oleate and penta particles were similar with previous reported works, which showed repeatability of the process (37, 63).

4.2.2. Stability Studies of Phase Transferred IONPs

The temperature stability study (shown in Figure 3.4 – a) and b)) showed almost little to no change in hydrodynamic sizes and zeta potentials for both phase transferred IONPs_oleate and penta particles. This showed that sodium citrate coating on IONPs was also stable at temperatures of 45 °C and 60 °C. Later in this work, hybrid NGs (NGs containing phase transferred IONPs) were synthesized, and its properties were studied at higher temperatures of 45 °C and 60 °C. Henceforth, this study was important to understand the individualistic effect of temperature on phase transferred particles.

Storage of nanoparticles for extended periods of time are a big challenge due its extremely high specific surface area and reactivity (79). Thus, time-based stability study for period of two months

was also performed as shown in Figure 3.4 – c) and d), respectively. The hydrodynamic sizes (nm) and zeta potential (mV) for both system of particles, IONPs_oleate and IONPs_penta for extended periods of two months showed good stability.

The human biological systems have varying pH conditions starting from mildly alkaline to acidic like in digestive systems (80). Hence, pH stability range was also studied (shown in Figure 3.5 – a) and b)), as these particles will be later used for potential biomedical applications. At acidic conditions (pH ~ 3), increase in size resulting from agglomeration of the particles were observed. This is due to reducing electrostatic stability of the systems. During electrostatic stabilization of IONPs with sodium citrate, the carboxylic acid groups of sodium citrate remain in dissociated state forming carboxylate ions and Na^+ ions. The positive charge of Na^+ ions of sodium citrate get electrostatically balanced with negative OH^- ions, thus forming an electrical double layer. Sodium citrate has three ionizable carboxylic groups with pKa values (3.13, 4.76 and 6.4) at 25°C.(81) At acidic conditions, when the pH of the environment is lower or close to the pKa values of carboxylic groups of sodium citrate, dissociation of carboxylic groups into carboxylate ions and Na^+ ions become hindered, which in turn disrupts formation of the electrostatic double layer and the stability of the entire system showing agglomeration effects. The pH stability window for phase transferred IONPs_oleate particles (3.5 – 7) was broader as compared to IONPs_penta particles (4 – 7). This could also be linked to the fact that the hydrodynamic sizes of phase transferred IONPs_penta particles (355 ± 37 nm, -41 ± 7 mV) were larger and zeta potentials were smaller as compared to IONPs_oleate particles (236 ± 32 nm, -50 ± 2 mV). Henceforth, the phase transferred IONPs_oleate particles were comparatively more stable which was also seen from larger pH stability window.

4.2.3. Magnetic Properties of Phase Transferred IONPs

The saturation magnetization (Ms) of phase transferred IONPs_oleate particles (26.1 emu/g) was significantly higher as compared to phase transferred IONPs_penta particles (0.6 emu/g) as shown in Figure 3.6 – a) and b). The Ms of phase transferred IONPs_oleate and IONPs_penta particles were significantly reduced as compared to its parent IONPs_oleate and IONPs_penta particles. Saturation magnetization is a property that indicates the statistical average of magnetic moments in the direction of the externally applied magnetic field. In case of phase transferred particles, sodium

citrate was present with IONPs, but only IONPs have magnetic response and this property is divided by the total mass of the system (i.e., IONPs + sodium citrate). Thus, it is expected that surface modified IONPs present lower Ms. values in comparison with unmodified IONPs (82).

Optimization of heat production from phase transferred IONPs_oleate particles under different magnetic field conditions is discussed next.

4.2.4. Heat production from Phase Transferred IONPs with Alternating Magnetic Field

The background heat contribution from MQ water (dispersion media) generated from eddy currents needs to be accounted for while analyzing heat production from phase transferred particles (discussed in detail in Chapter 2, Section 2.3, Subsection 2.3.10). The highest detectable temperature increase for the particles was seen at AMF condition (587 kHz, 12 mT) with least deviation from eddy currents. In Figure 3.7 – b) and c), the negative values of average temperatures plotted vs time should be discussed. At AMF frequencies, 154 kHz, and 162 kHz, respectively no production of heat from phase transferred particles were observed. Exposing the particles under above-mentioned frequencies was similar to baseline run (with only MQ water). Thus, the negative temperatures were due to experimental noise originating from temperature variations from eddy currents (baseline).

SAR values are quantification of the amount of power dissipated from the phase transferred particles in the form of heat energy (discussed in Chapter 1, Section 1.6). The temperature profiles obtained were used to calculate specific absorption rates (SAR) (W/g) at different AMF conditions. The highest SAR (1.7 ± 0.4 W/g) was seen at AMF condition (587 kHz, 12 mT). The heat energy produced from magnetic nanoparticles is due to flipping of magnetic moments on exposure to AMF. Two main mechanisms – Neels relaxation and Brownian relaxation determine the production of heat from magnetic nanoparticles (discussed in detail in Chapter 1, Section 1.6). In this study, it is difficult to determine the dominant mechanism determining heat production from phase transferred particles without knowledge of actual sizes, distribution and interparticle interaction of the system. At later stages of the work, the optimized AMF condition (587 kHz, 12 mT) was utilized for studying magnetically controlled drug release systems.

Previous works have shown magnetite (Fe_3O_4) NPs synthesized by co-precipitation technique to produce high SAR values (> 100 W/g) (83). The synthesis procedure for magnetite NPs is attached in Appendix A. The temperature increase vs time and SARs for magnetite NPs were significantly higher as compared to phase transferred IONPs_oleate particles as shown in Figure 3.8 – a) and b), respectively. The increase in temperature after 10 mins for phase transferred IONPs_oleate was ~ 1.3 °C and for magnetite NPs was ~ 73.8 °C. It is difficult to control heat production from magnetite NPs and therefore, it can lead to heat cytotoxicity effects affecting healthy tissues by impairing DNA, RNA synthesis, repair, and overall cell respiration (84). On the other hand, the heat energy produced from phase transferred IONPs are lower and controllable and below heat cytotoxic threshold levels. Henceforth, the heat generation from phase transferred particles are in line with the motivation of the work, which involves production of controlled heat to trigger release of specific bioactive agents, reducing side effects to minimum.

The properties of bare NGs; which will be later utilized with the phase transferred particles to synthesize hybrid NGs is discussed next section.

4.3. N-isopropyl Acrylamide-Acrylic Acid Nanogels

pNIPAm-aac (NGs) are thermal and pH responsive polymeric structures which will be later used with phase transferred IONPs to synthesize hybrid NGs. In this section, the thermal and pH properties of NGs will be discussed.

4.3.1. Thermo-responsive Properties

Seven batches of NGs with comparable sizes at 25 ºC and 45 ºC showed repeatability of the synthesis process (69). NGs bond with water molecules through amide side chains. The hydrophobic effect caused by the isopropyl groups become dominant above Volume Phase Transition Temperature (VPTT) of the system, thus entropically favoring release of bound water due to breakage of hydrogen bonds (discussed in Chapter 1, Section 1.8). Hence, polymer-polymer interactions grow stronger than polymer-solvent interaction and the polymer attains a coiled structure resulting in phase separation. The average VPTT of NGs was 35.9 ± 0.3 ºC calculated from heating and cooling curves (shown in Figure 3.9 – b)).

4.3.2. pH-responsive Properties

The combined effect of temperature and pH on NGs in terms of hydrodynamic sizes (nm) is shown in Figure 3.10. At more acidic pH (3.5), the hydrodynamic sizes were smaller and hence higher collapses of NGs were seen. An explanation for the above stated observation is discussed. The dissociation (pKa) value for acrylic acid is 4.2. At pH (3.5) which is below 4.2, acrylic acid does not dissociate, and relatively the system collapses more. This occurs due to an overall reduction in surface charge due to non-dissociation of acrylic acid. This in turn lowers the electrostatic repulsion in between the polymeric chains allowing them to come closer thereby reducing the overall matrix size of NGs (1, 69). Hence, incorporating pH sensitive properties in NGs can be utilized for producing targeted drug delivery systems in the field of oncology (53).

The important trend to note is that at temperatures above VPTT of the NGs system (~ 36 °C), the effect of pH on hydrodynamic diameter became less pronounced. For instance, at 25 °C, an additional decrease in hydrodynamic diameter (~ 64 nm) was observed at more acidic pH (3.5) as compared to pH (4.2). Whereas at 40 °C, a much smaller additional decrease in hydrodynamic diameter (~ 6 nm) was noted at above-specified pH conditions. A possible explanation is discussed. At a specific temperature, the NGs have a particular size to which it can collapse. For temperatures (25 °C), which is below the VPTT of NGs systems, the hydrophobic effect from isopropyl groups is negligible and hence the effect of acidic pH is dominant on the hydrodynamic sizes of NGs. Whereas at temperatures (40 °C and 45 °C) above VPTT of NGs systems, hydrophobicity of NGs has much more dominant effect on collapses in size as compared to acidic pH conditions. Henceforth, a size difference of only 6 nm and 1 nm for acidic pH (3.5) at elevated temperatures of 40 °C and 45 °C is seen, respectively.

4.4. Hybrid NGs: NGs with Phase Transferred IONPs

Hybrid NGs were synthesized using three different techniques with the idea of producing hybrid systems with different physico-chemical properties which could open up new opportunities. In this section, first hybrid NGs with phase transferred IONPs_oleate will be discussed, which will be followed by hybrid NGs with penta particles.

4.4.1. NGs with Phase Transferred IONPs_oleate Particles

The NGs with phase transferred IONPs_oleate particles synthesized using three different techniques – 1) in-situ, 2) post, 3) addition is referred to as NGs_insitu, NGs_post and NGs_added (as previously stated in Chapter 3, Section 3.4). The thermal, pH and magnetic properties is discussed next.

4.4.1.1. Thermo-responsive Properties

The synthesis of hybrid NGs with in situ technique involved addition of the phase transferred particles during start of the reaction (discussed in Chapter 2, Section 2.2, Subsection 2.2.9). All hydrodynamic sizes (nm) of NGs_insitu systems synthesized with different amounts of phase transferred particles (mg) was higher as compared to the average size obtained for bare NGs (250 ± 20 nm). The size of NGs_insitu system containing particles (4 mg) was 323 ± 4 nm while that of bare NGs was 250 ± 20 nm. This suggests that within NGs_insitu system, there might be two population of particles – 1) hybrid NGs particles (which contained phase transferred particles) and 2) bare NGs. But this difference in size between the two population of particles was not significant as small amounts of phase transferred particles were used during in situ synthesis technique (shown in Table – 3.4). This is to overcome the difficulty of sticking of phase transferred particles to magnetic stirrer during the reaction. The highest amount of particles used was 4 mg. Above particle amount (4 mg), considerable wastage of phase transferred particles occurred due to sticking with magnetic stirrer which would have made it difficult to quantitatively understand the amount of particles present in NGs_insitu systems at the end of reaction. An image of magnetic stirrer with the sticking problem is shown in Figure 4.1, when 4.7 mg of particles were used in the process.

Figure 4.1 – Image of magnetic stirrer showing sticking problem, when phase transferred particles (4.7 mg) was used during in situ reaction.

Thus, within NGs_insitu systems the population of hybrid NGs particles (which contained phase transferred particles) were considerably small as compared to population of bare NGs. Therefore, the system seemed bare NGs dominated. The VPTT of NGs_insitu system (36.8 ± 0.2 °C) was higher by ~ 1 °C as compared to bare NGs (35.9 ± 0.3 °C). This small increase in VPTT for NGs_insitu system can be attributed to relatively much smaller populations of hybrid NGs particles (containing phase transferred particles). A possible hypothesis for increase in VPTT of NGs_insitu system is that the phase transferred particles got incorporated inside polymeric NGs structures, which allowed less space for the chains to collapse, in turn increasing the VPTT of the system (85). The increase in VPTT of NGs_insitu systems can also be discussed based on hydrophilic-lipophilic balance (HLB) of NGs polymeric network. An inherent property of the phase transferred particles are its hydrophilicity. Therefore, overall hydrophilicity of hybrid NGs might increase when particles are incorporated, increasing the solubility of the system and in turn pushing VPPT to higher temperatures (51). A rough schematic of above stated hypothesis is shown in Figure 4.2.

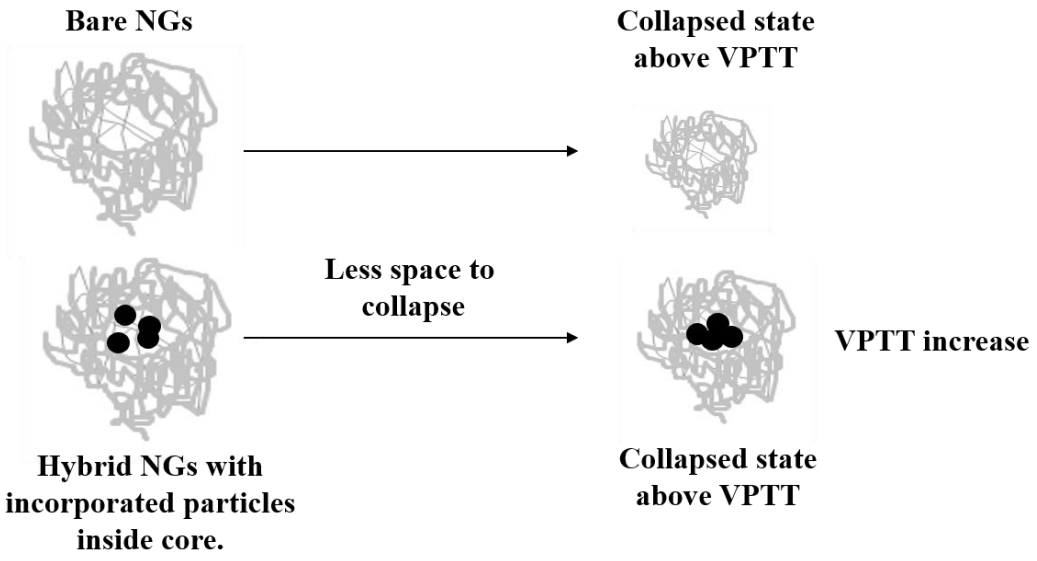

Figure 4.2 – Schematic showing the hypothesis if particles get incorporated inside the polymeric NGs matrix.

Due to high water stability of phase transferred particles; another probable scenario needs to be considered. The particles may be distributed both in the core and in the porous shell matrix forming crosslinking structures with BIS which is used as crosslinker in the reaction (discussed in Chapter

1, Section 1.8). This may give rise to two counter interactive effects - 1) incorporation of the particles inside the polymer core, which might hinder the collapse of the hydrophobic hydrocarbon chain of NGs at higher temperatures due to less space and hence increase in VPTT could be expected, (discussed above), 2) particles present on the outer regions of porous gel matrix forming crosslinking structures with (BIS), could also enhance the overall collapse capacity of the system (51, 85). For instance, both the VPTT (36.8 ± 0.2 °C) and VCE (%) (97 %) of NGs_insitu system (discussed above) was higher, as compared to bare NGs (shown in Figure 3.12 a) and Table – 3.6). These values are in accordance with the above stated hypothesis, which might suggest that phase transferred particles get distributed both in the core and porous shell matrix of bare NGs. A schematic of above stated hypothesis is shown in Figure 4.3. But from only DLS data, it is not possible to draw precise conclusion on particle distribution and interaction with polymeric chains of NGs and understand its associated effects.

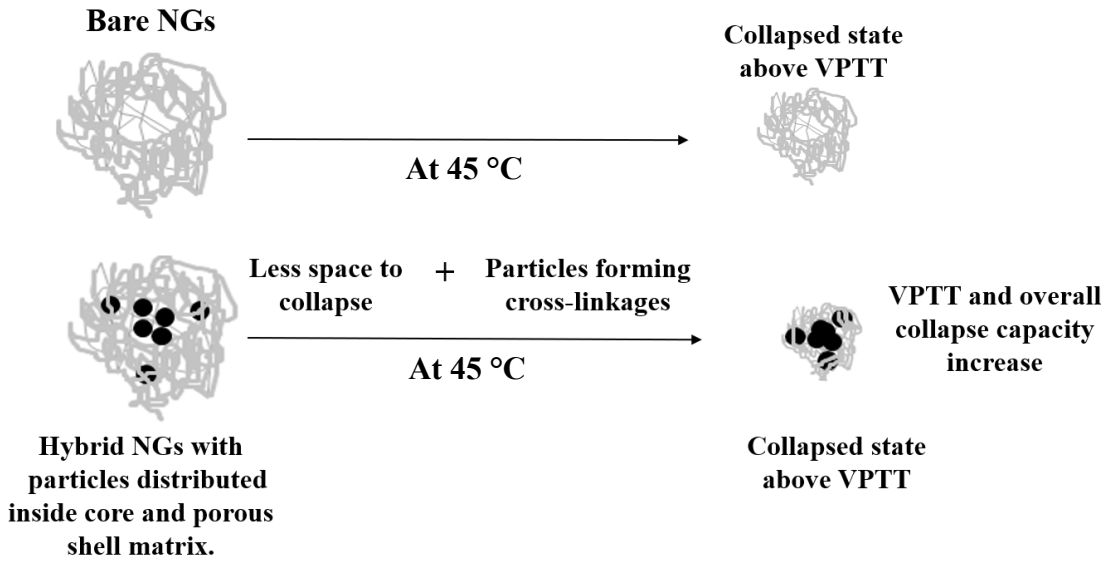

Figure 4.3 - Schematic showing the hypothesis, if particles get distributed both in core and porous shell matrix of polymeric NGs.

The synthesis of hybrid NGs with post technique involved reacting phase transferred IONPs with freeze dried bare NGs (i.e., NGs synthesized, dialyzed, and dried) with stirring (discussed in Chapter 2, Section 2.2, Subsection 2.2.9). The amount of phase transferred particles with bare NGs, used in this case was also 4 mg, so that the system could be comparable to NGs_insitu. Similar to NGs_insitu system, the NGs_post system could also be assumed dominated by bare

NGs as very less amount of phase transferred IONPs (4 mg) was used. During in situ technique, there was probability that the particles get incorporated in the core of the NGs as discussed above. Whereas in case of post technique, the probability of particles getting incorporated in the core of NGs is much less as seen from previous works of Anthony et al. with bare NGs and gold nanoparticles system (65). But the major challenge, is to understand whether the particles are getting into the porous polymeric shell network forming cross-linkages with BIS or interacting externally forming terminal bridging structures in between two bare NGs particles. A rough schematic of two plausible interactions of bare NGs with phase transferred particles during post synthesis technique is shown below in Figure 4.4.

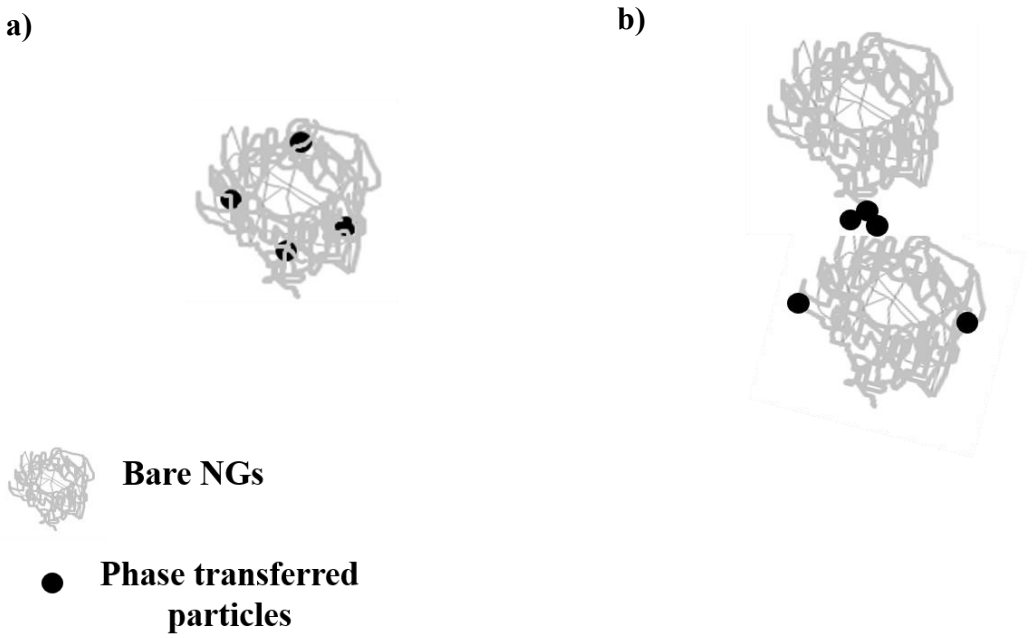

Figure 4.4 – Schematic showing two possible interaction of phase transferred particles with bare NGs during post synthesis technique. a) Particles forming cross-linkages with porous shell of bare NGs. b) particles forming external terminal bridges in between NGs.

In previous studies, possible argumentation of particles forming cross-linkages in porous shell matrix of NGs was given for post systems containing NGs with gold nanoparticles (69). In that system, the size of gold nanoparticles (hydrodynamic size ~ 50 nm) was suggested smaller as compared to the pore size of bare NGs, hence scenario as shown in figure 4.4 – a) was more probable. Previous studies by Raghunathan et al. have also reasoned similar scenario with NGs

and gold nanoparticle systems, when the size obtained for gold NPs was 60 nm (86). But in our system, the sizes of phase transferred IONPs are significantly larger (236 ± 32 nm) and scenario shown in Figure 4.4 – b) where the particles are forming external terminal bridges in between NGs are more probable. The VPTT of NGs_post system (35.7 ± 0.2 °C) was similar to bare NGs (35.9 ± 0.3 °C) which might again suggest above stated scenario, because if the particles formed cross-linkages with BIS in porous shell of NGs (shown in Figure 4.4 – a)) a significant decrease in VPTT of the system would have been expected (65, 86). If we assume that in our case the scenario shown in Figure 4.4 – b) is dominant during post synthesis technique, then in theory NGs_post system should have comparatively larger sizes than NGs_insitu system. But the hydrodynamic size of NGs_post system was smaller by (47 nm) as compared to NGs_insitu system at 25 °C as shown in Figure 3.11 – a). It is difficult to conclusively comment on this difference in sizes seen between NGs_post and NGs_insitu systems as there are several contributing variables like particle number, interaction of phase transferred particles with NGs and size deviation of bare NGs population.

The synthesis of hybrid NGs with addition technique involved addition of the phase transferred particles (4 mg) into as-synthesized NGs and then the samples were dialyzed and freeze dried (discussed in Chapter 2, Section 2.2, Subsection 2.2.9). The main idea of performing this experiment was to study whether the phase transferred particles will interact with NGs without the effect of stirring or elevated temperature. The main difference to be noted in this system as compared to NGs_post, was that the particles without stirring or application of heat were added to as-synthesized NGs before dialysis. Then the sample solution was dialyzed and freeze dried to obtain NGs_added system in powder form. The purpose of dialysis for 24 hours was to remove unwanted polymeric residues from the system which had not completed the polymerization process to form 3-D polymeric NGs (discussed in Chapter 2, Section 2.2, Subsection 2.2.8). Henceforth, there was possibility of interaction of the phase transferred particles with the incompletely polymerized structures. The VPTT of NGs_added (37.6 ± 0.1 °C) was higher as compared to bare NGs, NGs_insitu and NGs_post systems. This might suggest some interaction of phase transferred particles with the unreacted residues, abruptly altering the VPTT of the entire system.

Next, the magnetic and pH-responsive properties of NGs_insitu, NGs_post and NGs_added systems will be discussed, which is important for synthesizing stimuli-responsive drug delivery

systems.

4.4.1.2. pH-responsive and Magnetic Properties

The combined effect of temperature and pH on NGs_insitu and NGs_post systems in terms of hydrodynamic sizes (nm) are shown in Figure 3.13 – a) and b) respectively. Both the systems showed similar kind of pH response as compared to bare NGs (discussed in Section 4.3). At more acidic pH (3.5), the hydrodynamic sizes were smaller and hence higher collapses of NGs_insitu and NGs_post systems were seen. This can be again attributed to non-dissociation of acrylic acid at pH values less than 4.2 which causes the polymeric chains to come closer due to reduced electrostatic repulsion, showing more collapse (69). Henceforth, from the pH studies it was shown that incorporating phase transferred IONPs (4 mg) with NGs using different techniques did not have significant effect on the pH-responsivity of the system.

All the hybrid NGs retained superparamagnetism with zero hysteresis loss at room temperature as shown in Figure 3.14 – a). This suggests no major agglomeration of phase transferred IONPs in the hybrid NGs systems, as agglomeration can introduce magneto crystalline energy which could disrupt superparamagnetic properties (87). The Ms value seen for NGs_post (0.06 emu/g) was highest as compared to NGs_insitu (0.03 emu/g) and NGs_added (0.01 emu/g) systems when exposed to an external magnetic field of 1 T. It is difficult to comment on small differences in Ms values seen between three systems which might be attributed to different distributions of phase transferred IONPs within and outside polymeric NGs population. Another important point was that the measurements were also performed only once. In all the three systems, the magnetization values were significantly reduced as compared to values obtained for phase transferred IONPs. This was due to small amount of particles (4 mg) present in ~ (160 – 170 mg) of NGs (shown in Table 3.4). In case of hybrid NGs, the amount of NGs present with phase transferred IONPs was ~ 40 – 42.5 times more.

The saturation magnetizations increased with increase in mass of phase transferred particles (shown in Figure 3.14 – b)). This showed that Ms values of hybrid NGs can be tuned while retaining superparamagnetic properties.

All the three hybrid systems, NGs_insitu, NGs_post and NGs_added were dominated by bare NGs population. Henceforth, the magnetic part, which might contain phase transferred particles interacted with bare NGs was separated using a neodymium magnet and its thermo-responsive properties is discussed next.

4.4.1.3. Magnetically Separated Hybrid NGs

Magnetic separation of hybrid NGs were performed to study interacted phase transferred IONPs particles with bare NGs. Increase in hydrodynamic sizes (shown in Figure 3.15) were seen for the magnetically separated systems as compared to parent hybrid NGs which largely contained bare NGs. This may be attributed to two possible reasons. Firstly, magnetically separated particles were considerably larger as compared to bare NGs due to presence of NGs with interacted phase transferred particles. Secondly, there might be aggregation during the magnetic separation process. All the magnetically separated systems showed collapse at 45 °C, which confirmed that there was interaction of phase transferred particles with bare NGs for all the three different synthesis techniques implemented. If there was no interaction between the phase transferred IONPs and bare NGs, then no collapse in size would have been observed for the magnetically separated particles, as the phase transferred particles do not show significant decrease in size with increasing temperature (shown in in Section 3.2, Figure 3.4 – a)). The maximum collapse of bare NGs was seen up to temperature 45 °C while the magnetically separated systems showed collapse up to temperature 60 °C. This might suggest that with magnetic separation process, the properties of the magnetic part start to show significance which was otherwise overshadowed with relatively high population of bare NGs. There might be little to no presence of bare NGs in the magnetically separated systems. From previous studies, it has been seen that magnetic separation and cleaning processes are effective in removing non-magnetic part (bare NGs) (88). It is difficult to exactly comment on collapses seen up to 60 °C for magnetically separated systems. One possible reason might involve larger sizes of magnetically separated particles requiring higher temperatures to reach maximum collapse. The sizes of NGs_post particles (1081 ± 6 nm) were larger as compared to NGs_insitu particles (916 ± 101 nm). This could be due to possible hypothesis of phase transferred particles forming external terminal bridging structures connecting bare NGs (shown in Figure 4.4 – b)).

The NGs_added magnetically separated particles also showed collapse at 45 °C and 60 °C, respectively. This showed that the phase transferred particles interacted with bare NGs during addition technique, which was implemented without stirring and heating. For NGs_added magnetically separated system, a significantly smaller collapse in size (119 nm) was observed between temperature points (45 °C and 60 °C) as compared with NGs_insitu (365 nm) and NGs_post magnetically separated (366 nm) systems as shown in Figure 3.15. It is difficult to conclusively comment on the above stated observation, but a possible hypothesis can be drawn. In addition technique, the phase transferred IONPs are added in the as-synthesized NGs without stirring or application of heat and then the entire system is dialyzed and freeze dried. Collapses of NGs_added magnetically separated systems at elevated temperatures showed interaction between phase transferred particles and bare NGs in the added procedure. An important point to note, is that the phase transferred particles were added before the dialysis step. Thus, there was probability of interaction between the phase transferred particles and residual polymeric structures which then could not be removed by dialysis. Therefore, the magnetically separated system could get divided in two populations – 1) residual polymeric structures with phase transferred particles 2) NGs with phase transferred particles. The population of NGs with particles could be assumed similar to post system, where external interaction of phase transferred IONPs with NGs forming bridges is more probable (shown in Figure 4.4 – b)). The collapse of residual polymeric structures interacted with phase transferred particles is probably less as compared to NGs with particles. This in turn could bring down the overall collapse of the system. This hypothesis shows accordance with relatively small collapses in size between 45 °C and 60 °C for NGs_added as compared to NGs_insitu and NGs_post magnetically separated systems. A rough schematic of the above discussed hypothesis showing difference in NGs_added and NGs_post magnetically separated systems is shown in Figure 4.5 – a) and b), respectively.

After the magnetic separation process, the obtained masses of magnetically separated systems were significantly lower than 3.3 mg. 3.3 mg was the mass of nanogel samples used to load cytochrome C (discussed in Chapter 2, Subsection 2.2.10, Figure 2.11). Thus, these systems were not used for drug delivery devices in this study. Bare NGs, NGs_insitu, NGs_post and NGs_added systems were used for loading of cytochrome C and the effect on release mechanisms of cyt C based on their subtle differences in physico-chemical properties is studied and discussed in Section 4.5.

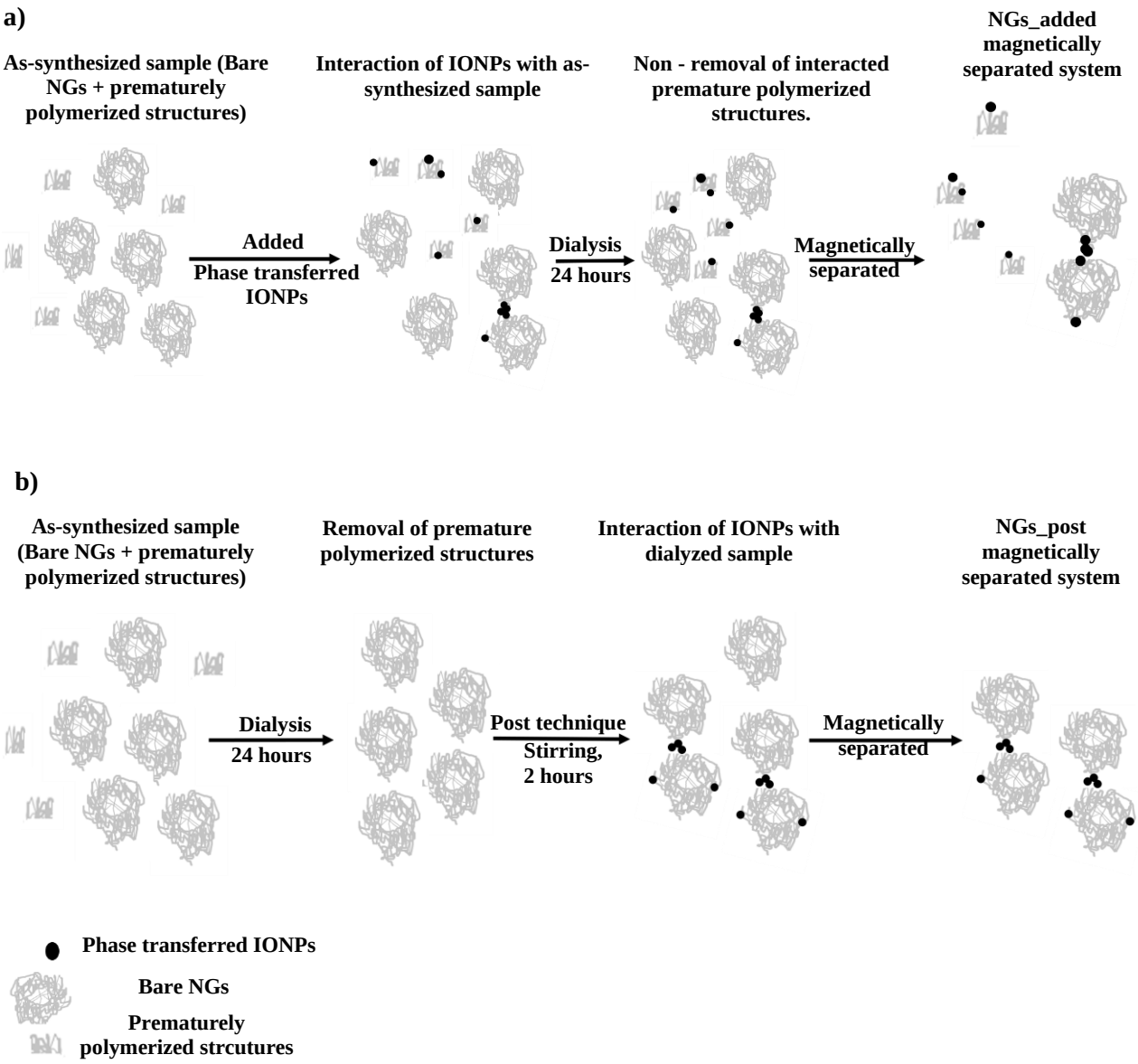

Figure 4.5 – a) and b) Rough schematic hypothesizing NGs_added and NGs_post magnetically separated systems, respectively.

4.4.2. NGs with Phase Transferred IONPs_penta Particles

The bare NGs with phase transferred IONPs_penta particles were also synthesized using in situ and post techniques. The thermal and magnetic properties of these systems are discussed next.

4.4.2.1. Thermal and Magnetic Properties

The synthesis of hybrid NGs with in situ technique involved addition of the phase transferred IONPs_penta particles during start of the reaction. The hydrodynamic sizes (nm) of NGs_insitu systems synthesized with different amounts of phase transferred particles (mg) was comparatively higher as compared to average size obtained for bare NGs (shown in Figure 3.16 – a)). The highest mass of phase transferred IONPs_penta particles used during in-situ technique was 4 mg. The same mass of phase transferred IONPs_oleate particles were also used to synthesize NGs_insitu systems, so that both the systems were comparable.

All the NGs_insitu systems, synthesized with different masses of IONPs_penta particles showed increase in size as compared to bare NGs (shown in Figure 3.16 – a)). The obtained hydrodynamic size (nm) of NGs_insitu system (308 ± 8 nm) with particle (4 mg) was in close range with size seen for NGs_insitu system with phase transferred IONPs_oleate particles (323 ± 4). The normalized volumetric collapses as function of temperature (25 – 60 °C) shown in Figure 3.16 – b) was similar to bare NGs and other hybrid NGs systems containing IONPs_oleate particles. This was again due to small amount of phase transferred particles used in the process and the system remains dominated with bare NGs population. The VPPT calculated for NGs_insitu system (36.8 ± 0.1 °C) (shown in Table 3.9) was higher by ~ 1 °C as compared to bare NGs (35.9 ± 0.3 °C). The VPTT obtained for this system was similar to NGs_insitu systems with phase transferred IONPs_oleate particles. The VCE (%) (97 %) at 45 °C for this system (shown in Figure 3.16 – d)) was also similar to NGs_insitu systems with phase transferred IONPs_oleate particles. From above discussed thermal data, it can be assumed that both NGs_insitu systems containing phase transferred IONPs_oleate and IONPs_penta particles, respectively showed similar thermo-responsive properties. This might be attributed to the fact that both IONPs_oleate and IONPs_penta particles had same phase transferring agent (sodium citrate) on their surface, leading to similar kind of chemical interactions with bare NGs. Henceforth, hypothesis shown in Figure 4.2 and 4.3 could also be used for possible explanation of increased VPTT and VCE (%) at 45 °C of NGs_insitu system as compared to bare NGs.

The average hydrodynamic size of phase transferred IONPs_penta particles (355 ± 37 nm) were larger as compared to IONPs_oleate particles (236 ± 32 nm). Thus, it could be assumed that in

NGs_insitu system with phase transferred IONPs_penta particles, hypothesis (shown in Figure 4.4 – b)) is even more likely to happen as compared to NGs with phase transferred IONPs_oleate particles. So, there is higher probability of phase transferred IONPs_penta particles forming external bridging structures with NGs. Based on the above-mentioned statement, in theory NGs_post system should have comparatively larger sizes than NGs_insitu system. But the hydrodynamic size of NGs_post system was smaller by (58 nm) as compared to NGs_insitu system at 25 °C as shown in Figure 3.16 – c). It is again difficult to comment conclusively and could possibly be connected to (discussion in 4.4.1.1, Paragraph 5), where several variables like total particle number in the system, interaction of phase transferred particles with NGs and size deviation of bare NGs population may be contributing to difference in sizes between NGs_insitu and NGs-post systems.

The NGs_insitu system retained superparamagnetism with zero hysteresis loss at room temperature as shown in Figure 3.17. The Ms value seen for NGs_insitu system (0.0013 emu/g) with phase transferred IONPs_penta particles was ~ 23 times less as compared to values obtained with phase transferred IONPs_oleate particles (0.03 emu/g). This might be attributed to the fact that Ms value for phase transferred IONPs_oleate particles (26.1 emu/g) was also higher as compared to IONPs_penta particles (0.6 emu/g) (shown in Chapter 3, Figure 3.2 - c)).

Due to significantly better magnetic properties of hybrid NGs with phase transferred IONPs_oleate particles, these systems were chosen over IONPs_penta systems for synthesizing magnetically controlled drug delivery systems which is discussed in upcoming two Sections 4.5 and 4.6, respectively.

4.5. Release Study of Cytochrome C

Hybrid NGs with phase transferred IONPs_oleate particles were used to load a model protein cytochrome C (cyt C) and the release studies were performed to understand how physico-chemical of hybrid NGs influence the release mechanisms. The release studies were performed at different conditions of elevated temperatures and acidic pH for period of 20 hours. This section is divided in two subsections. Firstly, loading and encapsulation efficiencies (L.E and E.E) of different hybrid NGs will be discussed. Later, the release profiles of the hybrid NGs will be compared with standard

drug delivery models and its kinetics will be studied.

4.5.1. Loading and Encapsulation Efficiencies

Loading efficiency (L.E) is defined as mass (%) of drug loaded in a system whereas encapsulation efficiency (E.E) is defined as mass of drug loaded per unit weight of system (69). The loading efficiencies were calculated using absorbance peaks of cyt C in wavelength range (409 – 411 nm) obtained using UV-Vis spectroscopy and cyt C calibration curve (plotted absorbance values as function of concentration (mg/mL)). The calibration curve of cyt C, formulae and method used for calculating L.E and E.E is attached in Appendix C. Cytochrome C was loaded in bare and hybrid NGs via breathing in mechanism; in which the uptake of the drug happens due to swelling of NGs in aqueous media when the temperature is below the VPTT of the system. The highest L.E values were calculated for bare NGs systems (85 ± 12 %) (shown in Table 3.10). This might be due to absence of phase transferred IONPs in bare NGs system. Thus, at room temperatures swelled up, water dispersed NGs were able to uptake larger amounts of cyt C as compared to NGs_insitu systems. The L.E and E.E values shown for bare NGs system were in close range with previous studies performed by Sharma et al. (69). The NGs_insitu system, showed comparatively lower L.E (70 ± 10 %), as compared to bare NGs. One possible reason is due to presence of phase transferred IONPs inside the core of system, thereby leaving less space for uptake of cyt C. This view is in accordance with previous study performed with gold nanoparticles coated with NGs systems (69). The L.E seen for NGs_post system (91 %), was higher as compared to NGs_insitu and NGs_added systems. A possible explanation could be connected to hypothesis (shown in 4.4.1.1, Figure 4.4 – b)). In NGs_post system, there is likelihood of phase transferred IONPs interacting externally with bare NGs. Hence, spaces might be available inside core and porous shell matrix of bare NGs for cyt C to get loaded, which gives high L.E as compared to NGs_insitu systems. The L.E of NGs_added system (68.1 %) was lowest among all the systems. A possible reason is discussed. The added phase transferred IONPs might interact with prematurely formed polymeric structures which then could not be removed by dialysis as hypothesized in (4.4.1.3, Figure 4.5 – a)). It can be assumed that the loading efficiency of cyt C with premature polymeric structures is lower in comparison to bare NGs and hybrid NGs particles, due to availability of less space. As, these structures form a part of the loaded sample, it could in turn lower the overall L.E of the system. But it is important to note that loading experiment of cyt C with NGs_post and NGs_added systems

were performed only once which poses question on repeatability of the L.E values.

4.5.2. Release Kinetics of Cytochrome C

A common mechanism of drug release from porous and polymeric gel structures is based on diffusion where concentration gradient plays most important role in transport phenomenon. Other mechanisms involve release of drug due to swelling and collapse of gel structures based on external stimuli conditions, via chemical reactions inside carrier structures or due to slow degradation of the system (89). In some systems, two or more mechanisms happen (69). Hence, different mathematical models are used to understand the release mechanisms (discussed in Chapter 1, Section 1.10).

In this study, the release of cyt C was performed from bare NGs and hybrid NGs systems at condition of 40 °C and pH (3.5) (shown in Figure 3.21), to understand influence of their physico-chemical properties on release kinetics. The release as function of time from NGs samples was monitored from the progressive decrease of cyt C absorbance peak measured using UV-Vis. A sample calculation of release (%) from changes in absorbance peak is attached in Appendix D. Presence of different release modes within the same release profile were inferred for all the systems. For instance, bare NGs, NGs_insitu and NGs_post system showed rapid release of cyt C for time scales up to 2, 3 and 1.5 hours respectively, after which the release profile decreased progressively. The differences in release modes for all these systems were not visually understandable and preliminary trial and error fittings were performed to make approximate division of its release profiles. Hence for bare NGs and all the three hybrid NGs, the entire release profiles were divided in two parts. All the parts were fitted with four most common mathematical models – 1) Zero-order, 2) First order, 3) Higuchi and 4) Korsmeyer-Peppas (power law). The efficient fits for each part are shown and discussed while the rest are attached in Appendix E. The four different systems are discussed in order – Bare NGs, NGs_insitu, NGs_post and NGs_added, respectively.

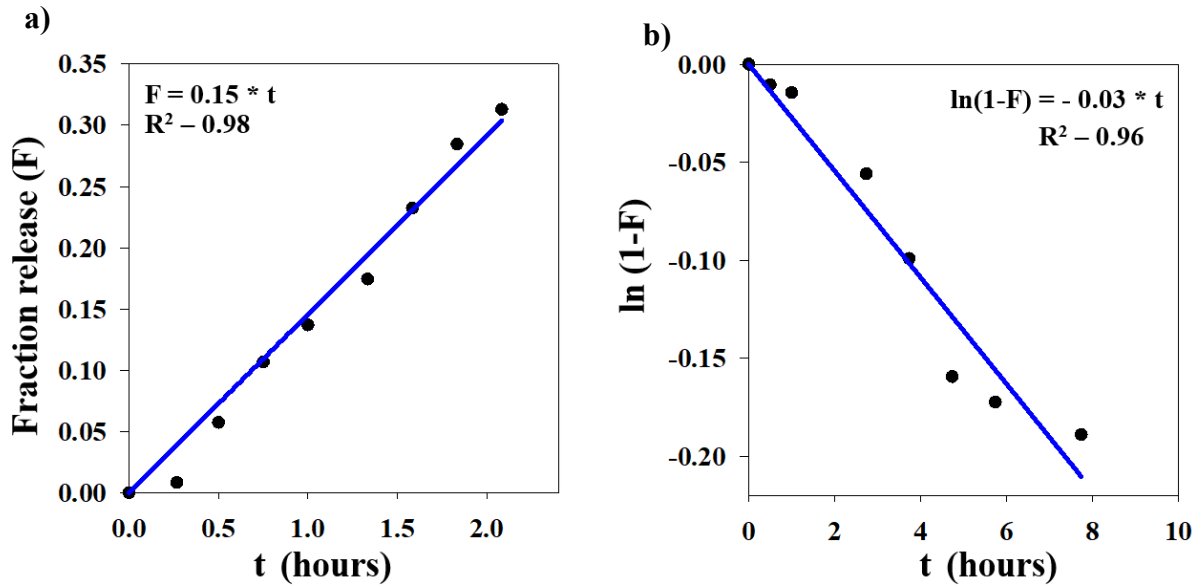

Figure 4.6 – Fitted models for bare NGs. a) Part-I fitted with zero order model, b) Part-II fitted with first order model.

The bare NGs system with which release study was performed had a L.E of 87.4 %. The release study from bare NGs system was performed for ~ 11 hours. The entire release profile obtained was divided into two parts and analyzed. Part-I consisted up to ~ 2 hours and consequently, the rest ~ 9 hours was Part-II. The best fit for part-I was seen with zero order model (shown in Figure 4.6 – a) and the release constant (K) value (0.15 hour $^{-1}$) was obtained (shown in Table 4.1). The release in part-I shows good accordance with zero order kinetics, where the release is independent of concentration of cytochrome C present inside the polymeric systems. This is also in line with previous studies performed with bare NGs systems, where the initial release was dominant by stimuli-responsive collapse of polymeric chains of NGs following concentration independent zero order kinetics (65).

With progression of release, the amount of drug in the system decreases, and the release profiles starts showing dependance on drug concentration present inside the polymeric systems at specific instances in time. Hence with ongoing release, the drug amount would decrease which would in turn decrease the release rates. This was observed from K values obtained for part-II (0.03 hour $^{-1}$) fitted from first order model, which was significantly smaller (5 times) as compared to Part-I (shown in table 4.1). In part-II, the best fit was seen with first order model shown in Figure 4.6 - b). This suggests that the dominant release mechanism was non-Fickian accelerated diffusion

(concentration dependent) release. It is important to note that though best fitted models have been shown for part-I and part II, both zero and first order models show good fitting in both the parts and it is mathematically difficult to find a distinctive boundary between the two mechanisms based on time scale.

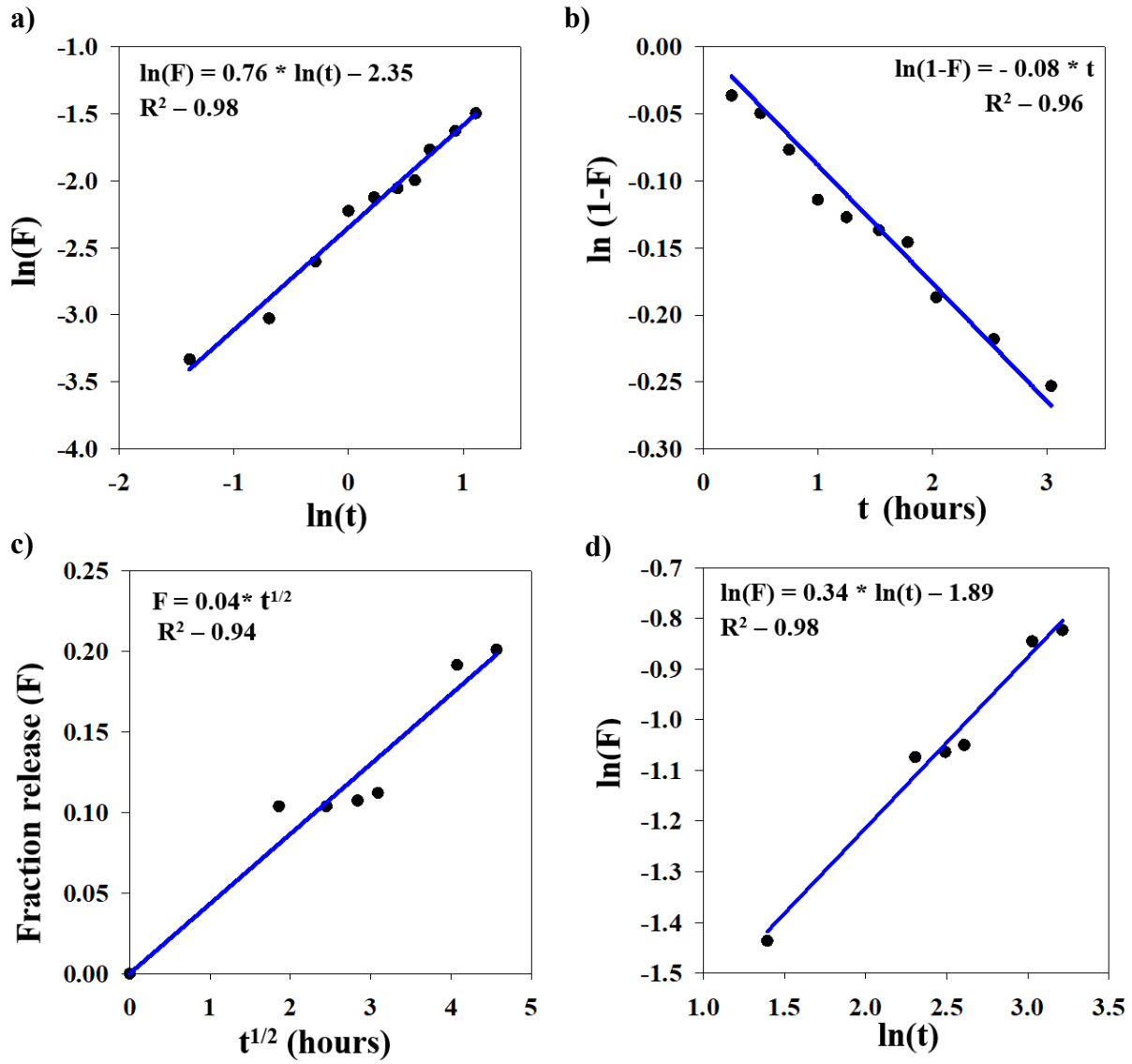

Figure 4.7 – Fitted models for NGs_insitu system. a) and b) Part-I fitted with power model and first order model, c) and d) Part-II fitted with Higuchi and power law models, respectively.

Part-I for NGs_insitu system was taken from 0 to ~ 3.2 hours. The power and first order models fit best as seen from R^2 values in Figure 4.7 – a) and b). The L.E of NGs_insitu system (~ 80 %) was relatively lower as compared to bare NGs system used. Therefore, the transition of dominant release mechanism from zero order (concentration independent) to anomalous transport

(concentration dependent) was relatively faster as compared to above discussed bare NGs due to less amount of drug present in the system at the start of release. This fine transition between different mechanisms could not be detected within Part-I and overall, Part-I showed dominated anomalous transport mechanism. The release exponent (n) value (0.76) obtained from power law model also showed dominant anomalous transport in part-1 as shown in Table 4.2. The K value fitted from first order model was 0.08 $hour^{-1}$ for Part-1 as shown in Table 4.1. The K value obtained in Part-I for bare NGs system is compared with K value for NGs_insitu system in Part-1. Both the parts had close time scales (~ 2.5 hours) for comparison. The K value for NGs_insitu system was lower by a factor of 2 as compared to bare NGs. This shows lower release rates of cytochrome C from NGs_insitu system in the above stated time scale. This might be due to higher VPPT of NGs_insitu systems (36.8 ± 0.2 °C) as compared to bare NGs (35.9 ± 0.3 °C), in turn having comparatively slower collapse of its polymeric chains (discussed in detail in Section 4.4, Subsection 4.4.1). But another variable which needs to be considered is L.E, which was different in both systems. Difference in L.E can effect the release mechanism (like transition from zero to first order releases), within a specified time scale which can also cause variation in release rates. The effect of different L.E on initial release rates of NGs_insitu system is attached in Appendix F. Henceforth, further experimentations with similar L.E between the two systems is required, to confirm lower release rates from NGs_insitu system, showing formation of slow or sustained drug delivery systems.

In Part-II, which was taken from (~ 3.2 – 22 hours), power model was best fitted as seen from R^2 values (shown in Figure 4.7 - d)). The n value obtained from power law (0.34), does not fall under ranges shown in Table 4.2. Previous studies have shown that n values obtained from power law can go below 0.40 for systems containing porous hydrophilic polymeric matrix, due to polydispersity of its pores (90). But still Higuchi diffusion can be considered as dominant mechanism with n values below 0.40. Higuchi or Fickian diffusion is a slower diffusion process as compared to anomalous transport and for swelling and collapsing polymeric structures, it is generally observed at later stages of the release when the drug concentration in the system becomes low. The difference in Higuchi diffusion as compared to anomalous transport, is that the diffusion process is independent of change in polymeric structure (discussed in detail in Chapter 1, Subsection 1.9.1). Henceforth, in Part-II, extended Higuchi release was dominant as the drug

concentration reduced with release progression. The Higuchi dissolution coefficient k_H was 0.04, which was obtained from fitted Higuchi model (shown in Table 4.1).

The NGs_post system was also divided in two parts. Part-I extended from (0 – 1.5 hours) while Part-II was taken over larger extension of time (~ 1.5 – 24 hours). The L.E of NGs_post sample used was 91 %. Part-I fitted well with both zero and first order models as seen from R^2 values (shown in Figure 4.8 – a) and b)) respectively. Again, in this regime, both zero order and first order mechanisms might be happening. The K value obtained in this part (0.28 hour $^{-1}$) was fitted from first order model (shown in Table – 4.1).

In Part-II, best fit was seen with Higuchi and power models. Extended Part-II also showed dominant Higuchi diffusion as compared to Part-II of NGs_insitu systems due to low amounts of cytochrome C present in the system after long periods of release. Thus, the release becomes independent of the collapse of its polymeric chains. The n value fitted from power model was 0.23, which was again outside the range of n values shown in Table 4.2. This could be attributed to the same fact stated for Part-II regime of NGs_insitu system. The Higuchi dissolution constant k_H in this case was 0.06 (shown in Table 4.1). The k_H value (0.06) was comparable to the value (0.04) obtained in Part-II Higuchi dominated region for NGs_insitu system. This shows that at longer time scales and at low concentrations of drug, slow Fickian diffusion is dominant which becomes independent of the collapse of the system. This type of release profiles could be interesting in biomedical fields where prolonged treatments over weeks, days or years are necessary, for e. g. treating of immunological disorders and psychiatric diseases (91).

An overall interesting point to note is the half-life ($t_{1/2}$) of cytochrome C release for NGs_post system. Half-life is defined at the time point where 50 % of the drug gets released from the system. The $t_{1/2}$ of NGs_post system (9.2 hours) was comparable with $t_{1/2}$ of bare NGs (9.8 hours) (shown in Figure 3.18). This might hint close thermo-responsive properties between bare NGs and NGs_post systems which can be further hinted from very similar VPTT values of 35.9 ± 0.3 °C and 35.7 ± 0.2 °C. This difference in $t_{1/2}$ of 0.6 hours can be attributed to difference in L.E of 3.4 % between the systems.

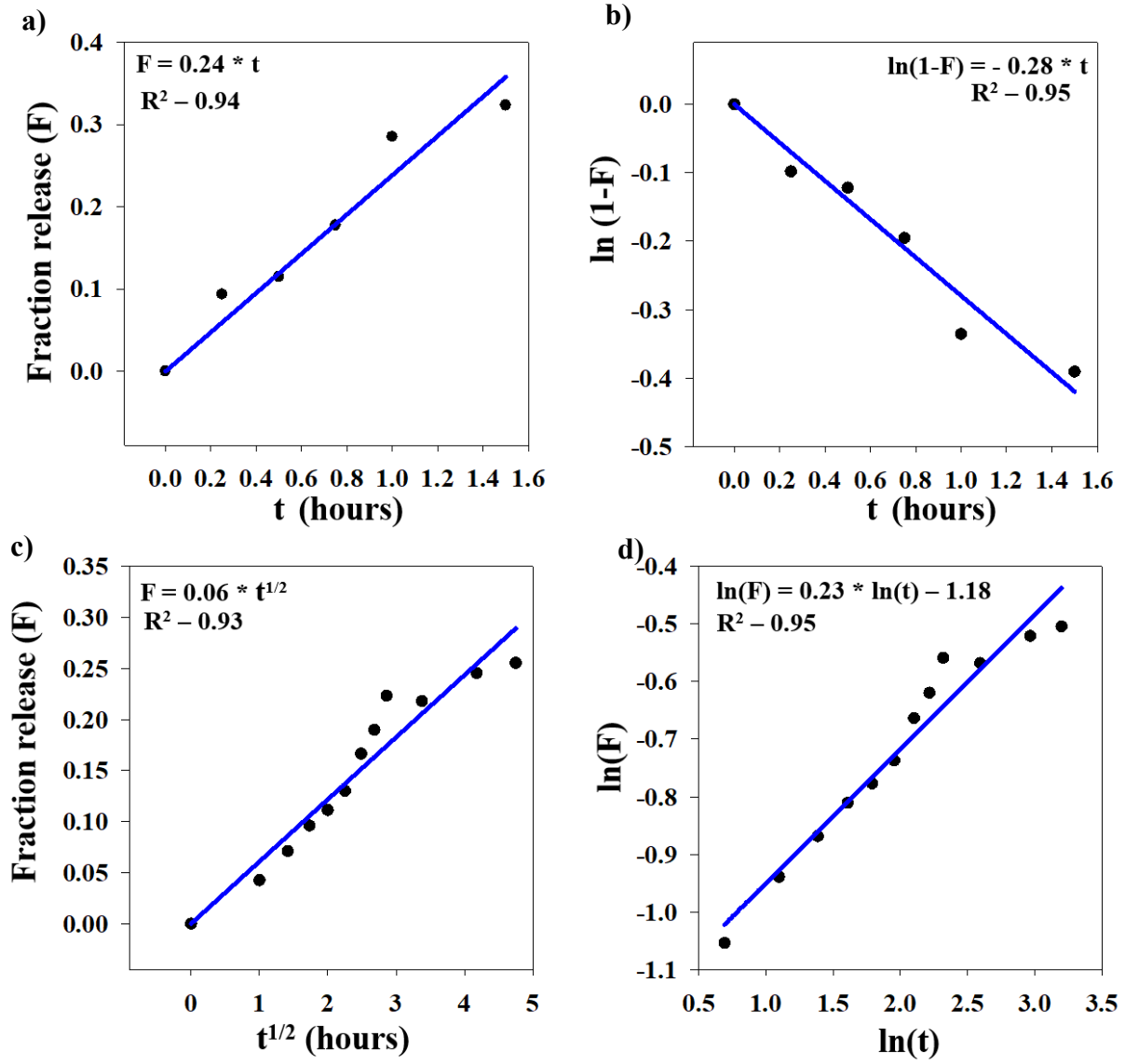

Figure 4.8 – Fitted models for NGs_post system. a) and b) Part-I fitted with zero order model and first order model. c) and d) Part-II fitted with Higuchi and power law models, respectively.

NGs_added system was also divided in two parts for better analysis. Part-I extended for period (0 – 1.6 hours), Part-II (~ 1.6 – 21 hours). For NGs_added system, Part-I is discussed in order to understand any difference in initial release mechanisms with respect to bare NGs, NGs_insitu and NGs_post systems. Part-II did not form efficient fit with any of the four mathematical models and is attached in Appendix E. Part-I showed best fitting with Higuchi and power law models as seen from R^2 values (shown in Figure 4.9 – a) and b)). Part-I of NGs_added system predicted different release mechanism as compared to Part-I of bare NGs and other hybrid NGs systems. The n value

obtained from slope of power law model was 0.45 (shown in Figure 4.9 – b) and Table 4.1). This predicts that the initial dominant release was due to Higuchi diffusion. It is difficult to conclude why slow Higuchi diffusion was seen at start of the release which generally becomes dominant at later stages due to decrease in amount of loaded drug with progression in time. A plausible explanation is given below. NGs_added system was different as compared to other three above discussed systems in terms of phase transferred IONPs addition step and cleaning processes employed. In NGs_added system, the phase transferred IONPs were added before dialysis which might show interaction with prematurely formed polymeric structures as hypothesized (in Section 4.4, Figure 4.5 – a)). These interacted polymeric structures do not get removed via dialysis step and forms part of the system. Thus, possibly a hindrance effect is created by these structures which effects the mobility of cyt C released from hybrid NGs particles to reach the walls of the dialysis membrane, before diffusing out into the sink.

In this section, release of cyt C at 40 °C and 3.5 pH was studied from bare and hybrid NGs. The effect of small differences in physico-chemical properties between bare NGs and hybrid NGs systems on loading and release of cyt C was discussed. In the next section, release of cyt C from bare and hybrid NGs on exposure to external alternating magnetic field (AMF) conditions was studied using Magnetherm setup.

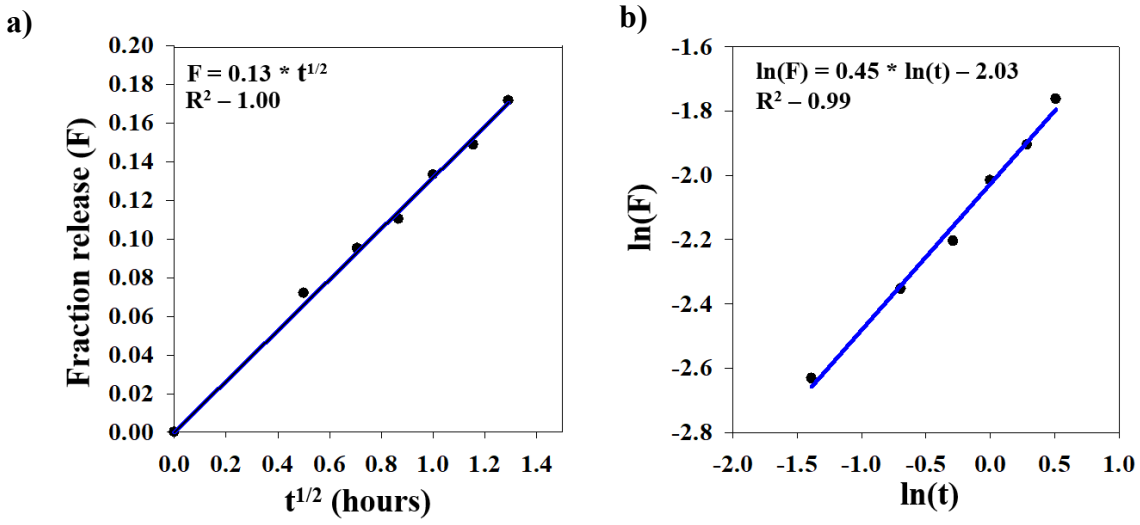

Figure 4.9 – Fitted models for NGs_added system. a) and b) Part-I fitted with Higuchi and power law models, respectively.

Table 4.1 – Showing rate constant K (hour $^{-1}$) of each part for bare NGs, NGs_insitu, NGs_post and NGs_added systems, respectively with corresponding dominant release mechanisms for each part.

Samples	**Parts**	**Release constant K (hour $^{-1}$)**	**Dominant Mechanism**
Bare NGs	Part-I	0.15	Zero order
	Part-II	0.03	First order
NGs_insitu	Part-I	0.08	First order
	Part-II	0.04	Higuchi
NGs_post	Part-I	0.28	First order
	Part-II	0.06	Higuchi
NGs_added	Part-I	0.13	Higuchi
	Part-II	0.02	Zero/First order
	Part-III	0.002	Zero/First order

Table 4.2 - Showing different release mechanisms based on different values of release exponent (n) in power law model (60).[2]

Release mechanism model	**Release exponent (n)**
Fickian diffusion	0.43 - 0.5
Anomalous transport	0.50<n>1,0
Case I transport	0.85 - 1.0
Super Case II transport	0.85 - 1

[2] This table have been reused again from Chapter 1, Section 1.9, Subsection 1.9.1 for easier and faster comparison with obtained release exponents (n) from power model.

4.6. Release Study of Cytochrome C: with Alternating Magnetic Field (AMF)

The release study of cyt C from bare and hybrid NGs was performed on exposure to AMF and the release conditions were tracked real-time. This section is divided in two subsections. In the first subsection, optimization of dynamic release conditions was discussed. Later, the release profiles performed for 10 hours with and without AMF is discussed.

4.6.1. Dynamic Release Conditions

Studies were performed with Magnetherm setup to understand the effect of alternating magnetic field (AMF) on release of cyt C from hybrid NGs. Release was also done without AMF which served as control of the study. The main aim was to maintain a condition of 37 ºC with and without AMF for the release study thus trying to emulate human biological conditions. But in experimental scenario, it was not possible to expose the samples at constant temperature of 37 ºC, the reason for which is discussed below. Readings for studying the release of cytochrome C using UV-vis were taken each hour. While performing UV-vis, the samples cooled down to room temperature. When samples were again placed in the magnetherm setup for the next hour of release, a certain lapse of time was required for the samples to reach 37 ºC. Thus, samples were not exposed to constant condition of 37 ºC for the entire duration of 1 hour. This was due to small size of in-built sink of magnetherm; providing smaller area of contact with the samples causing slow heat transfer (discussed in Chapter 2, Section 2.3, Subsection 2.3.10). Therefore, real time temperature profiles were recorded for each hour and the release was performed at dynamic condition (TP_WMF) (shown in Figure 3.19 – a).

Another challenge was faced when exposed to AMF. There was unwanted heat production from eddy currents in sink water. In this case, the heat from eddy currents was utilized to increase the temperature of the sink. Henceforth, the real time temperature of the system was again monitored. The temperature profile with AMF (TP_MF) is shown in Figure 3.19 – b).

Therefore, heat originating from two different heat sources – a) conventional heating from water bath and b) heating from eddy currents were optimized with each other so that the generated heating profiles will be close to each other. Thus, TP_MF provided similar heating conditions to TP_WMF, but with addition of alternating magnetic field (AMF). Figure 4.10 represents a

schematic of the exposed dynamic conditions – TP_WMF and TP_MF at which release study of cyt C was performed.

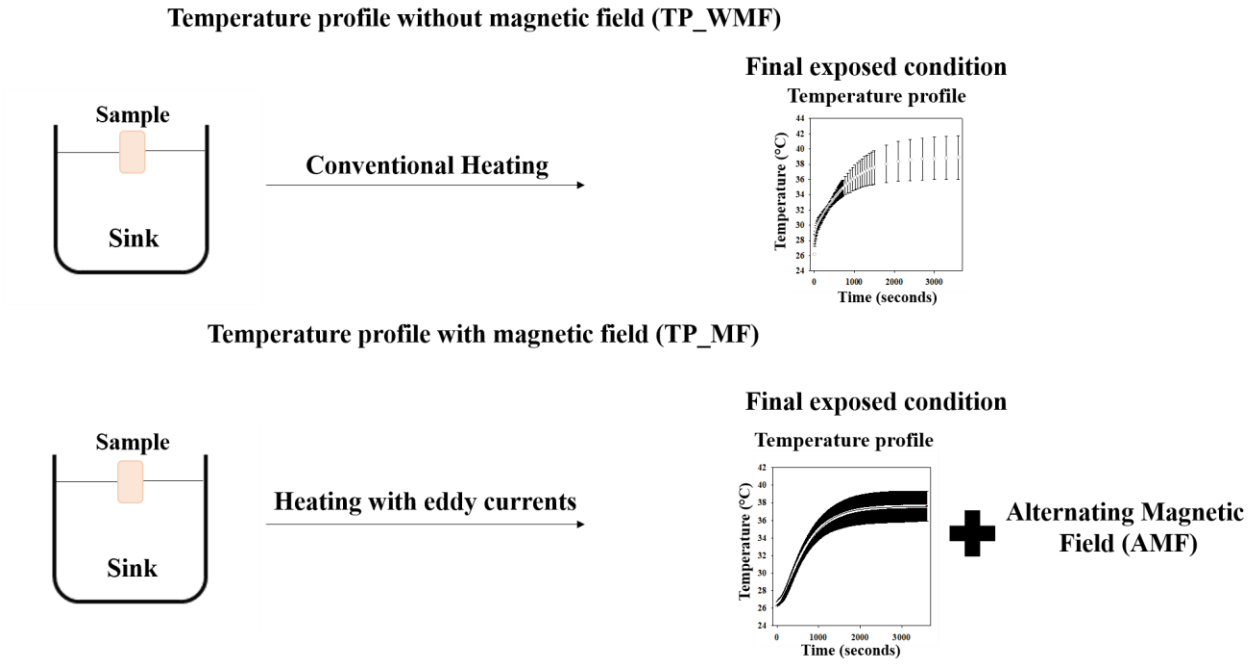

Figure 4.10 – Schematic showing the dynamic temperature conditions – TP_WMF, TP_MF at which release of cyt C was performed.

4.6.2. Release of Cytochrome C: With Alternating Magnetic Field

The main idea for performing release of cyt C with AMF, was to detect any triggered release due to heat production from the magnetic part (phase transferred IONPs particles) present with hybrid NGs. Release study of NGs_insitu system was performed at both conditions – TP_MF and TP_WMF for 10 cycles (shown in Figure 3.20 – a)). TP_WMF functioned as control condition in the study. For TP_MF, the magnetic field parameters were set to 587 kHz, 12 mT which was optimized for production of maximum heat from IONPs_oleate particles (discussed in Section 4.2, Subsection 4.2.4). The same field conditions were used with NGs_insitu system mainly due to two reasons. Firstly, the NGs_insitu system showed no major change in magnetic properties as compared to IONPs_oleate particles (discussed in Section 4.4, Subsection 4.4.1). Secondly, the fibre optic temperature probe of magnetherm setup (shown in Chapter 2, Section 2.3, Figure 2.18 – a)) was not able to detect any increase in temperature of NGs_insitu system (attached in

Appendix G). Thus, it was not possible to perform SAR optimization of NGs_insitu system, and release study were carried out at the best field conditions obtained for phase transferred IONPs_oleate particles. The diameter of magnetherm temperature probe was 120 um. Any heat production below space regime (120 um) would not be detected by the temperature probe. This non-measurable heat will be referred to as local heat and the measurable heat will be referred to as global heat for the entire study. Due to small amount of magnetic content, no global heat production from NGs_insitu system was observed, which was also previously shown by Riedinger et al. with polyethylene glycol (PEG) coated IONPs systems (4). Henceforth, any local heat production from NGs_insitu system could only be detected via a thermal nano sensor (in our case NGs) releasing some bioactive agent as function of heat (in our case cyt C).

NGs_insitu, bare NGs and Loaded NGs_added samples had similar L.E (77 ± 1 %). The release profiles were fitted with mathematical models – 1) zero order, 2) first order, 3) Higuchi 4) power law for 4 hours to compare the initial release rates and dominant release mechanisms involved. The best fit models are discussed while the rest are attached in Appendix H.

NGs_insitu system showed lower cyt C release (%) under condition TP_MF (~ 16 %) as compared to condition TP_WMF (control condition) (21 %) at the end of 4 hours (shown in Figure 3.20 - a)). Zero order model fitted best for NGs_insitu system under both release conditions (shown in Figure 4.11 – a) and b)). The K value obtained for NGs_insitu system was higher under condition TP_WMF (0.06 $hour^{-1}$) as compared to condition TP_MF (0.04 $hour^{-1}$) (shown in Table 4.3). This is attributed to the fact that the fitted average temperature values for condition TP_MF was comparatively lower to condition TP_WMF (shown in Figure 3.19 – c)), in turn higher release and K values of cyt C from NGs_insitu systems was seen under condition TP_WMF. Effect of 5 °C increase in temperature on release profiles of cyt C is attached in Appendix I. This might suggest, local heat produced on exposure to AMF did not show detectable change in release profile of cyt C. The release signal due to local heat from NGs_insitu system got lost in the signal which originated from temperature variation seen between TP_WMF and TP_MF release conditions.

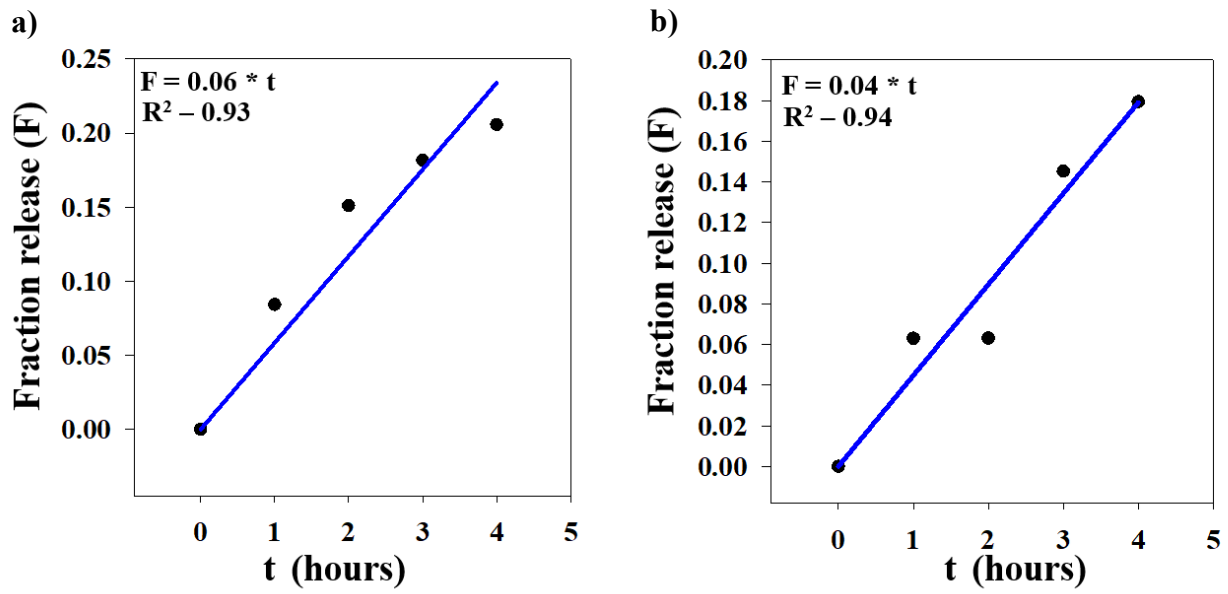

Figure 4.11 – a) and b) Fitted zero order models for NGs_insitu system under conditions TP_WMF and TP_MF, respectively.

Another attempt was made to detect any change in cyt C release profile from NGs_insitu system due to production of local heat. Thus, cyt C release profiles from bare NGs (control sample) and NGs_insitu system were compared under same condition – TP_MF (shown in Figure 3.20 – b)). Bare NGs and NGs_insitu systems showed best fit with zero order model (shown in Figure 4.12 – a) and b)). The K value for bare NGs (0.08 $hour^{-1}$) was 2 times more than NGs_insitu system (0.04 $hour^{-1}$) (shown in Table 4.3). This again makes it difficult to analyze the effect of local heat production on release of cyt C from NGs_insitu system as it gets masked due to significantly higher releases from bare NGs which was considered as control sample in this study. An important point was that the L.E for both bare NGs and NGs_insitu systems was similar in this study (77 ± 1 %) and due to lower release rates of cyt C from NGs_insitu system, the previous discussion (Section 4.5, Subsection 4.5.2, Paragraph 5) of NGs_insitu systems forming slower or sustained drug delivery systems as compared to bare NGs is strengthened.

Lastly, phase transferred IONPs_oleate particles (10 mg) was simply added in bare NGs system, loaded with cytochrome C and the release was performed under condition TP_MF (shown in Figure 3.20 – b)). This was performed to analyze any measurable change in cyt C profile due to production of global heat in the system. In contrary, the release rates of cyt C from Loaded

NGs_added system (0.03 hour^{-1}), fitted best with zero order model was significantly lower as compared to bare NGs and NGs_insitu systems (shown in Figure 4.12 - b)). This might be due to hindrance effect caused by added phase transferred particles in the system effecting the mobility of released cytochrome to reach the walls of the dialysis membrane, before diffusing out into the sink, which was also seen in NGs_added system as previously discussed (Section 4.5, Subsection 4.5.2, Paragraph 10). Henceforth, the effect of local heat production on release of cyt C from Loaded NGs_added system becomes non-commentable due to hindrance effect caused by added phase transferred IONPs.

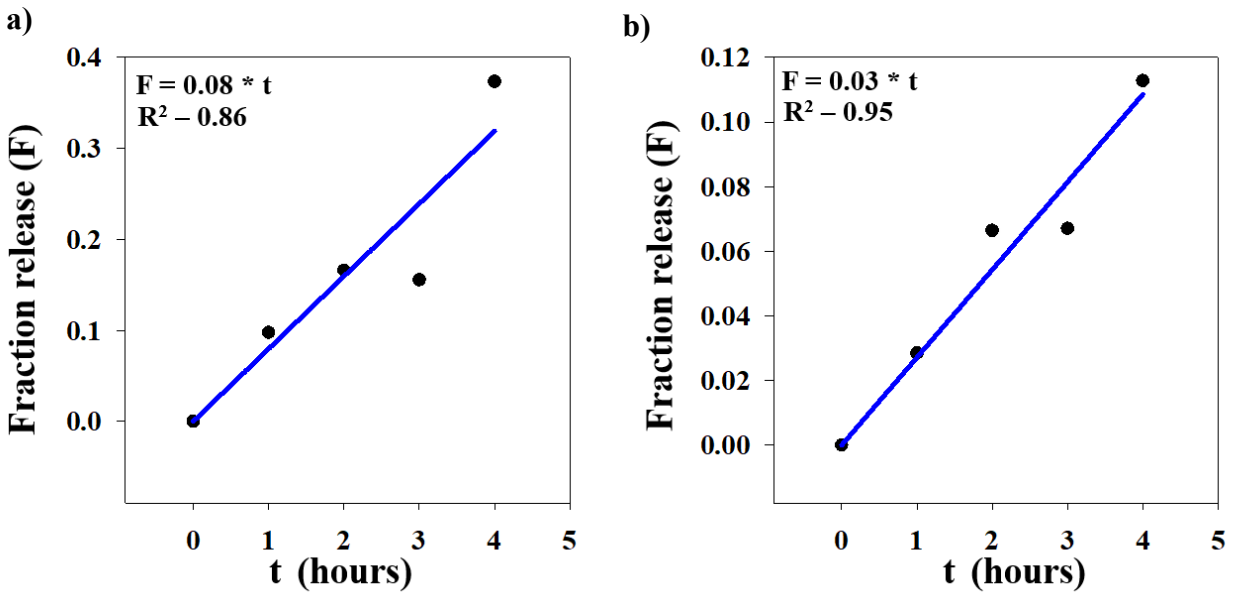

Figure 4.12 – a) and b) Fitted zero order model for bare NGs and Loaded NGs_added systems under condition TP_MF.

Table 4.3 - Showing rate constant K (hour $^{-1}$) for NGs_insitu, bare NGs and Loaded NGs_added systems under release conditions – TP_MF and TP_WMF, respectively with corresponding dominant release mechanisms.

Samples	**Release condition**	**Release constant (K) (hour $^{-1}$)**	**Dominant Mechanism**
NGs_insitu	TP_MF	0.04	Zero order
	TP_WMF	0.06	Zero order
Bare NGs	TP_MF	0.08	Zero order
Loaded NGs_added	TP_MF	0.03	Zero order

In this section, release study of cyt C was performed from NGs_insitu, bare NGs and Loaded NGs_added systems on exposure to AMF. Two different controls were used to understand effect of local heat production on release of cyt C from hybrid NGs. Firstly, release studies were performed from NGs_insitu system under two different conditions – TP_WMF (control condition) and TP_MF. Secondly, release profiles of bare NGs (control sample) and NGs_insitu systems were obtained on AMF exposure. In both cases, production of local heat was not detectable due to comparatively higher contributing effects of control on release profiles of cyt C. Lastly, cyt C release profiles for Loaded NGs_added system was obtained to analyze effect of global heat on release. Due to presence of phase transferred IONPs in Loaded NGs_added system, hindrance effect on mobility of cyt C was observed which made effects of global heat on cyt release also non-detectable.

Therefore, considering natural eddy currents originating in water on exposure to AMF, finer optimization of release conditions and innovative ways to increase magnetic content in hybrid NGs systems are required to detect and further optimize magnetically triggered releases.

Chapter 5: Conclusion

Iron oxide nanoparticles (IONPs), due to their size controllable synthesis techniques, superparamagnetism and tunable biocompatibility, have shown wide potential in biomedicine that involve, both imaging and therapeutic applications. Engineered IONPs, with organic and inorganic materials can have multi-functional properties like pH, light, thermal and magnetic sensitivity which can be utilized for *in-vivo* bioimaging, bio-separation of proteins, lipids, DNA and RNA, and target specific drug delivery systems.

In this study, synthesis of monodisperse IONPs in organic solvents were done using two different iron precursors – iron oleate (IONPs_oleate) and iron pentacarbonyl (IONPs_penta). The synthesized IONPs showed reproducible and repeatable sizes of 16 ± 2 nm and 8 ± 1 nm for IONPs_oleate and IONPs_penta, respectively, with low polydispersity index (PDI) for both (~0.1). The crystallographic properties of two system of particles were studied using XRD. Both the system of particles showed presence of magnetite crystallographic phases, but due to enhanced peak broadening effect contributed from small size of IONPs, it was not possible to quantify composition of phases and there might have been presence of other iron oxide phases. IONPs_penta particles were amorphous in nature, whereas the IONPs_oleate particles were relatively crystalline. The saturation magnetization (Ms) value of IONPs_oleate particles (74.3 emu/g) was significantly higher as compared to IONPs_penta particles (21.9 emu/g), but both the systems showed superparamagnetic at room temperature. The difference in Ms of the two systems showed the concept of nanoscale Kirkendall effect, which causes diffusion of iron core from the core-shell structure of IONPs_penta systems, resulting in lower Ms values.

Both of the IONPs systems were phase transferred to aqueous phase with sodium citrate, to be able to utilize them for biomedical application. Repeatability of the phase transfer process was shown as 10-12 batches of experiments were performed, resulting in hydrodynamic sizes of 236 ± 32 nm and 355 ± 37 nm for IONPs_oleate and IONPs_penta, respectively. The efficacy of the phase transfer process was shown from high zeta potential values on the negative scale measured using DLS, which showed stability of phase transferred IONPs_oleate (-50 ± 2 mV) and IONPs_penta particles (-41 ± 7 mV) in water. The stability of these systems was tested over two months, elevated

temperatures and pH values ranging from acidic to alkaline. Both the systems were stable with little to no change in hydrodynamic sizes and zeta potentials over long periods and high temperatures. The pH stability window for phase transferred IONPs_oleate was observed ~ (3.5 pH – 7 pH) and for IONPs_penta was ~ (4 pH– 7 pH), which showed good stability range for application in different parts of the human biological systems, starting from slightly alkaline regions (blood and brain) to more acidic regions (stomach and gastrointestinal tract). Due to significantly higher Ms value for phase transferred IONPs_oleate particles (26.1 emu/g) as compared to IONPs_penta particles (0.6 emu/g), oleate system of particles were chosen for heat production study on exposure to AMF conditions. At AMF condition (587 kHz, 12 mT), the highest SAR value (1.7 ± 0.4 W/g) was obtained for phase transferred IONPs_oleate particles that was compared with magnetite NPs (150 ± 80 W/g). Much less heating effects were seen from phase transferred particles showing potential for producing controlled heat, which could be utilized for synthesizing target specific drug delivery systems with minimal side effects from unwanted heating.

Poly- (N-isopropyl acrylamide-acrylic acid) (NGs), a thermo and pH-responsive polymer was used with phase transferred IONPs to synthesize hybrid NGs. Hence, seven batches of NGs were synthesized with average hydrodynamic diameter (250 ± 20 nm) obtained at 25 ºC, which showed repeatability of the process. Thermo-responsive properties were studied by seeing their collapses at 45 ºC. All the batches collapsed, and the reduced average hydrodynamic diameter (95 ± 2 nm) was seen for seven batches. The calculated volume phase transition temperature (VPTT) of NGs was 35.9 ± 0.3 ºC. pH characterization was also performed which showed reduction in sizes of NGs (~ 63 nm) at acidic condition (3.5 pH). Henceforth, thermal and pH responsive properties of NGs combined with superparamagnetic properties of phase transferred IONPs could be utilized to synthesize drug delivery devices with many functionalities.

Hybrid NGs were synthesized using three different techniques - (i. In-situ, ii. Post, iii. Addition), with the idea of producing hybrid systems with different physico-chemical properties which could open up new opportunities as multi-functional drug delivery systems. The hybrid NGs synthesized using different techniques showed differences in sizes and thermo-responsive properties. The highest possible amount of phase transferred IONPs (4 mg) was used with bare NGs during all the

three synthesis techniques for comparison. The hydrodynamic sizes obtained for NGs_insitu system (323 ± 4 nm) was higher as compared to bare NGs (250 ± 20 nm) which suggested presence of phase transferred IONPs with NGs structures. The VPTT obtained for NGs_insitu system (36.8 ± 0.2 ºC) was ~ 1 ºC higher as compared to bare NGs (35.9 ± 0.3 ºC). The NGs_insitu system (97 %) also showed higher volumetric collapse efficiency (VCE) (%) at 45 ºC as compared to bare NGs (94 %). From small differences in thermo-responsive properties between bare NGs and NGs_insitu systems, it was difficult to conclusively comment on the distribution of phase transferred particles with NGs structures, but a possible hypothesis was shown where the particles might be present both internally and externally with NGs structures. The VPTT obtained for NGs_post system (35.7 ± 0.2 ºC) was similar with bare NGs (35.9 ± 0.3 ºC). Based on previous cited works by other research groups on post synthesis technique, a possible hypothesis was discussed for our NGs_post system, which suggested phase transferred particles forming external bridging structures between bare NGs. Lastly, addition technique was implemented to study if the phase transferred particles could be interacted with NGs structures without using stirring or heating. The magnetic bottom product separated from NGs_added systems, showed collapses at elevated temperatures of 45 ºC and 60 ºC which confirmed interaction between phase transferred particles and NGs. The VPTT obtained for NGs_added system (37.6 ± 0.1 ºC) was higher as compared to bare NGs and other hybrid NGs. This was attributed to interaction of phase transferred IONPs with unwanted polymeric structures, which might have been present in NGs_added system due to its different cleaning process. All the three systems showed superparamagnetism at room temperature which further confirmed presence of phase transferred IONPs with NGs structures. The pH-sensitive properties of NGs_insitu and NGs_post systems were similar to bare NGs which showed reduction in sizes at acidic pH condition (3.5 pH). It was shown that utilizing phase transferred IONPs with NGs did not have considerable effect on the pH sensitivity of NGs. Henceforth, hybrid NGs showed thermal, pH and magneto-responsive properties.

Hybrid NGs were utilized to load and release a model protein cytochrome C (cyt C) under condition 40 ºC and pH (3.5). The effect of subtle differences in physico-chemical properties between hybrid NGs on release of cyt C were studied by mathematically fitting with common drug delivery models. The initial part of the release profiles (~ 2.5 hours) showed best fit with zero order models. As compared to initial release rates of bare NGs (K value – 0.15 $hour^{-1}$), the

NGs_insitu system showed significantly slower releases (K value - 0.08 $hour^{-1}$) suggesting formation of slower or sustained drug delivery devices. The release profile for NGs_post system was similar to bare NGs, which can be attributed to close themo-responsive properties between these systems (also seen from similar VPTT values). The initial release profiles (~ 1.5 hours) for NGs_added system showed best fit with Higuchi model, showing Fickian diffusion (independent of collapse of polymeric chains of hybrid NGs). This suggested a hindrance effect on mobility of released cyt C, as predicted due to presence of unreacted polymeric structures in NGs_added systems. Henceforth, the subtle differences in thermo-responsive properties between the hybrid systems originating from different synthesis techniques has significant effect on release profiles of cyt C, in turn giving rise to different drug delivery devices.

After investigating thermal and pH responsive properties of hybrid NGs on cyt releases, the magneto-responsive properties were also studied. The main challenge faced while performing release studies from hybrid NGs, under AMF condition, was production of background heat from eddy currents. Inorder to compensate for background heating effects, two dynamic conditions – temperature profile with magnetic field (TP_WMF) and temperature profile without magnetic field (TP_MF) were optimized, at which release studies were performed. Three studies were done to analyze the effect of AMF on release from hybrid NGs. Firstly, release study from NGs_insitu systems were carried out for 10 cycles (10 hours) under both conditions TP_WMF and TP_MF. TP_WMF was used as the control condition in the study. The initial release from NGs_insitu systems for first 4 hours was best fitted with zero order model. NGs_insitu system under condition TP_MF (0.04 $hour^{-1}$) showed slower release rates as compared to releases performed under condition TP_WMF (0.06 $hour^{-1}$). This was attributed to differences between release conditions TP_WMF and TP_MF. Thus, effect of AMF on release of cyt C from hybrid NGs was not detectable due to noise from control condition – TP_WMF. In the second study, releases from bare NGs (control sample) were compared with NGs_insitu system under condition TM_MF. The obtained release rate from bare NGs (0.08 $hour^{-1}$) was higher as compared to NGs_insitu system (0.04 $hour^{-1}$) for first four hours. This again made it difficult to understand the effect of AMF on releases, as bare NGs (control sample) showed higher release rates. Lastly, Loaded NGs_added system (containing higher amount of phase transferred IONPs than hybrid NGs) was compared with bare NGs (control). In this case, the release rates obtained for Loaded NGs_added system

(0.03 hour $^{-1}$) was also significantly lower than the control used (0.08 hour^{-1}), thus making it uncommentable on the effect of AMF on release of cyt C. Hence, finer optimization of release conditions and innovative ways to increase magnetic content in hybrid NGs systems are required to detect release of cyt C under AMF condition.

In summary, effective phase transfer of IONPs from organic to aqeuous mdia was shown. The stability of the phase transferred particles were studied under different conditions. Next, these particles were used to synthesize novel hybrid NGs with thermal, pH and magneto-responsive properties. It was also shown that implementing different synthesis techniques for hybrid NGs, can be used to engineer thermo-responsive properties of the system. The effects of physico-chemical properties of hybrid NGs were studied on loading and release of cytochrome C from these systems. Slower or sustained drug delivery system (NGs_insitu) was produced as compared to previously cited bare NGs system. Finally, releases from hybrid NGs were performed on exposure to AMF condition, to understand the effect of magneto-resposive properties of hybrid NGs.

Future Scope

Synthesis of hybrid NGs with thermal, pH and magneto-responsive properties, having good drug loading and release properties have been shown successfully within the scope of this study. The distribution of phase transferred IONPs with the NGs structures was studied using Dynamic Light Scattering Technique (DLS) and probable hypothesis was drawn. However, other characterization techniques could be utilized like Fourier Transform Infrared Spectroscopy (FTIR) to understand chemical interactions between particles and NGs population. Similarly, Small Angle X-ray Scattering (SAXS) could also be used to analyze distribution of particles with NGs populations.

Future studies should be performed trying to increase the magnetic content in hybrid NGs systems, in order to make the magneto-responsive properties of these systems more pronounced. Innovative methodologies could be implemented like use of glass stirrers or non-magnetic impellers during the synthesis process, in order to overcome the sticking problem of IONPs to magnetic stirrers. This could in turn allow to increase the amount of IONPs during the synthesis process.

A general breathing-in approach was provided based on previous experimental observations, as how cyt C gets loaded with NGs and hybrid NGs. Different techniques like FTIR and Raman spectroscopy could be utilized, to examine chemical interactions between cyt C and nanogel structures.

For studying magneto-responsive releases under dynamic conditions using Magnetherm setup, finer optimization of release conditions is required to compensate for eddy currents generating unwanted background heat. This would help to analyze the release signal of cyt C from hybrid NGs on exposure AMF conditions.

Having shown that hybrid NGs have good loading and release properties with cyt C, the study can be extended to investigate the loading and release capacities of these systems with other more commercially used drugs such as L-Dopa, Coumarin and Doxorubicin. Lastly, release studies could be performed in more realistic environments, like serum cultures emulating close human biological conditions.

Appendices

Appendix A

Synthesis of Magnetite Nanoparticles

The magnetite (Fe_3O_4) nanoparticles were synthesized using concept of co-precipitation from previous well developed works reported elsewhere (92). The magnetite nanoparticles were abbreviated in our study as magnetite NPs. Magnetite NPs were prepared using iron chloride tetrahydrate ($FeCl_2 \cdot 4H_2O$) (1.5 g) and iron chloride hexahydrate ($FeCl_3.6H_2O$) (3.0 g), with molar ratio of ferric (Fe^{3+}): ferrous (Fe^{2+}) ions taken 1:2 and dissolved in MQ water (100 ml) with vigorous stirring. In parallel, NH_4OH (25 wt %) in MQ water (10 ml) was prepared. The Fe^{3+}/Fe^{2+} ions solution was gently poured dropwise using a burette in the ammonia and water solution. The solution color changed from orange to black rapidly. The formed magnetite nanoparticles were magnetically separated and thoroughly washed with MQ water three times. The final particles were redispersed in MQ water (30ml). A reaction schematic is shown in Figure A.1.

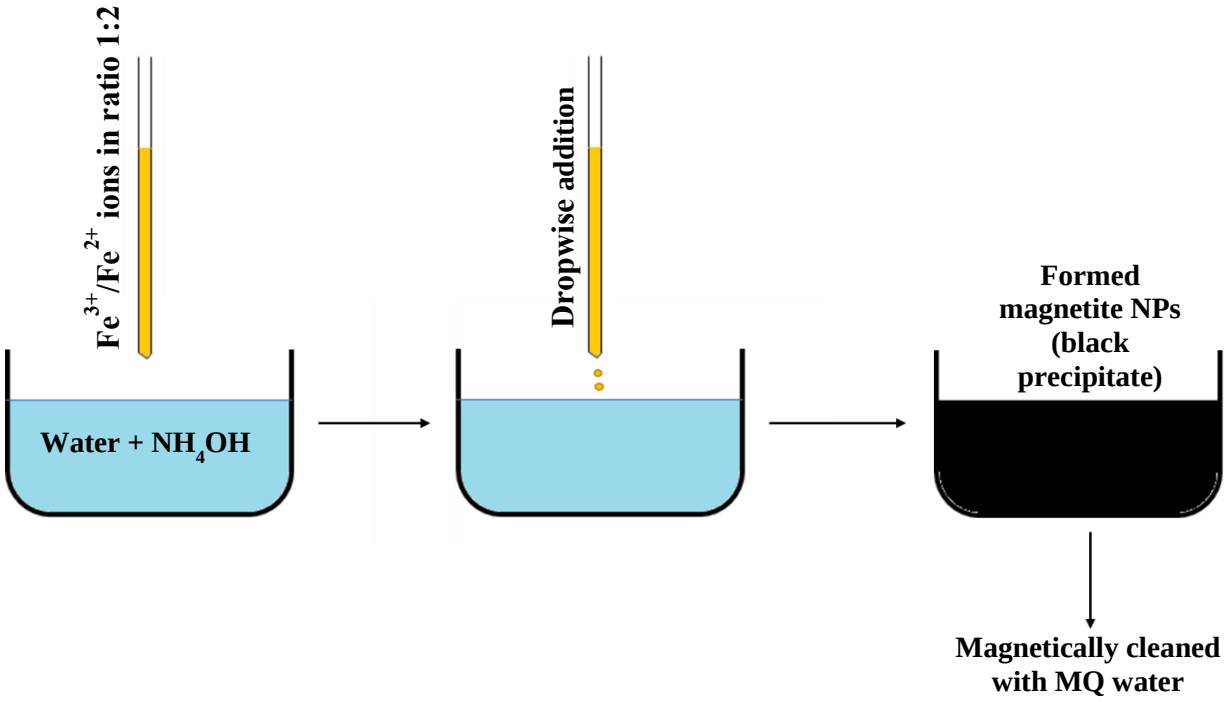

Figure A.1– Schematic showing synthesis of magnetite NPs via co-precipitation concept.

Appendix B

Synthesis of Loaded NGs_added System

This system was synthesized by first loading NGs system with cyt C. The loaded NGs system (2 mL) was then taken in a glass vial, into which phase transferred IONPs_oleate particles (10 mg) was simply added without stirring or heating. In our study this system was abbreviated as Loaded NGs_added system. Loaded NGs_added system was then taken for release studies under condition TP_MF. A flowchart of the above stated synthesis is shown in Figure A.2.

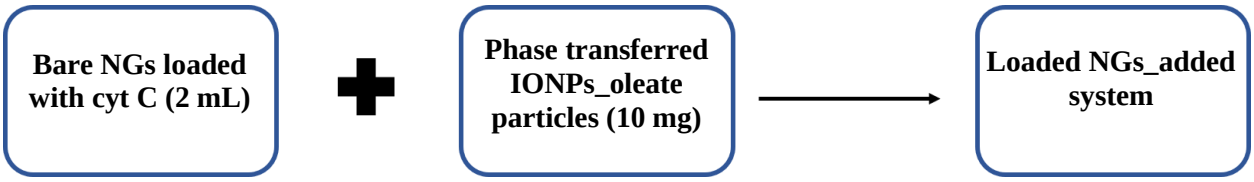

Figure A.2 – Flowchart showing synthesis of Loaded NGs_added system.

Appendix C

Calibration Curve of Cytochrome C

The calibration curve of cyt C was obtained by measuring peak absorbance values using UV-vis spectroscopy (409-411 nm) as function of concentration (shown in Figure A.3). The plotted values showed linear fit which is in accordance with Beer-Lambert law (93). The calibration curve was used to calculate peak absorbance value for concentration of cyt C used for loading NGs and hybrid NGs systems. The initial concentration of cyt C used for loading was 0.50 mg/ml. After loading, the samples were diluted 3 times before any release studies (discussed in Chapter 2, Section 2.3, Subsection 2.3.8). Theoretically, hundred percent loading efficiency of cyt C would correspond to concentration 0.20 mg/ml. Henceforth, for concentration (0.20 mg/ml), the absorbance value (1.70) was calculated from the calibration curve (shown in black dotted line in Figure A.3). Based on this value, the loading (L.E) and encapsulation efficiencies (E.E) of the samples were calculated which is shown next.

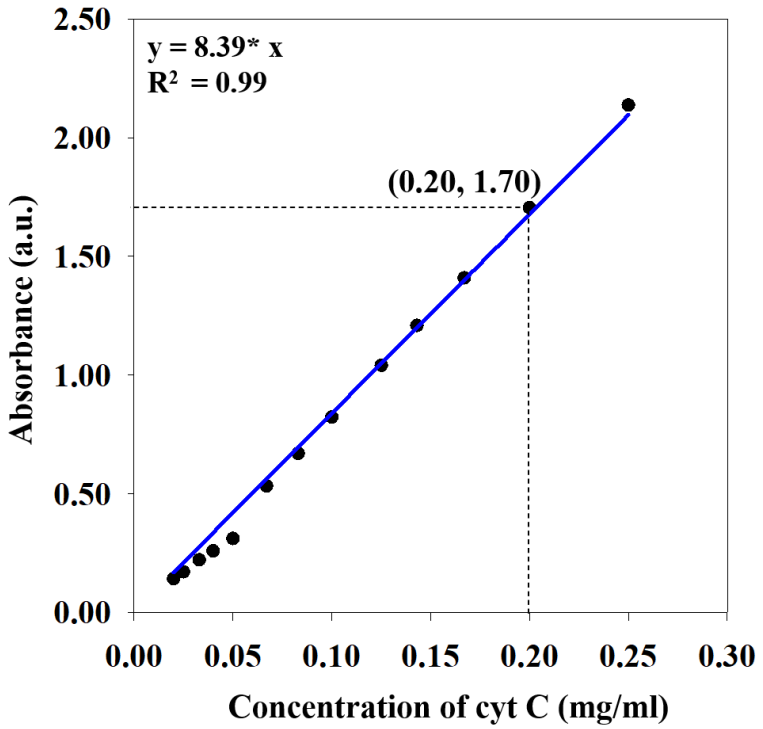

Figure A.3 – Calibration curve of cyt C obtained at different concentrations (mg/ml) as function of absorbance value using UV-vis spectroscopy. Points best fitted with linear plot (R^2 = 0.99).

Calculation of Loading and Encapsulation Efficiencies

The bare and hybrid NGs systems were loaded with cyt C. After the loading procedure, the L.E was calculated based on UV-vis absorption peaks. Theoretically, if hundred percent of cyt C gets loaded in a system, the absorbance value ($A_{100\%}$) is known from above discussed calibration curve. Hence, absorbance peak after loading ($A_{X\%}$) is used to calculate L.E with respect to $A_{100\%}$. The formula for calculating L.E is shown in Equation A.1.

$$L.E\ (\%) = (A_{X\%} / A_{100\%}) * 100 \qquad (A.1)$$

The encapsulation efficiency (E.E) was defined as mass of cyt C loaded per unit mass of nanocarrier system (NGs or hybrid NGs) (shown in Equation A.2).

$$E.E = \frac{(L.E\ (\%) * Mass\ of\ Drug\ used)}{(Mass\ of\ nanocarrier\ system)}\ \left[\frac{ug}{mg}\right] \qquad (A.2)$$

A sample has been demonstrated by the following example using NGs_insitu system as shown by Figure A.4.

$A_{X\%}$ = 1.35

$A_{100\%}$ = 1.70

$L.E = (1.35\ /1.70)\ * 100 = 80\ \%$

Mass of drug used for loading = 1000 µg

Mass of NGs_insitu system = 3.3 mg

$E.E = (80 * 1000)/(100 * 3.3) = 242$ µg/mg

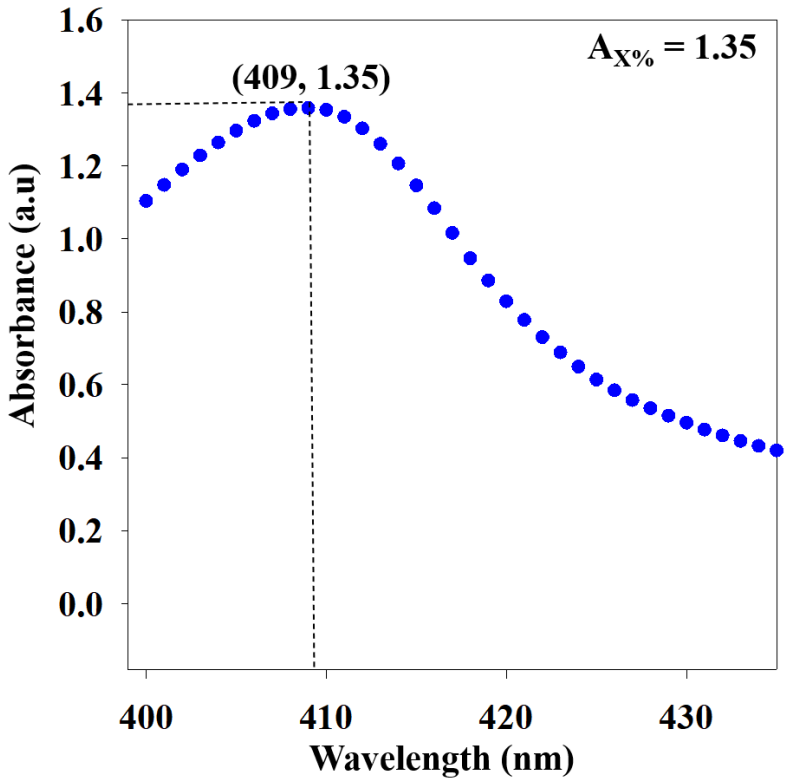

Figure A.4 – UV-vis spectra of NGs_insitu system conducted for calculating L.E.

Appendix D

Release Studies of Cytochrome C using UV-vis Spectroscopy

The release percentage of cyt C from NGs and hybrid NGs systems were calculated as follows:

$$Drug\ Release\ (\%) = [((t_o) - (t))/\ (t_o)]\ X\ 100 \quad \text{(A.3)}$$

where,

t_o = Peak absorbance value of the system at the start of release

t = Peak absorbance value of the system at the time of measurement

$$Cumulative\ Mass\ Released\ (Mt) = [Drug\ Release\ (\%) * L.E\ (\%) * Mass\ of\ drug\ used\ for\ loading] \quad \text{(A.4)}$$

$$Cumulative\ Fraction\ Released\ (F) = [(Mt)/(L.E\ (\%) * Mass\ of\ drug\ used\ for\ loading)] \quad \text{(A.5)}$$

A sample calculation has been shown using the release profile for NGs_insitu system. Figure A.5 shows the decrease in absorbance peaks with cyt C release with time using UV-vis. The value of absorbance is noted at the start of release (t_0) (shown in Figure A.5). The following calculation is shown ~ 20 hours after commencement of release of cyt C from NGs_insitu system.

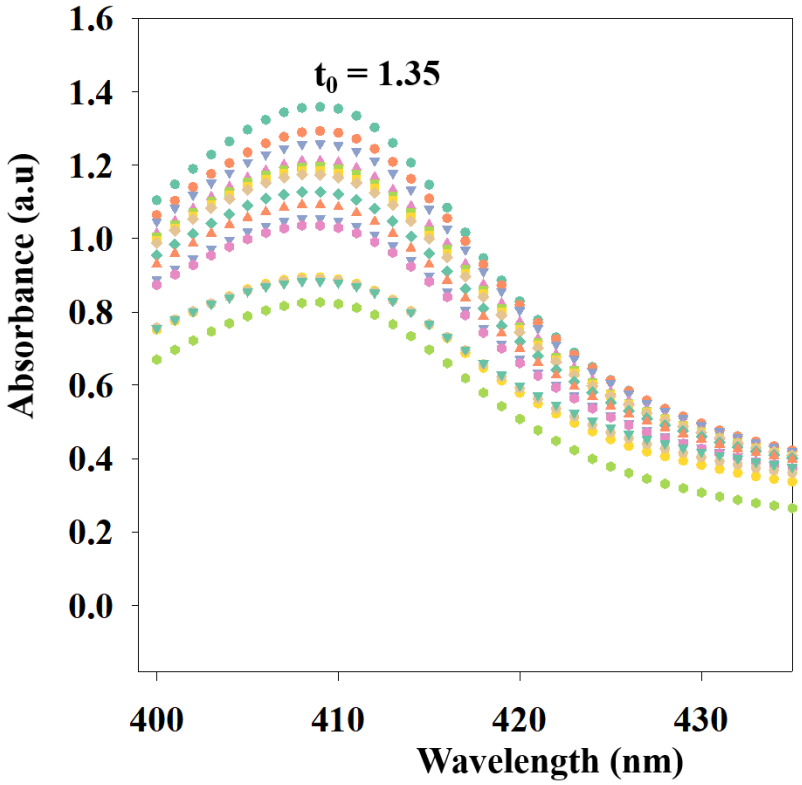

Figure A.5 - Release profiles of NGs_insitu system loaded with cyt C using UV-vis.

The calculations, at t = 20 hours, are as follows:

$Drug\ Release\ (\%)$ = [(1.35-0.78)/ (1.35)] X 100 = 42.22 %

$Cumulative\ Mass\ Released\ (Mt) = [\left(\frac{42.22}{100}\right) * (\frac{80}{100}) * 1000]$ = 337.76 µg

$Cumulative\ Fraction\ Released\ (F) = \left[\frac{337.76}{800}\right]$ = 0.42

Table A.1 provides the values of various parameters used to determine the release kinetics for NGs_insitu system.

Table A.1 – Release kinetics data for NGs_insitu system used for model fitting.

Time (hours)	Release (%)	Mt (ug)	F	ln(F)	ln(1-F)	t^0.5	ln(t)
0	0	0	0			0	
0.25	3.57	28.4107	0.03565	-3.334	-0.0363	0.5	-1.3863
0.5	4.84	38.5477	0.04837	-3.0288	-0.0496	0.70711	-0.6931
0.75	7.4	58.9626	0.07399	-2.6038	-0.0769	0.86603	-0.2877
1	10.79	85.9536	0.10786	-2.2269	-0.1141	1	0
1.25	11.96	95.2342	0.11951	-2.1244	-0.1273	1.11803	0.22314
1.54	12.8	101.939	0.12792	-2.0564	-0.1369	1.23828	0.42744
1.79	13.58	108.152	0.13572	-1.9972	-0.1459	1.33542	0.57848
2.04	17.06	135.888	0.17052	-1.7689	-0.187	1.42595	0.70968
2.54	19.61	156.227	0.19604	-1.6294	-0.2182	1.59164	0.92954
3.04	22.37	178.196	0.22361	-1.4978	-0.2531	1.74165	1.10966
4.04	23.78	189.43	0.23771	-1.4367	-0.2714	2.00832	1.39459
10.04	34.17	272.222	0.3416	-1.0741	-0.4179	3.16754	2.30591
12.09	34.51	274.996	0.34508	-1.064	-0.4232	3.47611	2.49183
13.59	35	278.862	0.34993	-1.05	-0.4307	3.68556	2.60884
20.65	42.94	342.154	0.42936	-0.8455	-0.561	4.54423	3.02772

Appendix E

Release Kinetics Model Fits of Bare NGs

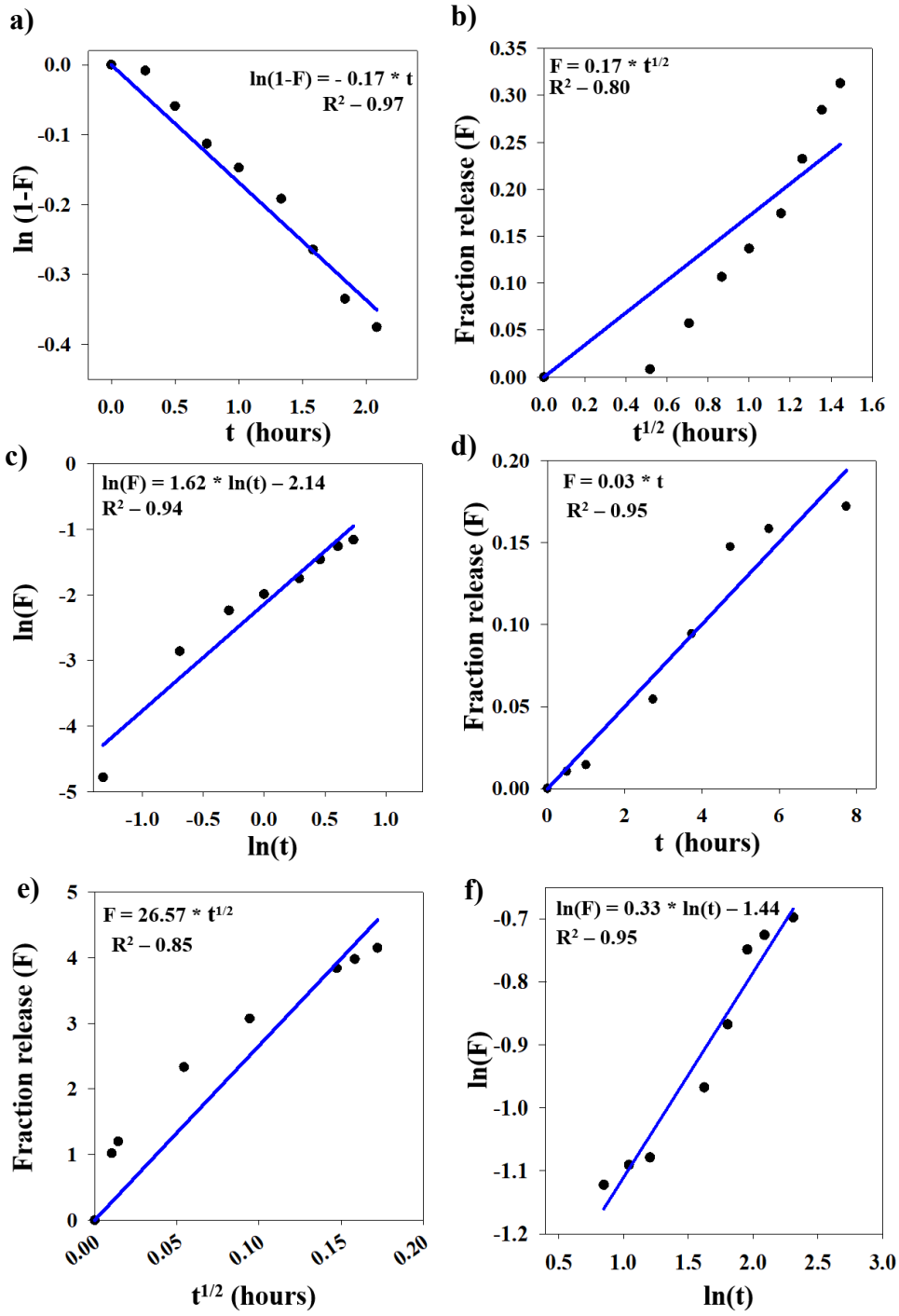

Figure A.6 – a), b), c) Part-I fit with first order, Higuchi, and power law, respectively. d), e), f) Part-II fit with zero order, Higuchi and power model.

Release Kinetics Model Fits of NGs_insitu System

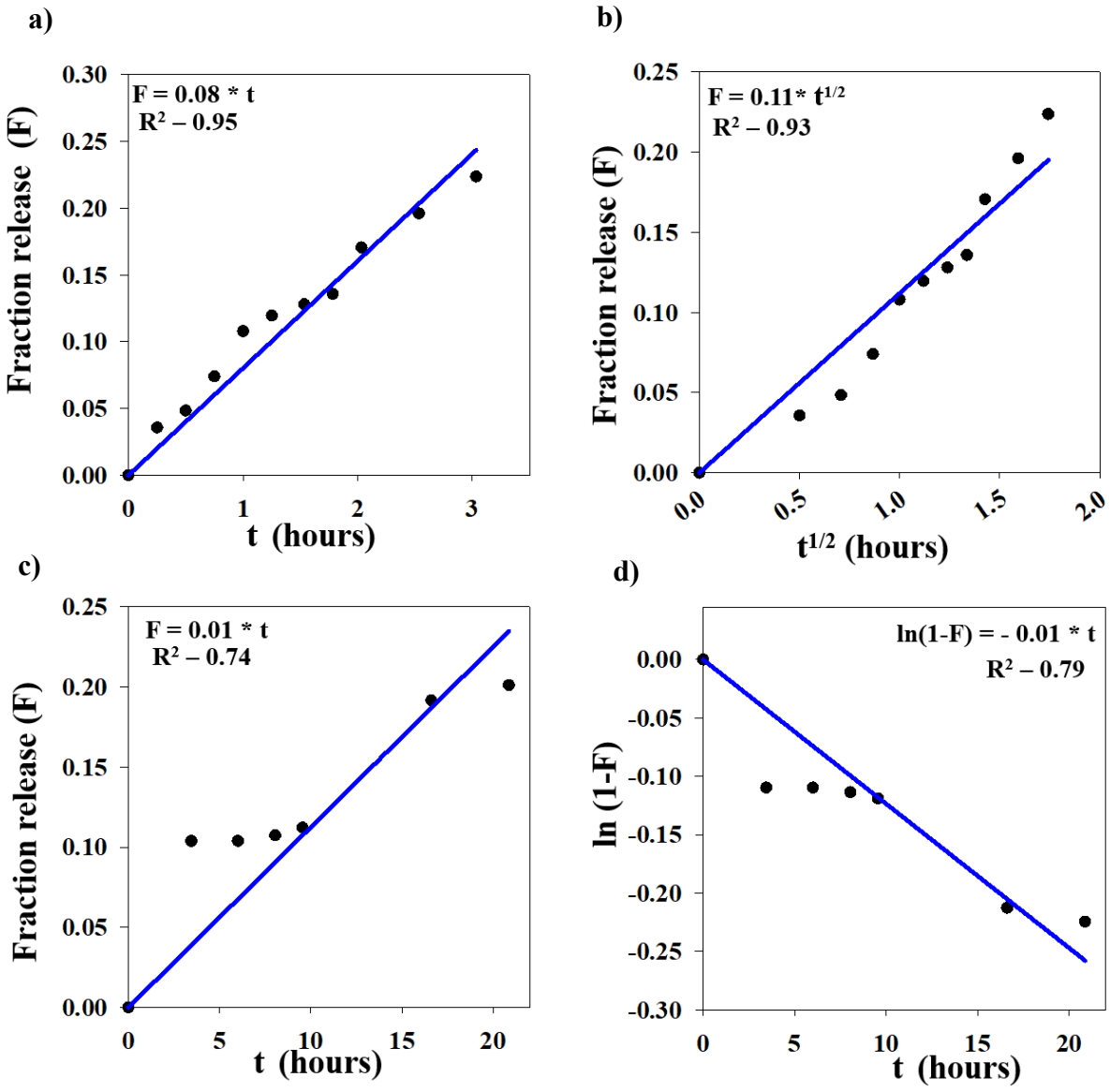

Figure A.7 – a), b) Part-I fit with zero order and Higuchi models. c), d) Part-II fit with zero and first order models.

Release Kinetics Model Fits of NGs_post System

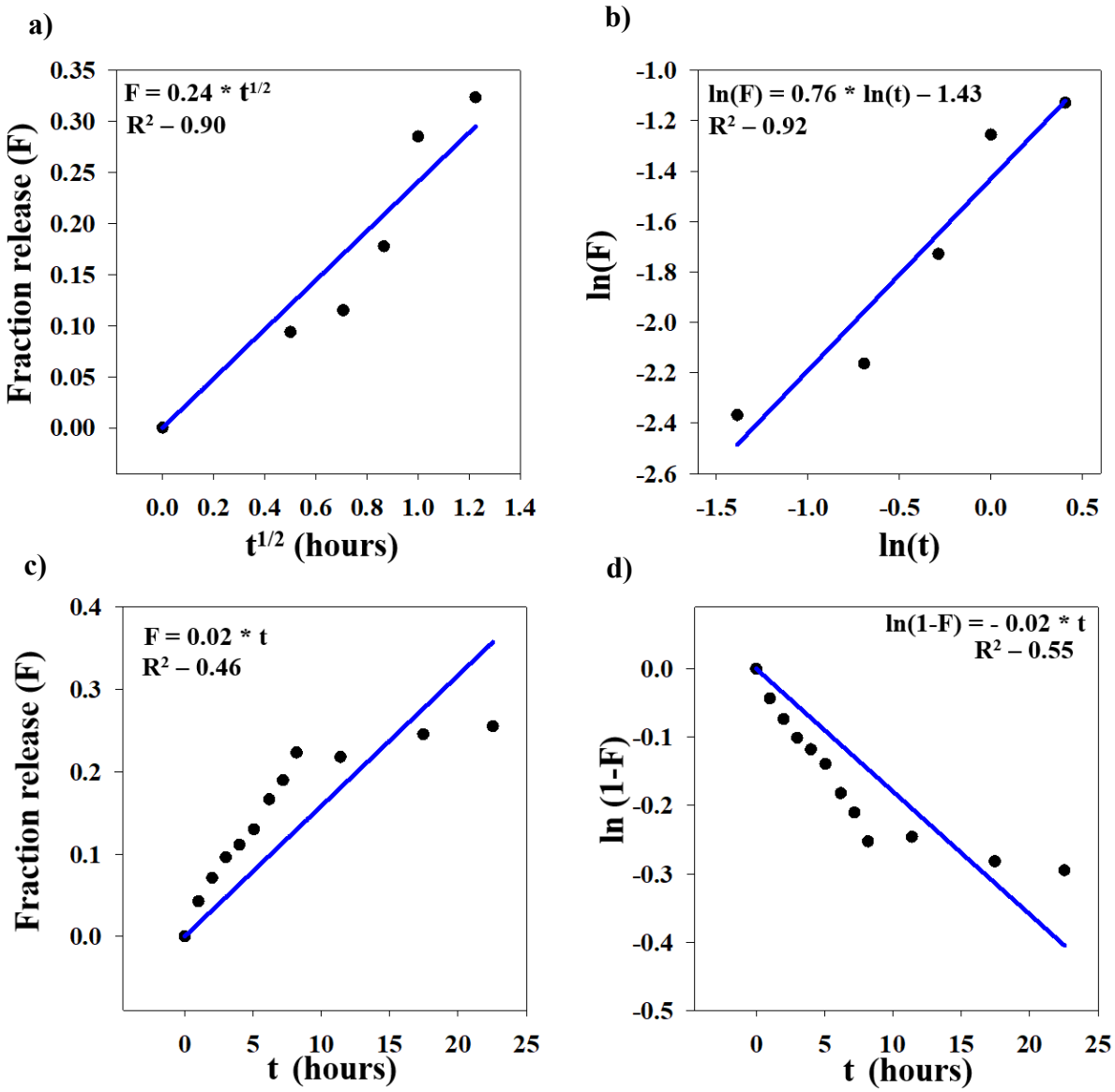

Figure A.8 – a), b) Part-I fit with Higuchi and Power law model. c) and d) Part-II fit with zero and first order models.

Release Kinetics Model Fits of NGs_added System

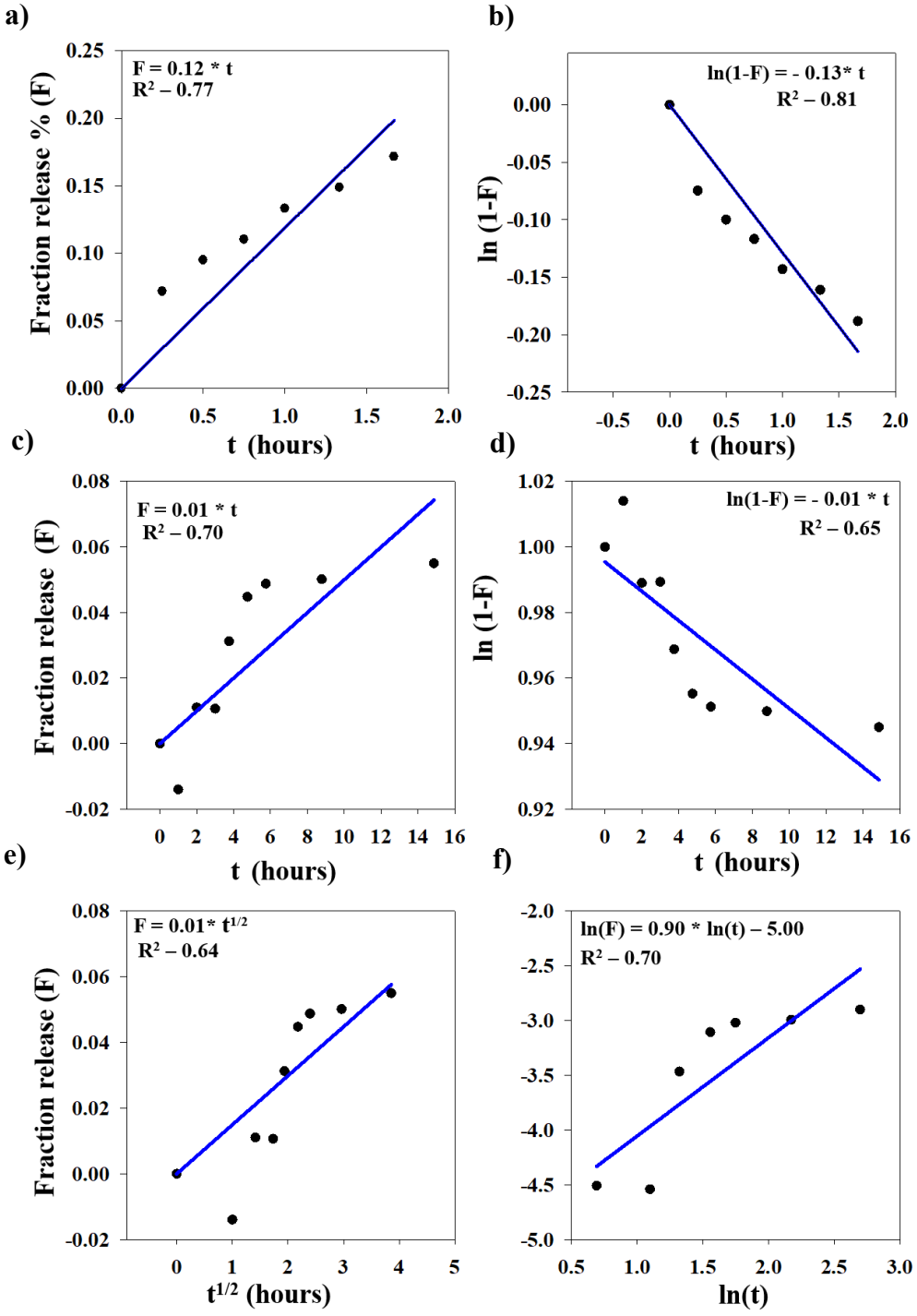

Figure A.9 – a), b) Part-I fit with zero and first order models. c), d) Part-II fit with zero, first order, Higuchi, and power law models.

Appendix F

Effect of Loading Efficiency (L.E) on cyt C Release from NGs_insitu Systems

It is important to point out that the releases at two different L.E (shown in Figure A.10) was carried out same release condition of 40 ºC and 3.5 pH.

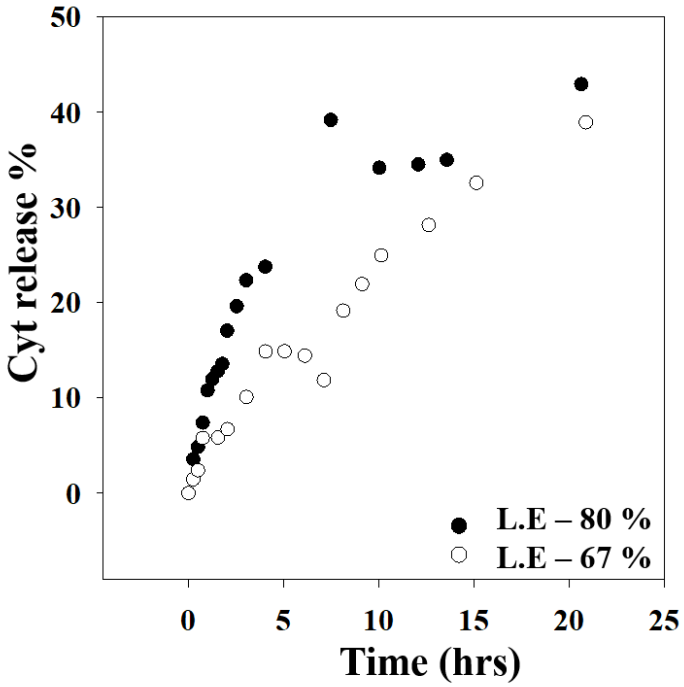

Figure A.10 – Effect of L.E on cyt C release from NGs_insitu system

Appendix G

Heat generation from NGs_insitu system on exposure to AMF

The heat profile as function of temperature for NGs_insitu system on exposure to AMF condition (587 kHz, 12 mT) is shown in Figure A.11. The shaded region shows the standard deviation in heat production. Almost no heating effect was monitored for NGs_insitu system as the heat signal from the sample got overshadowed in background heat contributed from formation of eddy currents in MQ water. Also low SAR value (0.76 ± 0.12 W/g) was calculated.

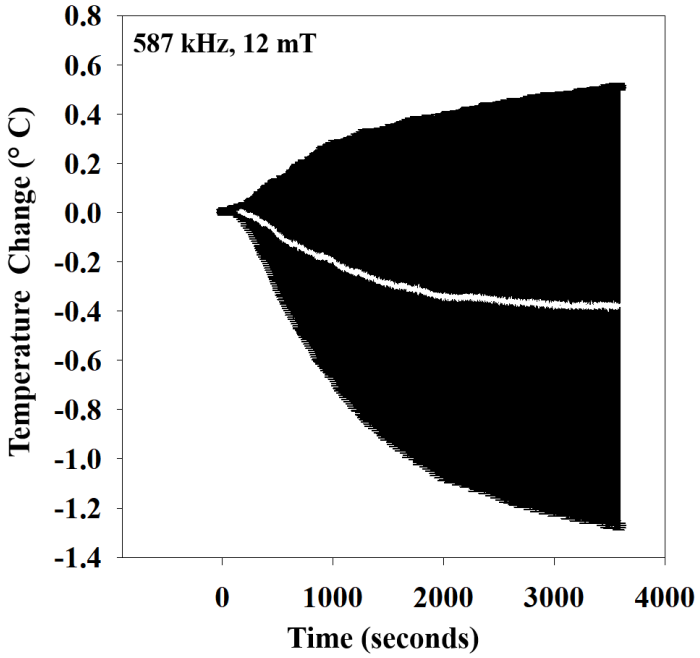

Figure A.11 - Shows the temperature change as function of time under AMF condition (587 kHz, 12 mT) for NGs_insitu system. The shaded region (shown in black) shows the standard deviation in temperature produced.

Appendix H

Release Kinetics Model Fit of bare NGs and hybrid NGs under condition TP_MF

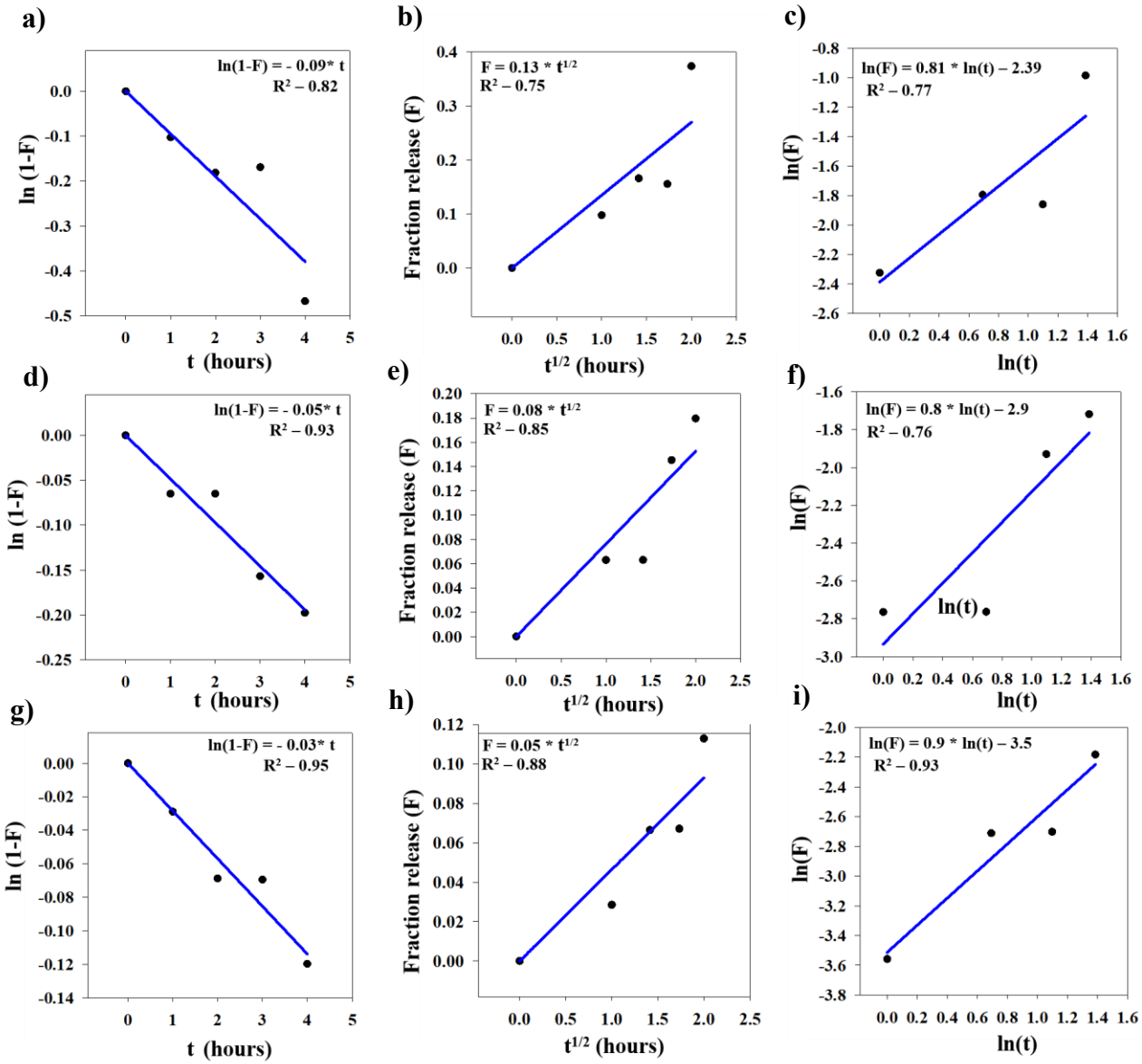

Figure A.12 – a), b), c) Release from bare NGs for 10 cycles fit with first order, Higuchi, and power models, respectively. d), e) and f) Release from NGs_insitu for 10 cycles fit with first order, Higuchi, and power models, respectively. g), h) and i) Release from Loaded NGs_insitu for 10 cycles fit with first order, Higuchi, and power models, respectively. All the release data was obtained under condition TP_MF.

Release Kinetics Model Fit of NGs_insitu System under condition TP_WMF

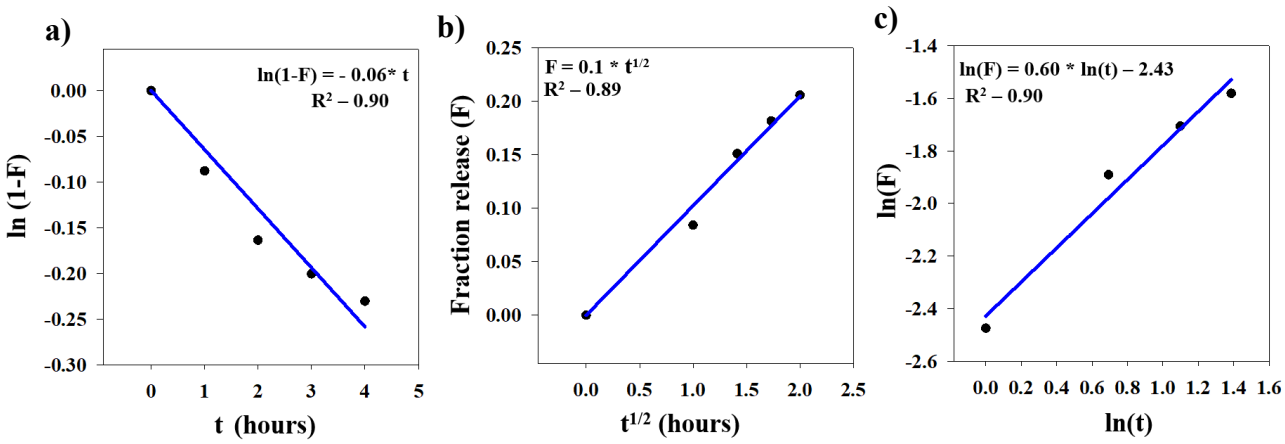

Figure A.13 - Release from NGs_insitu for 10 cycles fit with first order, Higuchi, and power models, respectively under condition TP_WMF.

Appendix I

Effect of Temperature on cyt C Release from NGs_insitu Systems

The cyt C release from NGs_insitu system was done at two different temperatures 40 ºC and 45 ºC, respectively as shown in Figure A.14. Due to increase of 5 ºC, much higher initial release rates were observed. But it should be pointed out that the effect of L.E was also involved in the data shown. The NGs_insitu sample (at 45 ºC) had L.E (80 %) while the sample (at 40 ºC) had L.E (67 %). Henceforth, there is significant increase in initial release rates caused by a difference of 5 ºC, but it should not be overestimated.

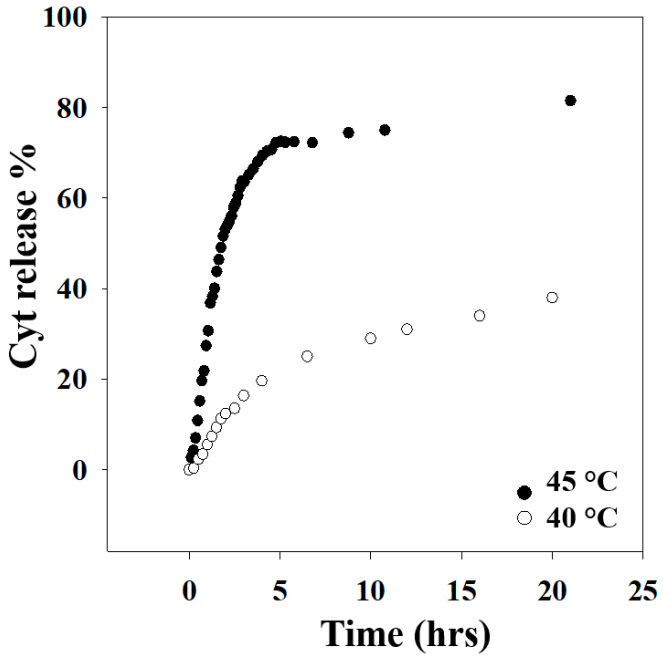

Figure A.14 – Effect of temperature on cyt C release from NGs_insitu system.

References

1. Bandyopadhyay S, Andersen MK, Alvi MAA, Sharma A, Raju R, McDonagh BH, et al. Incorporation of Fe@ Au nanoparticles into multiresponsive pNIPAM-AAc colloidal gels modulates drug uptake and release. Colloid and Polymer Science. 2016;294(12):1929-42.
2. Halperin A, Kröger M, Winnik FM. Poly (N-isopropylacrylamide) phase diagrams: fifty years of research. Angewandte Chemie International Edition. 2015;54(51):15342-67.
3. Bronstein LM, Huang X, Retrum J, Schmucker A, Pink M, Stein BD, et al. Influence of iron oleate complex structure on iron oxide nanoparticle formation. Chemistry of materials. 2007;19(15):3624-32.
4. Riedinger A, Guardia P, Curcio A, Garcia MA, Cingolani R, Manna L, et al. Subnanometer local temperature probing and remotely controlled drug release based on azo-functionalized iron oxide nanoparticles. Nano letters. 2013;13(6):2399-406.
5. Deatsch AE, Evans BA. Heating efficiency in magnetic nanoparticle hyperthermia. Journal of Magnetism and Magnetic Materials. 2014;354:163-72.
6. Khandhar AP, Ferguson RM, Krishnan KM. Monodispersed magnetite nanoparticles optimized for magnetic fluid hyperthermia: Implications in biological systems. Journal of applied physics. 2011;109(7):07B310.
7. Silva GA. Introduction to nanotechnology and its applications to medicine. Surgical neurology. 2004;61(3):216-20.
8. Ragusa A, García I, Penadés S. Nanoparticles as nonviral gene delivery vectors. IEEE transactions on nanobioscience. 2007;6(4):319-30.
9. Månsson S, Johansson E, Magnusson P, Chai C-M, Hansson G, Petersson JS, et al. 13 C imaging—a new diagnostic platform. European radiology. 2006;16(1):57-67.
10. Astruc D, Lu F, Aranzaes JR. Nanoparticles as recyclable catalysts: the frontier between homogeneous and heterogeneous catalysis. Angewandte Chemie International Edition. 2005;44(48):7852-72.
11. Murty BS, Shankar P, Raj B, Rath B, Murday J. Textbook of nanoscience and nanotechnology: Springer Science & Business Media; 2013.

12. Parveen S, Misra R, Sahoo SK. Nanoparticles: a boon to drug delivery, therapeutics, diagnostics and imaging. Nanomedicine: Nanotechnology, Biology and Medicine. 2012;8(2):147-66.

13. Wu W, Wu Z, Yu T, Jiang C, Kim W-S. Recent progress on magnetic iron oxide nanoparticles: synthesis, surface functional strategies and biomedical applications. Science and technology of advanced materials. 2015.

14. LaMer VK, Dinegar RH. Theory, production and mechanism of formation of monodispersed hydrosols. Journal of the American Chemical Society. 1950;72(11):4847-54.

15. Burda C, Chen X, Narayanan R, El-Sayed MA. Chemistry and properties of nanocrystals of different shapes. Chemical reviews. 2005;105(4):1025-102.

16. Khalil MI. Co-precipitation in aqueous solution synthesis of magnetite nanoparticles using iron (III) salts as precursors. Arabian Journal of Chemistry. 2015;8(2):279-84.

17. Park J, Joo J, Kwon SG, Jang Y, Hyeon T. Synthesis of monodisperse spherical nanocrystals. Angewandte Chemie International Edition. 2007;46(25):4630-60.

18. Arshadi S, Moghaddam J, Eskandarian M. LaMer diagram approach to study the nucleation and growth of Cu 2 O nanoparticles using supersaturation theory. Korean Journal of Chemical Engineering. 2014;31(11):2020-6.

19. Massart R. Preparation of aqueous magnetic liquids in alkaline and acidic media. IEEE transactions on magnetics. 1981;17(2):1247-8.

20. Hyeon T, Lee SS, Park J, Chung Y, Na HB. Synthesis of highly crystalline and monodisperse maghemite nanocrystallites without a size-selection process. Journal of the American Chemical Society. 2001;123(51):12798-801.

21. Laurent S, Forge D, Port M, Roch A, Robic C, Vander Elst L, et al. Magnetic iron oxide nanoparticles: synthesis, stabilization, vectorization, physicochemical characterizations, and biological applications. Chemical reviews. 2008;108(6):2064-110.

22. Lu AH, Salabas EeL, Schüth F. Magnetic nanoparticles: synthesis, protection, functionalization, and application. Angewandte Chemie International Edition. 2007;46(8):1222-44.

23. Zeng H, Sun S. Syntheses, properties, and potential applications of multicomponent magnetic nanoparticles. Advanced Functional Materials. 2008;18(3):391-400.

24. Yu WW, Chang E, Falkner JC, Zhang J, Al-Somali AM, Sayes CM, et al. Forming biocompatible and nonaggregated nanocrystals in water using amphiphilic polymers. Journal of the American Chemical Society. 2007;129(10):2871-9.

25. Park J, An K, Hwang Y, Park J-G, Noh H-J, Kim J-Y, et al. Ultra-large-scale syntheses of monodisperse nanocrystals. Nature materials. 2004;3(12):891-5.

26. Hufschmid R, Arami H, Ferguson RM, Gonzales M, Teeman E, Brush LN, et al. Synthesis of phase-pure and monodisperse iron oxide nanoparticles by thermal decomposition. Nanoscale. 2015;7(25):11142-54.

27. Roca A, Morales M, O'Grady K, Serna C. Structural and magnetic properties of uniform magnetite nanoparticles prepared by high temperature decomposition of organic precursors. Nanotechnology. 2006;17(11):2783.

28. Cotin G, Kiefer C, Perton F, Ihiawakrim D, Blanco-Andujar C, Moldovan S, et al. Unravelling the thermal decomposition parameters for the synthesis of anisotropic iron oxide nanoparticles. Nanomaterials. 2018;8(11):881.

29. Singh G, Kumar PA, Lundgren C, van Helvoort AT, Mathieu R, Wahlström E, et al. Tunability in crystallinity and magnetic properties of core–shell Fe nanoparticles. Particle & Particle Systems Characterization. 2014;31(10):1054-9.

30. Poth P. Corrosion Books: The Iron Oxides–Structure, Properties, Reactions, Occurences and Uses. By: RM Cornell, U. Schwertmann. Materials and Corrosion. 2004;55(9):704-.

31. Boxall C, Kelsall G, Zhang Z. Photoelectrophoresis of colloidal iron oxides. Part 2.—Magnetite (Fe 3 O 4). Journal of the Chemical Society, Faraday Transactions. 1996;92(5):791-802.

32. Fauzi AD. Theoretical study of the effect of oxygen vacancies on magnetism and charge transport of Fe3O4. March; 2017.

33. Jain A. Presentation on Magnetic materials. Science. 2016.

34. Xiao-Li L, Yong Y, Jian-Peng W, Yi-Fan Z, Hai-Ming F, Jun D. Novel magnetic vortex nanorings/nanodiscs: Synthesis and theranostic applications. Chinese Physics B. 2015;24(12):127505.

35. Fannin P, Charles S. On the calculation of the Neel relaxation time in uniaxial single-domain ferromagnetic particles. Journal of Physics D: Applied Physics. 1994;27(2):185.

36. Starks CM, Liotta CL, Halpern ME. Basic Concepts in Phase-Transfer Catalysis. Phase-Transfer Catalysis: Springer; 1994. p. 1-22.
37. Banerjee A. NTNU Specialization Project. 2019:34.
38. Bandyopadhyay S, Singh G, Sandvig I, Sandvig A, Mathieu R, Kumar PA, et al. Synthesis and in vitro cellular interactions of superparamagnetic iron nanoparticles with a crystalline gold shell. Applied surface science. 2014;316:171-8.
39. Arias LS, Pessan JP, Vieira APM, Lima TMTd, Delbem ACB, Monteiro DR. Iron oxide nanoparticles for biomedical applications: a perspective on synthesis, drugs, antimicrobial activity, and toxicity. Antibiotics. 2018;7(2):46.
40. Marinovich M, Tragni E, Corsini A, Galli CL. Quantification of in vitro cytotoxicity of surfactants: correlation with their eye irritation potential. Journal of Toxicology: Cutaneous and Ocular Toxicology. 1990;9(3):169-78.
41. Effendy I, Maibach HI. Surfactants and experimental irritant contact dermatitis. Contact dermatitis. 1995;33(4):217-25.
42. Goodman C, McCusker C, Yilmaz T, Rotello V. Bioconjugate Chem. 2004.
43. Roberts K, Alberts B, Johnson A, Walter P, Hunt T. Molecular biology of the cell. New York: Garland Science. 2002.
44. Buchholz FL, Graham AT. Modern superabsorbent polymer technology. John! Wiley & Sons, Inc, 605 Third Ave, New York, NY 10016, USA, 1998 279. 1998.
45. Harrison IP, Spada F. Hydrogels for atopic dermatitis and wound management: a superior drug delivery vehicle. Pharmaceutics. 2018;10(2):71.
46. Schild HG. Poly (N-isopropylacrylamide): experiment, theory and application. Progress in polymer science. 1992;17(2):163-249.
47. Li Y, Huang G, Zhang X, Li B, Chen Y, Lu T, et al. Magnetic hydrogels and their potential biomedical applications. Advanced Functional Materials. 2013;23(6):660-72.
48. Burkert S, Schmidt T, Gohs U, Dorschner H, Arndt K-F. Cross-linking of poly (N-vinyl pyrrolidone) films by electron beam irradiation. Radiation Physics and Chemistry. 2007;76(8-9):1324-8.
49. Wu C, Wang X. Globule-to-coil transition of a single homopolymer chain in solution. Physical review letters. 1998;80(18):4092.

50. Illeperuma WR, Sun J-Y, Suo Z, Vlassak JJ. Force and stroke of a hydrogel actuator. Soft Matter. 2013;9(35):8504-11.

51. Bandyopadhyay S. Fabrication and Application of Nanomaterials. 1st ed: New York (NY) Mc Graw Hill; 2019. 286 pages p.

52. Falamarzian M, Varshosaz J. The effect of structural changes on swelling kinetics of polybasic/hydrophobic pH-sensitive hydrogels. Drug development and industrial pharmacy. 1998;24(7):667-9.

53. Hao G, Xu ZP, Li L. Manipulating extracellular tumour pH: an effective target for cancer therapy. RSC advances. 2018;8(39):22182-92.

54. Khan MS, Khan GT, Khan A, Sultana S. Preparation and characterization of novel temperature and pH sensitive (NIPAM-co-MAA) polymer microgels and their volume phase change with various salts. Polymer Korea. 2013;37(6):794-801.

55. Zhang H. Controlled/“living” radical precipitation polymerization: a versatile polymerization technique for advanced functional polymers. European Polymer Journal. 2013;49(3):579-600.

56. Ma D. Hybrid Nanoparticles: An Introduction. Noble Metal-Metal Oxide Hybrid Nanoparticles: Elsevier; 2019. p. 3-6.

57. Shamim N, Hong L, Hidajat K, Uddin M. Thermosensitive polymer (N-isopropylacrylamide) coated nanomagnetic particles: preparation and characterization. Colloids and surfaces b: biointerfaces. 2007;55(1):51-8.

58. Jain KK. Drug delivery systems-an overview. Drug delivery systems. 2008:1-50.

59. Mehrotra N, Gupta M, Kovar A, Meibohm B. The role of pharmacokinetics and pharmacodynamics in phosphodiesterase-5 inhibitor therapy. International journal of impotence research. 2007;19(3):253-64.

60. Bruschi ML. Strategies to modify the drug release from pharmaceutical systems: Woodhead Publishing; 2015.

61. Tafani M, Karpinich NO, Hurster KA, Pastorino JG, Schneider T, Russo MA, et al. Cytochrome c release upon Fas receptor activation depends on translocation of full-length bid and the induction of the mitochondrial permeability transition. Journal of Biological Chemistry. 2002;277(12):10073-82.

62. Momtazi L, Bagherifam S, Singh G, Hofgaard A, Hakkarainen M, Glomm WR, et al. Synthesis, characterization, and cellular uptake of magnetic nanocarriers for cancer drug delivery. Journal of colloid and interface science. 2014;433:76-85.

63. Sharma A, Foppen JW, Banerjee A, Sawssen S, Bachhar N, Peddis D, et al. Magnetic Nanoparticles to Unique DNA Tracers: Effect of Functionalization on Physico-chemical Properties. Nanoscale Research Letters. 2021;16(1):1-16.

64. Chakraborty C, Pal S, Doss G, Wen Z-H, Lin C-S. Nanoparticles as' smart'pharmaceutical delivery. Frontiers in bioscience (Landmark edition). 2013;18:1030-50.

65. Anthny J. Understanding the growth and physicochemical

properties of multifunctional

nanoparticles. 2018:131.

66. Fuciños C, Fuciños P, Míguez M, Katime I, Pastrana LM, Rúa ML. Temperature-and pH-sensitive nanohydrogels of poly (N-Isopropylacrylamide) for food packaging applications: modelling the swelling-collapse behaviour. PLoS One. 2014;9(2):e87190.

67. Bandyopadhyay S, Sharma A, Glomm WR. The Influence of Differently Shaped Gold Nanoparticles Functionalized with NIPAM-Based Hydrogels on the Release of Cytochrome C. Gels. 2017;3(4):42.

68. Chenite A, Chaput C, Wang D, Combes C, Buschmann M, Hoemann C, et al. Novel injectable neutral solutions of chitosan form biodegradable gels in situ. Biomaterials. 2000;21(21):2155-61.

69. Sharma A. Different shaped hybrid nanocarriers for

theranostic applications. 2016:169.

70. Aldrich S. [Properties of Cytochrome C. Available from: https://www.sigmaaldrich.com/life-science/metabolomics/enzyme-explorer/learning-center/cytochrome-c.html.

71. Stigliano RV, Shubitidze F, Petryk JD, Shoshiashvili L, Petryk AA, Hoopes PJ. Mitigation of eddy current heating during magnetic nanoparticle hyperthermia therapy. International Journal of Hyperthermia. 2016;32(7):735-48.

72. Pusey P. The effect of polydispersity on the crystallization of hard spherical colloids. Journal de physique. 1987;48(5):709-12.

73. Korpany KV, Mottillo C, Bachelder J, Cross SN, Dong P, Trudel S, et al. One-step ligand exchange and switching from hydrophobic to water-stable hydrophilic superparamagnetic iron oxide nanoparticles by mechanochemical milling. Chemical Communications. 2016;52(14):3054-7.

74. Xu C, Sun S. Monodisperse magnetic nanoparticles for biomedical applications. Polymer International. 2007;56(7):821-6.

75. Ghasemi E, Mirhabibi A, Edrissi M, Aghababazadeh R, Brydson R. Study on the magnetorheological properties of Maghemite-Kerosene ferrofluid. Journal of nanoscience and nanotechnology. 2009;9(7):4273-8.

76. Shukla S, Jadaun A, Arora V, Sinha RK, Biyani N, Jain V. In vitro toxicity assessment of chitosan oligosaccharide coated iron oxide nanoparticles. Toxicology reports. 2015;2:27-39.

77. Peng S, Sun S. Synthesis and characterization of monodisperse hollow Fe3O4 nanoparticles. Angewandte Chemie. 2007;119(22):4233-6.

78. Balanda M. AC susceptibility studies of phase transitions and magnetic relaxation: Conventional, molecular and low-dimensional magnets. Acta Phys Pol A. 2013;124(6):964-76.

79. Guerrini L, Alvarez-Puebla RA, Pazos-Perez N. Surface modifications of nanoparticles for stability in biological fluids. Materials. 2018;11(7):1154.

80. Evans D, Pye G, Bramley R, Clark A, Dyson T, Hardcastle J. Measurement of gastrointestinal pH profiles in normal ambulant human subjects. Gut. 1988;29(8):1035-41.

81. (ECHA) ECA. [Trisodium citrate]. Available from: https://echa.europa.eu/registration-dossier/-/registered-dossier/15303/4/22.

82. Sosa-Acosta JR, Silva J, Fernández-Izquierdo L, Díaz-Castañón S, Ortiz M, Zuaznabar-Gardona JC, et al. Iron oxide nanoparticles (IONPs) with potential applications in plasmid DNA isolation. Colloids and Surfaces A: Physicochemical and Engineering Aspects. 2018;545:167-78.

83. Simeonidis K, Morales MP, Marciello M, Angelakeris M, de La Presa P, Lazaro-Carrillo A, et al. In-situ particles reorientation during magnetic hyperthermia application: Shape matters twice. Scientific reports. 2016;6(1):1-11.

84. Pietrangeli P, Mondovì B. On the biochemical basis of tumour damage by hypothermia. Hyperthermia in Cancer Treatment: A Primer: Springer; 2006. p. 110-8.

85. Dionigi C, Piñeiro Y, Riminucci A, Bañobre M, Rivas J, Dediu V. Regulating the thermal response of PNIPAM hydrogels by controlling the adsorption of magnetite nanoparticles. Applied Physics A. 2014;114(2):585-90.

86. Raghunathan K. Tailoring multifunctional nanoparticles

for encapsulation of bio-molecules. 2017:113.

87. Mahmoudi M, Simchi A, Imani M, Milani AS, Stroeve P. Optimal design and characterization of superparamagnetic iron oxide nanoparticles coated with polyvinyl alcohol for targeted delivery and imaging. The Journal of Physical Chemistry B. 2008;112(46):14470-81.

88. Banerjee A. Magnetic Energy Harvesting of Hybrid Iron Oxide Nanoparticles (IONPs) for Biomedical Applications. 2020:22.

89. Amsden B. Solute diffusion within hydrogels. Mechanisms and models. Macromolecules. 1998;31(23):8382-95.

90. Saurí J, Millán D, Suñé-Negre J, Colom H, Ticó J, Miñarro M, et al. Quality by design approach to understand the physicochemical phenomena involved in controlled release of captopril SR matrix tablets. International journal of pharmaceutics. 2014;477(1-2):431-41.

91. Benhabbour SR, Kovarova M, Jones C, Copeland DJ, Shrivastava R, Swanson MD, et al. Ultra-long-acting tunable biodegradable and removable controlled release implants for drug delivery. Nature communications. 2019;10(1):1-12.

92. Petcharoen K, Sirivat A. Synthesis and characterization of magnetite nanoparticles via the chemical co-precipitation method. Materials Science and Engineering: B. 2012;177(5):421-7.

93. Bouguer P. Essai d'Optique sur la Gradation de la Lumière. The British Institute of Radiology; 1922.